Spring 4-16-2020

THE ROLE OF LGR5+ EPITHELIAL STEM-LIKE CELLS IN 3D-ORGANOID MODELING AND PATHOGENESIS OF AMELOBLASTOMA

Ting-Han Chang
University of Pennsylvania, tinch@upenn.edu

THE ROLE OF LGR5+ EPITHELIAL STEM-LIKE CELLS IN 3D-ORGANOID MODELING AND PATHOGENESIS OF AMELOBLASTOMA

Abstract

Ameloblastoma (AM) is a benign yet locally aggressive tumor with high recurrences. Currently, the underlying pathophysiology remains elusive and radical surgery remains the most definitive treatment with severe morbidities. Our group first reported that AM harbors a subpopulation of tumor epithelial stem-like cells (AM-EpiSCs). Herein, this study further explored whether $LGR5^+$ epithelial cells in AM possess unique stem-like cell properties and their potential contribution to the pathogenesis and recurrence of AM. Our findings demonstrated that LGR5 and stem cell-related genes were simultaneously expressed in a subpopulation of AM epithelial cells, both *in vivo* and *in vitro*, which were markedly enriched under the 3D-spheroid culture condition. As compared to $LGR5^-$ counterparts, $LGR5^+$ AM epithelial cells showed increased expression of several critical genes involved in the regulation of epithelial-mesenchymal transition (EMT) and stem cell pluripotency, and functionally, exhibited enhanced capacity to form 3D-spheroids and generate human tumor 3D-organoids, which recapitulated characteristic histopathologic features of distinct subtypes of solid AM. Interestingly, AM derived mesenchymal stromal cells (AM-MSCs) and their secretomes or extracellular vesicles (EVs) significantly promoted the generation of $LGR5^+$ AM-EpiSCs both *in vitro* and *in vivo*. Furthermore, treatment with a selective $BRAF^{V600E}$ inhibitor, Vemurafenib, unexpectedly enriched the proportion of $LGR5^+$ AM-EpiSCs in AM 3D-organoids, which may explain the therapeutic resistant and recurrent properties of AM conferred by this unique subpopulation of AM-EpiSCs. Therefore, the tumor 3D-organoids generated by $LGR5^+$ AM-EpiSCs provided a novel *ex vivo* platform for mechanistic studies of human AM and high throughput screening of targeted therapeutic drugs. These findings suggest that $LGR5^+$ AM-EpiSCs play a pivotal role in pathogenesis and progression of AM and targeted inhibition of both BRAF and LGR5 potentially serves a novel non-surgical adjuvant therapeutic approach for this benign yet aggressively destructive jaw tumor.

Degree Type

Dissertation

Degree Name

DScD (Doctor of Science in Dentistry)

Primary Advisor

Anh D. Le

Keywords

Ameloblastoma, LGR5, Organoid, Epithelial Stem cells

Subject Categories

Dentistry | Oral and Maxillofacial Surgery

THE ROLE OF LGR5^{+} EPITHELIAL STEM-LIKE CELLS IN 3D-ORGANOID MODELING AND PATHOGENESIS OF AMELOBLASTOMA

TING-HAN CHANG

A DISSERTATION

Presented to the Faculties of the University of Pennsylvania

in

Partial Fulfillment of the Requirements for the

Degree of Doctor of Science in Dentistry

2020

Supervisor of Dissertation

Anh D. Le

Chair and Norman Vine Endowed Professor of Oral Rehabilitation, Department of Oral and Maxillofacial Surgery and Pharmacology, University of Pennsylvania School of Dental Medicine

Co-Supervisor of Dissertation

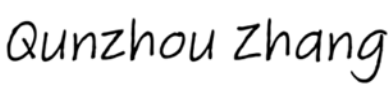

Qunzhou Zhang

Research Assistant Professor, Department of Oral and Maxillofacial Surgery and Pharmacology, University of Pennsylvania School of Dental Medicine

Graduate Group Chairperson

Claire H. Mitchell

Professor, Department of Basic & Translational Sciences, University of Pennsylvania School of Dental Medicine

Dissertation Committee

Faizan Alawi, Associate Dean for Academic Affairs Director, Penn Oral Pathology Services Associate Professor of Pathology, Department of Basic & Translational Sciences, University of Pennsylvania School of Dental Medicine

Rabie M. Shanti, Assistant Professor of Oral Surgery and Pharmacology, Department of Oral and Maxillofacial Surgery and Pharmacology, University of Pennsylvania School of Dental Medicine

Dedication

To my husband Da-Yo Yuh and our daughters

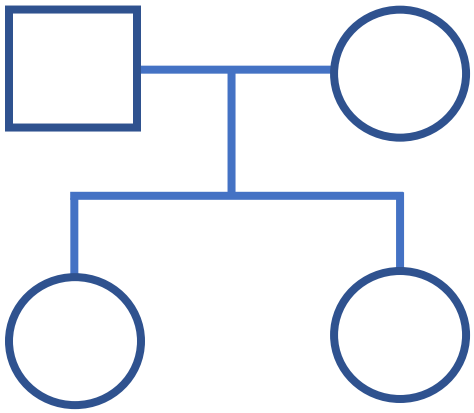

Agnes *Phoebe*

ACKNOWLEDGMENT

This work would not have been possible without endless support and patience from my mentors, Dr. Anh D. Le, and Dr. Qunzhou Zhang. I want to thank Dr. Le for allowing me to study this significant field—benign odontogenic tumor—of the dental medicine, and her inspirational encouragement that open an unlimited future for me. I always remember Dr. Le told me that “The way we treat a patient has never changed for 100 years, and we have to do something to improve it.’’ She taught me never to be satisfied with the current status and urged me to go high and go deep. I also want to thank Dr. Zhang for his patience and guidance. He always accompanied and helped me to face the troubles and trained me to be able to do research independently.

No thesis project is completed without the support and advice of a committee. The committee supervising this project was chaired by Dr. Claire H. Mitchell and included Dr. Faizan Alawi and Dr. Rabie M. Shanti, all of whom carried a unique perspective critical to the development of this project. I deeply appreciate the discipline of the rigorous attitude towards science that how you trained me and will keep it forever.

I would also like to thank all my friends and family who have given me encouragement and support, especially my parents, who give me endless love and support. Finally, I want to thank my husband, Dr. Da-Yo Yuh, whose accompany, love, and support help me struggle through every difficulty I encountered.

ABSTRACT

THE ROLE OF LGR5^{+} EPITHELIAL STEM-LIKE CELLS IN 3D-ORGANOID MODELING AND PATHOGENESIS OF AMELOBLASTOMA

Ting-Han Chang

Anh D. Le and Qunzhou Zhang

Ameloblastoma (AM) is a benign yet locally aggressive tumor with high recurrences. Currently, the underlying pathophysiology remains elusive and radical surgery remains the most definitive treatment with severe morbidities. Our group first reported that AM harbors a subpopulation of tumor epithelial stem-like cells (AM-EpiSCs). Herein, this study further explored whether LGR5^{+} epithelial cells in AM possess unique stem-like cell properties and their potential contribution to the pathogenesis and recurrence of AM. Our findings demonstrated that LGR5 and stem cell-related genes were simultaneously expressed in a subpopulation of AM epithelial cells, both *in vivo* and *in vitro*, which were markedly enriched under the 3D-spheroid culture condition. As compared to LGR5^{-} counterparts, LGR5^{+} AM epithelial cells showed increased expression of several critical genes involved in the regulation of epithelial-mesenchymal transition (EMT) and stem cell pluripotency, and functionally, exhibited enhanced capacity to form 3D-spheroids and generate human tumor 3D-organoids, which recapitulated characteristic histopathologic features of

distinct subtypes of solid AM. Interestingly, AM derived mesenchymal stromal cells (AM-MSCs) and their secretomes or extracellular vesicles (EVs) significantly promoted the generation of $LGR5^+$ AM-EpiSCs both *in vitro* and *in vivo*. Furthermore, treatment with a selective $BRAF^{V600E}$ inhibitor, Vemurafenib, unexpectedly enriched the proportion of $LGR5^+$ AM-EpiSCs in AM 3D-organoids, which may explain the therapeutic resistant and recurrent properties of AM conferred by this unique subpopulation of AM-EpiSCs. Therefore, the tumor 3D-organoids generated by $LGR5^+$ AM-EpiSCs provided a novel *ex vivo* platform for mechanistic studies of human AM and high throughput screening of targeted therapeutic drugs. These findings suggest that $LGR5^+$ AM-EpiSCs play a pivotal role in pathogenesis and progression of AM and targeted inhibition of both BRAF and LGR5 potentially serves a novel non-surgical adjuvant therapeutic approach for this benign yet aggressively destructive jaw tumor.

[1] The part of this dissertation was reorganized from the article accepted by the journal of *Cell Death & Disease*.

[2] These materials are not contained in the Footnote 1.

---

[1] $LGR5^+$ epithelial tumor stem-like cells generate a 3D-organoid model for ameloblastoma. **Ting-Han Chang**, Rabie M. Shanti, Yanfang Liang, Jincheng Zeng, Shihong Shi, Faizan Alawi, Lee Carrasco, Qunzhou Zhang, and Anh D. Le. Accepted for publication in *Cell Death & Disease*.

[2] Chapter 1.4-1.6, 2.13, 2.15, 3.8-3.10, 4.3-4.4. Table 1, 2 and Figure 1.1-1.3,1.5, 2.1-2.2, 3.18-23.

TABLE OF CONTENTS

LIST OF TABLES

LIST OF ILLUSTRATIONS

CHAPTER 1: INTRODUCTION

1.1 Classification and epidemiology of ameloblastoma

Ameloblastoma (AM), one of the most common odontogenic epithelial tumors, has an estimated global incidence of 0.5 cases per million, and most cases are diagnosed at 30-60 years of age. AM accounts for 1% of all oral tumors and 11.7 to 60.3% of all odontogenic tumors[1]. AM is a benign yet locally aggressive tumor with a high recurrent rate in comparison with other benign odontogenic cysts or tumors. The overall recurrent rate of AM is 31%, ranging from 65% for conservative surgery to 11% for radical surgery[2], even though its malignant transformation and/or metastasis are less reported. The WHO has recently updated the classification of AM into three categories, AM (solid/multicystic type), unicystic type, and peripheral/extraosseous type, among which the solid/multicystic type accounts for about 71.3% of all AM cases and manifests a high recurrence rate (Figure 1.1)[3,4]. For large and aggressive lesions, a radical surgical approach is usually recommended with at least 1 cm margin to prevent recurrence[5]; however, incurs severe morbidities associated with large jaw defects, impaired oral functions and facial esthetics that require comprehensive tissue reconstruction and oral rehabilitation, compromise patient quality of life and raise the overall health care cost[1,6]. To date, the pathophysiology of AM remains poorly understood. Previous studies have found several genetic mutations in AM, including mitogen-activated protein kinase

(MAPK) and non-MAPK pathway, such as sonic hedgehog pathway, phosphatidylinositol 3-kinase (PI3K) pathway and Wnt signaling pathway (Figure 1.2)[7,8]. Among these mutations, $BRAF^{V600E}$ is the most common one, accounting for 46-82%[7-12], but has no significant correlation with tumor recurrence (Figure 1.3 and Table 1). *BRAF* is the gene that encodes B-Raf protein, which is a member of the Raf kinase family involved in regulating the MAPK pathway. $BRAF^{V600E}$ is a point mutation at codon 600 where valine is replaced by glutamic acid. A specific $BRAF^{V600E}$ inhibitor, Vemurafenib, inhibits the activity of $BRAF^{V600E}$ kinase by binding to its ATP-binding site. Clinically, Vemurafenib has been utilized to treat melanoma, but a high drug resistance rate has been reported in melanoma patients[13]. Currently, an active clinical trial (NCT02367859) on AM therapy has been ongoing with the combinatory use of Dabrafenib (a BRAF inhibitor) and Trametinib (a MEK inhibitor), and only a partial response to the treatment with either a single BRAF inhibitor or combined a MEK inhibitor has been reported in AM patients (Table 2)[14-17]. Therefore, further studies are necessary to delineate the mechanisms underlying AM pathogenesis that may hold promises in the development of novel drugs as a non-surgical adjunctive treatment of this benign but aggressive odontogenic tumor.

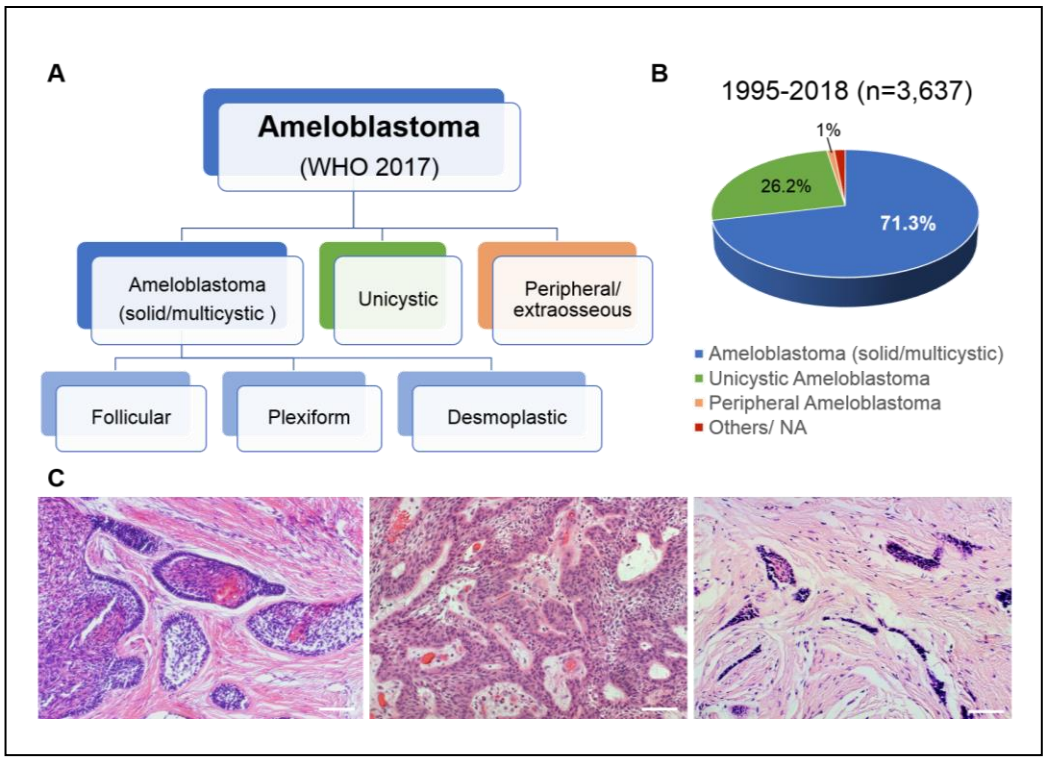

Figure 1.1 Classification of ameloblastoma (AM). A The Diagram was organized according to 2017 WHO classification of head and neck tumors[3]. The classification of AM has been updated into three categories, including AM (solid/multicystic), unicystic and peripheral/extraosseous. **B** The pie chart was modified from the global incidence of AM by Hendra, F. N. *et al.*[4], herein the most common type is solid AM with around 71.3%. **C** Histopathology of different subtypes of solid AM. Left, the follicular type is the most common type, which consists of islands of odontogenic epithelium surrounding with columnar to cuboidal peripheral cells (ameloblast-like). The epithelium arranges in a palisading pattern with hyperchromatic nuclei and reverses polarity. The inner cells resemble stellate reticulum with loosely arranged angular cells that may undergo cystic changes. The stroma is moderate to highly collagenized. Middle, the second common type is the plexiform type which consists of anastomosing strands with an inconspicuous stellate reticulum, and the peripheral epithelial cells are less pronounced than the follicular type. The connective tissue is loose and often undergoes cystic changes. Right, The desmoplastic type consists of cuboidal to flat peripheral cells with central spindle cells and densely collagenous stroma. Scale bar: 50μm.

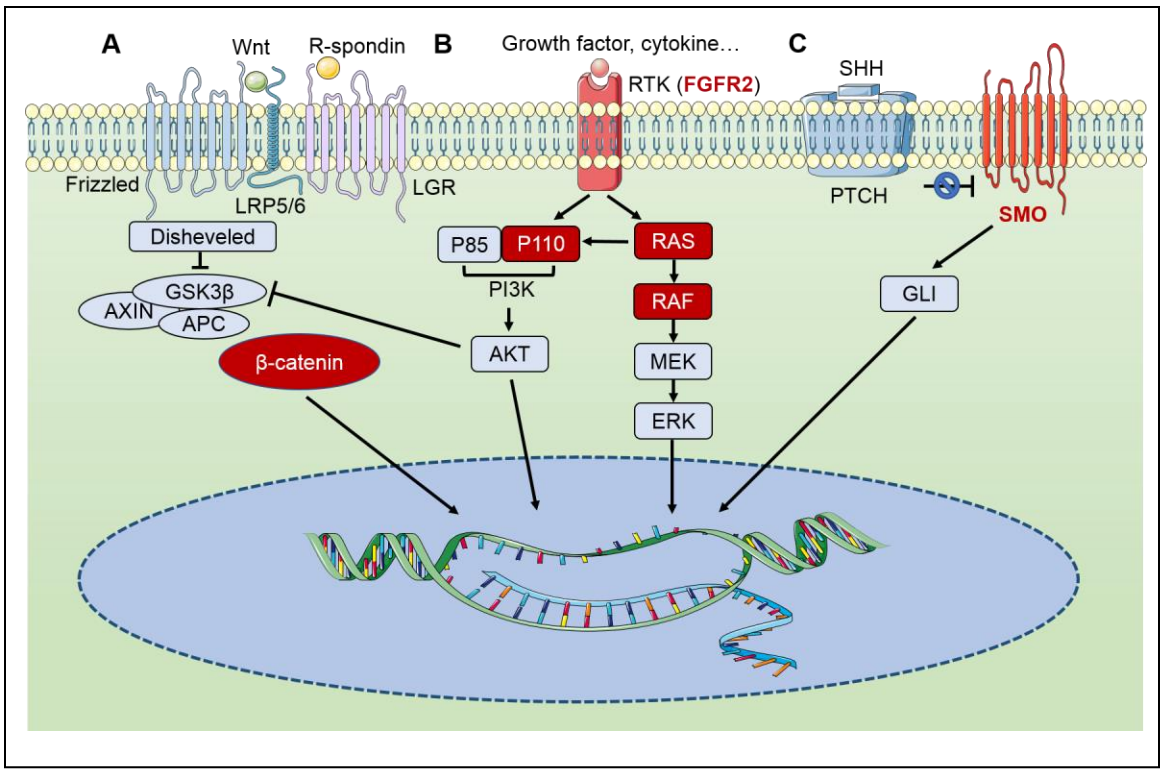

Figure 1.2 Mutations in signaling pathways of AM. The mutations in AM were marked with red color and these involved pathways are essential for cell proliferation and survival. **A** Somatic mutation of *CTNNB1*, a gene that encodes a protein called β-catenin in the canonical Wnt signaling pathway. **B** Mutation of FGFR2, a class V receptor tyrosine kinase (RTK), activates both MAPK (right) and PI3K signaling pathways (left). Right: both RAS and RAF in the downstream of MAPK pathway have mutations. Left: the mutation of PIK3CA, the gene that encodes p110 protein, a catalytic subunit of PI3K. **C** The smoothened (SMO) mutation in the hedgehog signaling pathway. The diagram was generated by using SMART SERVIER MEDICAL ART.

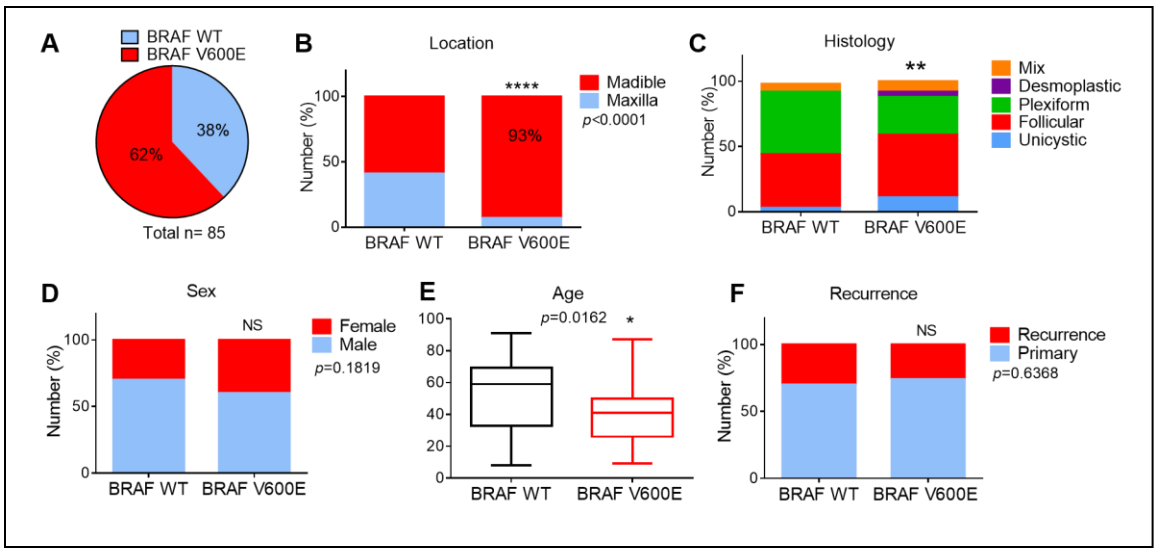

Figure 1.3 BRAF^{V600E} mutation in AM. Data are pooled from four original articles, and the raw data are presented in Table 1. **A** Around 62% BRAF^{V600E} mutation in 85 patients. **B** BRAF^{V600E} mutation is significantly higher in the mandible (93%) than the maxilla. p<0.0001, Fisher's exact test. **C** BRAF^{V600E} was found in both unicystic and solid AM, including different histologic subtypes of solid AM, but had a lower preference in plexiform AM compared with the wild type BRAF group. Besides, this dataset showed no desmoplastic AM in the wild type BRAF group. p=0.0071 Chi-square test. **D** BRAF^{V600E} had no significant different preference in sex distribution compared with the wild type BRAF group. NS= not significant. Fisher's exact test. **E** BRAF^{V600E} mutation occurred in younger diagnosis age. Data are mean ± SD, two-tailed unpaired Student's *t*-tests, *p<0.05. **F** No significant difference in the recurrent rate between BRAF^{V600E} mutation and wild type groups. NS=not significant. Fisher's exact test.

Table 1. BRAF^{V600E} mutation in AM.

ID (Author_case number)	Sex	Age	Location	Histological type	BRAF^{V600E}	Recurrence
Diniz et al._01[10]	F	23	Mandible	Unicystic	WT	NA
Diniz et al._07[10]	M	48	Mandible	Follicular	WT	NA
Diniz et al._08[10]	M	8	Maxilla	Follicular	WT	Primary
Kurppa et al._03[9]	M	61	Mandible	Plexiform	WT	Primary
Kurppa et al._07[9]	M	36	Mandible	Follicular	WT	Primary
Kurppa et al._09[9]	M	32	Mandible	Plexiform	WT	Recurrence
Kurppa et al._13[9]	M	84	Mandible	Follicular	WT	Primary
Kurppa et al._16[9]	F	61	Mandible	Mix	WT	Primary
Kurppa et al._17[9]	M	69	Mandible	Plexiform	WT	Primary
Kurppa et al._18[9]	M	77	Mandible	Plexiform	WT	Recurrence
Kurppa et al._19[9]	M	69	Mandible	Plexiform	WT	Primary
Kurppa et al._24[9]	M	31	Mandible	Follicular	WT	Primary
Soltani et al._10[12]	F	52	NA	Plexiform	WT	NA
Soltani et al._15[12]	F	16	NA	Plexiform	WT	NA
Soltani et al._22[12]	M	35	NA	Follicular	WT	NA
Soltani et al._25[12]	M	31	NA	Follicular	WT	NA
Soltani et al._28[12]	M	33	NA	Follicular	WT	NA
Sweeney et al._01[8]	F	57	Maxilla	Plexiform	WT	Primary
Sweeney et al._02[8]	M	73	Maxilla	Mix	WT	Recurrence
Sweeney et al._03[8]	M	70	Mandible	Follicular	WT	Primary
Sweeney et al._04[8]	M	66	Maxilla	Plexiform	WT	Recurrence
Sweeney et al._05[8]	F	51	Maxilla	Plexiform	WT	Recurrence
Sweeney et al._06[8]	F	29	Maxilla	Plexiform	WT	Primary
Sweeney et al._07[8]	NA	NA	Maxilla	Plexiform	WT	NA
Sweeney et al._08[8]	M	77	Maxilla	Plexiform	WT	Recurrence
Sweeney et al._09[8]	M	62	Maxilla	Plexiform	WT	Primary
Sweeney et al._23[8]	M	79	Mandible	NA	WT	Primary
Sweeney et al._24[8]	M	61	Maxilla	Follicular	WT	Primary
Sweeney et al._25[8]	M	65	Maxilla	Follicular	WT	Primary
Sweeney et al._26[8]	NA	NA	Mandible	Follicular	WT	NA
Sweeney et al._27[8]	F	91	Mandible	Follicular	WT	Primary
Sweeney et al._28[8]	F	47	Mandible	Plexiform	WT	Recurrence
Diniz et al._02[10]	M	NA	Mandible	Unicystic	Mutant	NA

ID (Author_case number)	Sex	Age	Location	Histological type	$BRAF^{V600E}$	Recurrence
Diniz et al._03[10]	F	10	Mandible	Unicystic	Mutant	NA
Diniz et al._04[10]	F	21	Mandible	Unicystic	Mutant	Primary
Diniz et al._05[10]	M	14	Mandible	Unicystic	Mutant	Primary
Diniz et al._06[10]	M	38	Maxilla	Unicystic	Mutant	Primary
Diniz et al._09[10]	M	NA	Mandible	Granular	Mutant	NA
Diniz et al._10[10]	F	41	Mandible	Follicular	Mutant	NA
Diniz et al._11[10]	M	46	Mandible	Follicular	Mutant	Primary
Diniz et al._12[10]	F	28	Mandible	Follicular	Mutant	NA
Diniz et al._13[10]	F	39	Mandible	Follicular	Mutant	Primary
Diniz et al._14[10]	F	9	Mandible	Plexiform	Mutant	NA
Diniz et al._15[10]	M	75	Maxilla	Follicular	Mutant	Primary
Diniz et al._16[10]	F	28	Maxilla	Desmoplastic	Mutant	Primary
Diniz et al._17[10]	M	25	Mandible	Desmoplastic	Mutant	Primary
Kurppa et al._01[9]	M	66	Mandible	Follicular	Mutant	Primary
Kurppa et al._02[9]	F	70	Mandible	Follicular	Mutant	Primary
Kurppa et al._04[9]	F	27	Mandible	Follicular	Mutant	Primary
Kurppa et al._05[9]	F	24	Mandible	Plexiform	Mutant	Primary
Kurppa et al._06[9]	F	50	Mandible	Plexiform	Mutant	Primary
Kurppa et al._08[9]	M	47	Mandible	Follicular	Mutant	Primary
Kurppa et al._10[9]	M	46	Mandible	Follicular	Mutant	Recurrence
Kurppa et al._11[9]	M	14	Mandible	Plexiform	Mutant	Primary
Kurppa et al._12[9]	F	34	Mandible	Follicular	Mutant	Recurrence
Kurppa et al._14[9]	F	18	Mandible	Follicular	Mutant	Primary
Kurppa et al._15[9]	M	16	Mandible	Plexiform	Mutant	Primary
Kurppa et al._20[9]	M	43	Mandible	Follicular	Mutant	Primary
Kurppa et al._21[9]	F	44	Mandible	Plexiform	Mutant	Primary
Kurppa et al._22[9]	M	33	Mandible	Follicular	Mutant	Recurrence
Kurppa et al._23[9]	F	46	Mandible	Plexiform	Mutant	Recurrence
Soltani et al._03[12]	M	87	NA	Follicular	Mutant	NA
Soltani et al._05[12]	M	58	NA	Follicular	Mutant	NA
Soltani et al._06[12]	M	46	NA	Plexiform	Mutant	NA
Soltani et al._09[12]	M	51	NA	Plexiform	Mutant	NA
Soltani et al._12[12]	M	30	NA	Plexiform	Mutant	NA
Soltani et al._16[12]	M	30	NA	Plexiform	Mutant	NA

ID (Author_case number)	Sex	Age	Location	Histological type	$BRAF^{V600E}$	Recurrence
Soltani et al._20[12]	M	78	NA	Follicular	Mutant	NA
Soltani et al._23[12]	F	50	NA	Plexiform	Mutant	NA
Soltani et al._24[12]	M	22	NA	Follicular	Mutant	NA
Soltani et al._26[12]	F	37	NA	Follicular	Mutant	NA
Soltani et al._29[12]	M	41	NA	Follicular	Mutant	NA
Soltani et al._33[12]	F	26	NA	Plexiform	Mutant	NA
Sweeney et al._11[8]	NA	NA	Mandible	Mix	Mutant	NA
Sweeney et al._12[8]	M	59	Mandible	Follicular	Mutant	Recurrence
Sweeney et al._13[8]	NA	NA	Mandible	Follicular	Mutant	NA
Sweeney et al._14[8]	M	45	Mandible	Follicular	Mutant	Primary
Sweeney et al._15[8]	M	70	Mandible	Mix	Mutant	Recurrence
Sweeney et al._16[8]	NA	NA	Mandible	Mix	Mutant	NA
Sweeney et al._17[8]	NA	NA	Frontal bone	Mix	Mutant	NA
Sweeney et al._18[8]	M	83	Mandible	Plexiform	Mutant	Primary
Sweeney et al._19[8]	NA	NA	Mandible	NA	Mutant	NA
Sweeney et al._20[8]	NA	NA	Mandible	NA	Mutant	NA
Sweeney et al._21[8]	NA	NA	Mandible	NA	Mutant	NA
Sweeney et al._22[8]	NA	NA	Mandible	NA	Mutant	NA

This table pools $BRAF^{V600E}$ and $BRAF^{WT}$ ameloblastoma cases from previous studies in the comparation of sex, age, location, histological type and recurrence. M, male; F, female; WT, wild type; NA, not available.

Table 2. Clinical reports of targeting $BRAF^{V600E}$ in AM.

Author	Sex	Age	Diagnosis	Mutation	Treatment	Follow up/ tool	Outcome
Kaye et al.[14]	M	40	Recurrent ameloblastoma of left mandible, bilateral neck and bilateral lung metastasis	BRAF V600E	Dabrafenib 150 mg BID; trametinib 2 mg QD	20 weeks/ CT scan	Partial response
Tan et al.[16]	M	85	Recurrent AM, left mandible with pathologic fracture	BRAF V600E	Dabrafenib 150 mg BID for 73 days, 1.5 months later under surgery treatment	75 days/ CT scan	Cystic change with same tumor size
						16 weeks/ surgical specimen	> 90% tumor volume reduction in the specimen
Faden et al.[15]	F	83	Recurrent AM, right mandible	BRAF V600E	Dabrafenib 75 mg BID (50% reduction of dose due to clinical comorbidities)	12 months/ MRI	75% reduction in tumor volume
Fernandes et al.[17]	F	29	Recurrent AM, left mandible status post operation Undiagnosed lesion of right cavernous sinus	BRAF V600E	Vemurafenib 960 mg BID	11 months/ MRI	Partial response
Brunet et al.[18]	F	26	Metastasis AM of bilateral lung	BRAF V600E	Dabrafenib 150 mg BID; trametinib 2 mg QD	12 weeks/ PET/CT scan;30 weeks/ NA	Complete response

This table is a summary of clinical case reports for advanced ameloblastoma cases treated with a $BRAF^{V600E}$ inhibitor (dabrafenib or vemurafenib) alone or combined with a MEK inhibitor (trametinib) orally. AM, ameloblastoma; M, male; F, female; QD, once daily, BID, twice daily; CT, computerized tomography; MRI, Magnetic resonance imaging; PET, positron emission tomography; NA, not available.

1.2 Plasticity of cancer stem cells— bidirectional EMT process, the hybrid EMT intermediate cells

Cancer stem cells (CSCs), or tumor-initiating cells (TICs), have the capabilities of self-renewal and differentiation into non-CSCs to repopulate the cancer mass. CSCs have been demonstrated to contribute to tumorigenesis, progression, metastasis, therapeutic resistance, and recurrence[19,20]. Epithelial-mesenchymal transition (EMT) is a dynamic process, during which epithelial cells undergo loss of cell junctions and spindle shape-like cell morphological changes and gain increased cell motility, all properties characteristic of mesenchymal cells[21,22]. EMT process plays a critical role in embryonic development, tissue remodeling/homeostasis, and wound healing, and a variety of pathological settings[22,23]. In tumor microenvironment, a portion of tumor epithelial cells undergo dynamic bidirectional EMT and mesenchymal-epithelial transition (MET) process, the determinant of cell plasticity that contributes to tumor initiation, CSC formation, and is closely associated with the development of several cancer hallmarks[22]. EMT intermediate cells, or hybrid cells, are endowed with both epithelial and mesenchymal cell features and contribute to tumor initiation, progression, metastasis, and drug resistance[21-23]. However, much less work has been done to explore the potential role of EMT and TICs in the development of benign epithelial tumors. Recently, our group has shown that AM tissues harbor a proportion of epithelial cells (AM epithelial cells) which simultaneously express EMT regulatory transcription factors (TFs) such as ZEB1, Slug, and Snail as well as stem cell-related markers such as ALDH1, BMI-1, and SOX2. These proteins

were up-regulated in AM epithelial cells when co-cultured with AM-derived mesenchymal stromal cells (AM-MSCs)[24], thus supporting the notion that the subpopulation of AM epithelial cells are endowed with both EMT and stem-like cell properties (AM-EpiSCs). However, to date, there is still a lack of consistent cell surface markers to identify these EMT intermediate cells with stem-like cell properties (AM-EpiSCs) and their potential role in the pathogenesis and progression of AM remains largely unknown.

1.3 LGR5^{+} stem cells in normal organs and tumors

Leucine-rich repeat-containing G-protein coupled receptor (LGR) proteins are a unique class of evolutionarily conserved seven-transmembrane (7TM) receptors characterized by a large extracellular region (ectodomain) that harbors multiple imperfect copies of leucine-rich repeat protein interaction domain (Figure 1.4 A)[25]. LGR5, a family member of LGR proteins, can activate Wnt/β-catenin pathway through binding with its ligands, R-spondin family (R-spondin 1 to 4) (Figure 1.4 B)[25,26], and has been identified as an epithelial stem cell marker in multiple developmental organs, such as the root cervical loop, taste bud, intestine, and hair follicle[25,27,28]. Meanwhile, LGR5 has also been reported as a putative marker for cancer stem cells (CSCs) in several types of malignant cancers, e.g. basal cell carcinoma, glioma, and gastrointestinal (GI) cancers[29-34]. Functionally, LGR5 has been shown to promote EMT process and metastasis in hepatocellular carcinoma, colon cancer, and glioma[33-35] and to predict poor survival of glioma patients[34]. The development of odontogenic tumors, including ameloblastoma,

has been linked to the enamel organ, e.g. remnants of odontogenic epithelium, the migrating epithelium at the cervical loop, and lining of odontogenic cyst[36,37]. Several studies have also reported LGR5 expression in odontogenic epithelial stem cells[38-41], suggesting that LGR5 may represent a putative epithelial stem cell surface marker in both normal and tumorous odontogenic tissues.

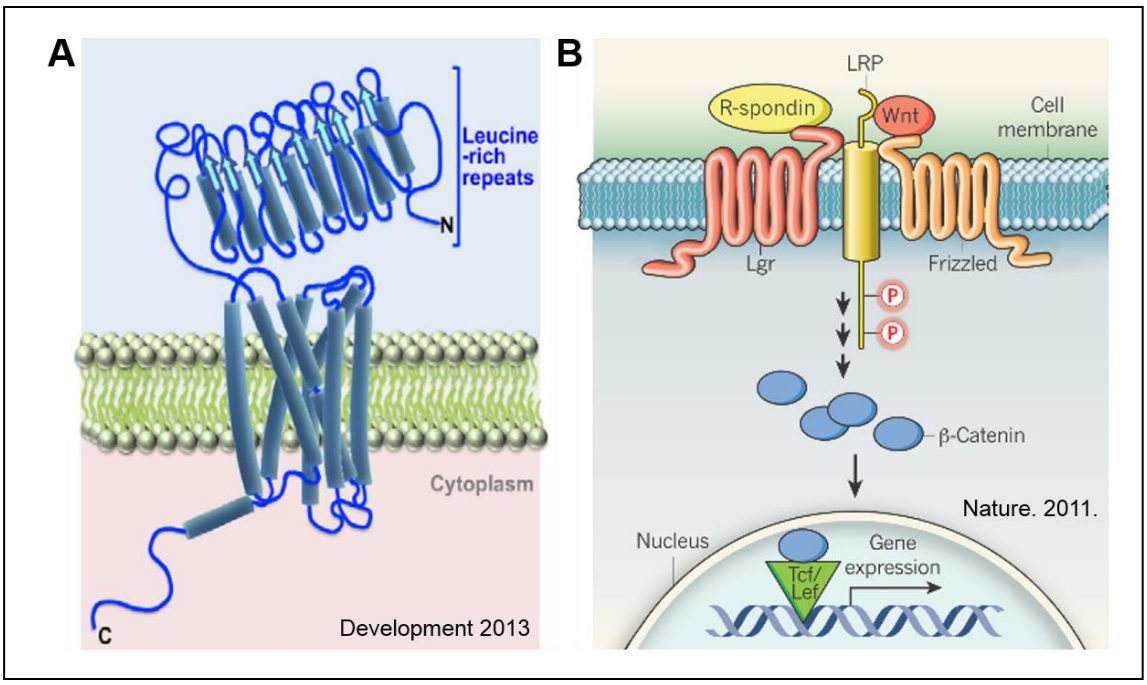

Figure 1.4 LGR5-mediated signaling pathways. A Leucine-rich repeat-containing G-protein coupled receptor (LGR) proteins are a unique class of evolutionarily conserved seven-transmembrane (7TM) receptors characterized by a large extracellular region (ectodomain) that harbors multiple imperfect copies of leucine-rich repeat (LRR) protein interaction domain. **B** R-spondins bind to LGR5 ectodomain at the horseshoe-shaped LRR surface, but not C-terminal cap, leading to the activation of the Wnt/β-catenin signaling pathway. In addition, the extended loop of the C-terminal LRR cap can bind to the antibody and activate LGR5 signaling in a ligand-independent manner[42].

1.4 Tumor microenvironment in the regulation of tumor progression

In epithelial tumor microenvironment, abundant stromal cells, particularly, the cancer associated fibroblasts (CAFs), surround epithelial tumor islands and play an important role in tumorigenesis and progression of various types of malignancies[43]. Recently, our group showed that AM-MSCs are essential for the survival of AM epithelial cells *in vivo* and AM-MSCs derived interleukin (IL)-6 can promote the expression of stem cell- and EMT-related genes in AM epithelial cells[24].

Paracrine secretomes contain a large panel of biological soluble factors. Exosomes, a subtype of extracellular vesicles (EVs) released by all kinds of cells, have a size ranged from 30~200nm and contain a variety of biological components such as proteins, lipids, and nucleic acid that play an important role in intercellular communication[44]. Recently, an increasing body of evidence has revealed the important role of cancer-derived exosomes in tumorigenesis and these circulating exosomes can be employed as biomarkers for early diagnosis and prognosis[45-47]. However, the role of AM-MSCs-derived secretomes in the regulation of $LGR5^+$ EpiSCs in AM is unknown.

1.5 Organoid model in the study of tumor biology

Two-dimensional (2D) monolayer cell culture is a popular and stable method to study tumor cell behavior *in vitro*. However, the 2D culture involves a single type of cells and fails to reflect *in situ* tumor structure and the heterogeneity of its tumor microenvironment[48,49]. To overcome the drawbacks of the conventional 2D

culture, researchers endeavored to develop 3D-spheroid culture, whereby cells in a suspension culture system aggregate into 3D-spheroid structures that can partially mimic certain properties, e.g. hypoxia and cell-cell interactions of *in vivo* tumor microenvironment[50]. In recent years, much progress has been made in the development of 3D-organoid culture, which is based on cell-cell and cell-extracellular matrix (ECM) interactions to generate organ-like structures[49]. The 3D-organoid model can recapitulate the major properties of the target tissues or organs, thus having provided a useful alternative *ex vivo* platform to replace animal models for mechanistic studies in stem cell biology, tissue homeostasis, and disease modeling[48,50]. Even though 3D-organoids have been extensively employed in the study of a variety of malignant tumors, much less is done in the field of benign tumor. Due to the lack of an established animal model for human ameloblastoma, herein, it is crucial to establish an AM-organoid model as an alternative for further mechanistic studies and therapeutic drug screening.

1.6 Hypothesis

LGR5 has been identified as an epithelial stem cell marker in multiple developmental organs and cancer stem cells (CSCs) [25,27-30]. CSCs have been demonstrated to contribute to tumorigenesis, progression, metastasis, therapeutic resistance, and recurrence[19,20]. EMT intermediate cells, or hybrid cells, are endowed with both epithelial and mesenchymal cell features and contribute to CSC capabilities, such as tumor initiation, progression, metastasis, and drug resistance[19-23]. Our group previously showed that AM-MSCs are

essential for the survival of AM epithelial cells *in vivo* and AM-MSCs derived interleukin (IL)-6 can promote the expression of stem cell- and EMT-related genes in AM epithelial cells[24]. Based on these findings, **I hypothesize that LGR5$^+$ AM epithelial cells represent a subpopulation of EMT hybrid cells with unique stem-like cell properties driven by stromal cell-derived secretomes, which contribute to the pathogenesis and recurrence of AM (Figure 1.5).** Studies in this thesis have demonstrated the potential role of LGR5$^+$ intermediate stem-like AM epithelial cells in the pathogenesis and organoid formation in ameloblastoma, and the tumor 3D-organoids formed by LGR5$^+$ AM-EpiSCs provided a novel *ex vivo* platform for further mechanistic studies and screening of targeted therapeutic drugs for the treatment of this benign yet aggressively destructive jaw tumor.

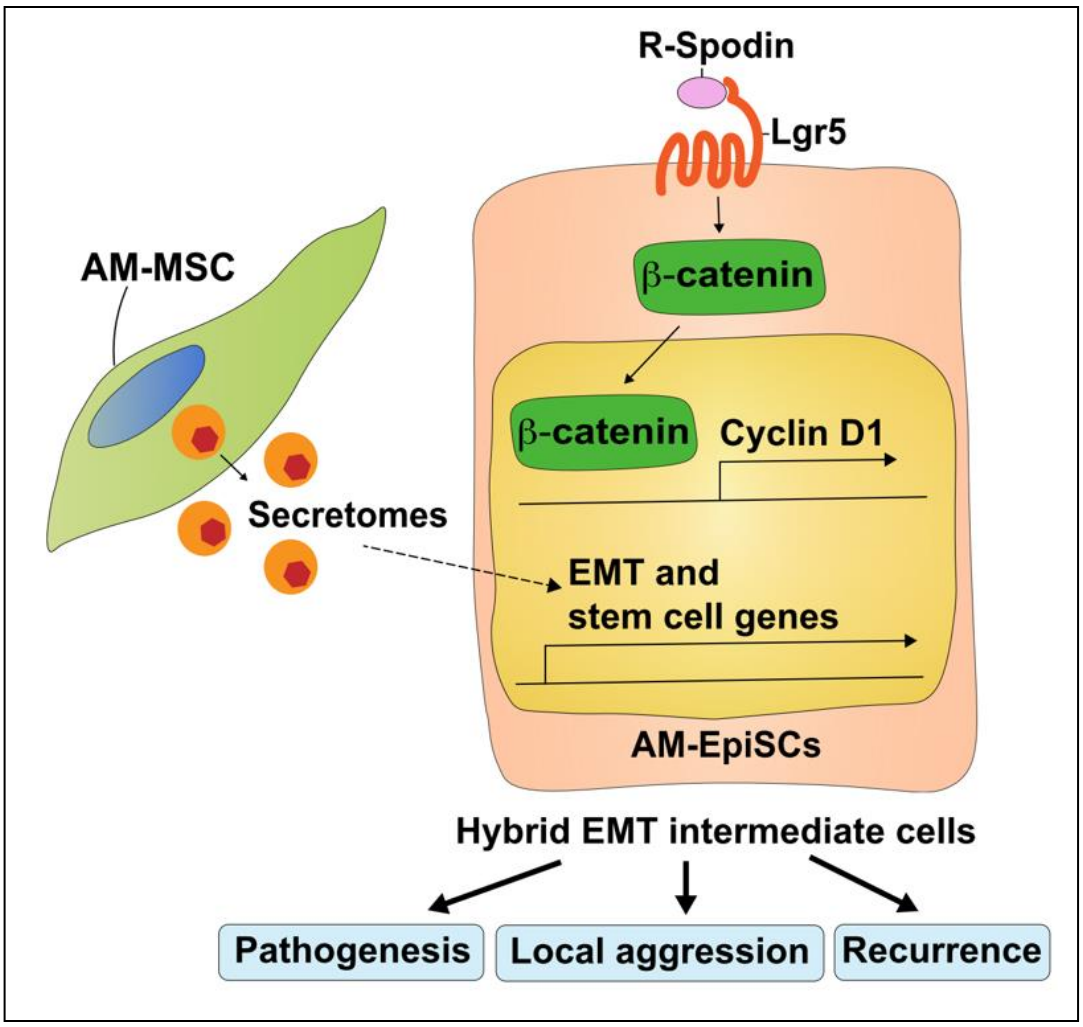

Figure 1.5 Hypothesis and aims. The central hypothesis is that LGR5$^+$ AM epithelial cells represent a subpopulation of tumor stem-like cells and confer EMT phenotypes. To confirm this hypothesis, this study proposed the following three specific aims. **Aim 1**: To explore whether LGR5$^+$ epithelial cells represent a subpopulation of epithelial stem-like cells in AM and their potential roles in the pathogenesis and recurrence of AM. **Aim 2**: To establish 3D organoids by using LGR5$^+$ AM epithelial cells, allowing for further mechanistic and therapeutic intervention studies. **Aim 3**: To uncover the role of AM-MSCs in the regulation of EMT process and stem cell properties in LGR5$^+$ AM epithelial cells.

CHAPTER 2: MATERIALS AND METHODS

2.1 Experimental design

Aim 1: To explore whether LGR5^{+} epithelial cells represent a subpopulation of epithelial stem-like cells in AM and their potential roles in the pathogenesis and recurrence of AM (Figure 2.1). This study collected fifteen human AM samples (three fresh tissues and twelve formalin-fixed paraffin-embedded tissues) to evaluate histological features and culture epithelial cells (AM-EpiCs) and mesenchymal cells (AM-MSCs). To determine the stem cell and EMT properties of LGR5^{+} AM epithelial cells in vitro, Lg5^{+} epithelial cells were sorted out and compared their properties and functions with parental, LGR5^{-} counterparts, including: (i) The expression of stem cell-related genes and EMT TFs; (ii) Self-renewal capability via sphere-forming assay; (iii) Migration capacities. To determine whether LGR5 is a functional marker, the proliferation and stem cell and EMT properties of AM-EpiCs after stimulated with its ligands (R-spondin 1 and 2) were evaluated.

Aim 2: To establish 3D organoids using LGR5^{+} AM epithelial cells (Figure 2.2). This study utilized both primary AM cells (follicular type) and one AM cell line (plexiform type) to create AM-organoids and optimized the culture conditions, e.g. culture media, cell density, and small molecules, for 3D organoid culture with LGR5^{+} AM epithelial cells alone or in combination with AM-MSCs. Then, I subcutaneously transplanted *ex vivo* cultured 3D AM-organoids into nude mice to

evaluate the stem cell properties of LGR5^{+} AM epithelial cells *in vivo* by comparison of the self-renewal, proliferation and propagation capabilities of parental, LGR5^{-}, and LGR5^{+} AM epithelial cells. Finally, this study determined whether a specific BRAF inhibitor can extirpate *ex vivo* organoid formation.

Aim 3: To uncover the role of AM-MSCs in the regulation of EMT process and stem cell properties in LGR5^{+} AM epithelial cells. The stromal effects on EMT and stem cell properties in LGR5^{+} AM epithelial cells were determined. Parental, sorted LGR5^{-}, and LGR5^{+} AM epithelial cells were co-cultured with AM mesenchymal stromal cells (AM-MSCs) or stimulated with AM-MSC derived secretomes, and then the expression of LGR5, EMT TFs, and stem cell-related genes was determined. Finally, the 3D AM-organoids derived from AM-EpiCs and AM-MSCs *ex vivo* (Figure 2.2) were established to create a platform for future mechanistic studies.

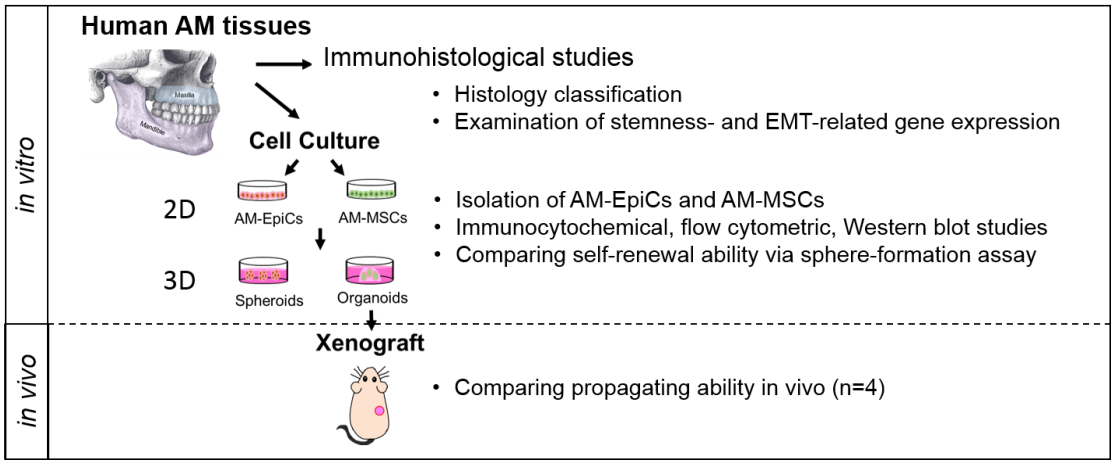

Figure 2.1 To identify whether LGR5^{+} AM epithelial cells represent a subpopulation of stem-like cells in AM. This study collected fifteen human AM tissues and analyzed the expression of LGR5 in both tissue samples and isolated primary epithelial cells form fresh tissues. Then, the stem cell- and EMT-properties in sorted LGR5^{-} and LGR5^{+} AM epithelial cells were compared both *in vitro* and *in vivo*.

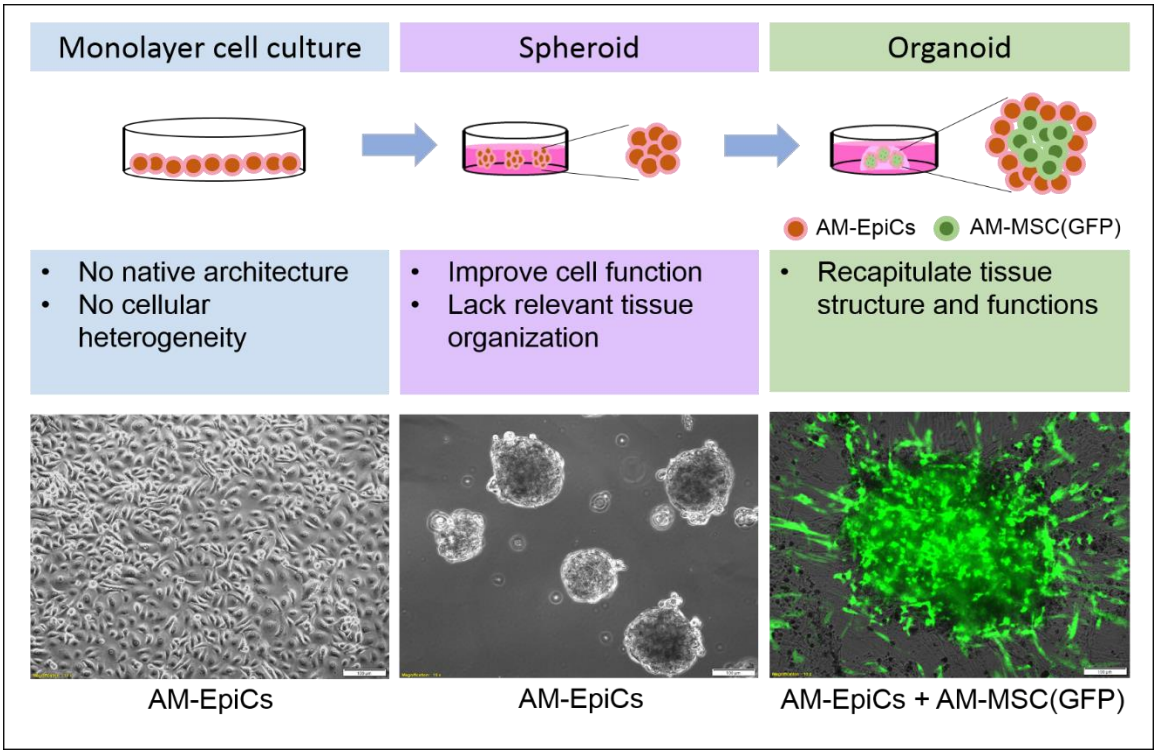

Figure 2.2 To generate AM-organoid models. The AM-organoid models were generated from either AM epithelial cells alone or combined AM epithelial cells and MSCs. Then, the *ex vivo* organoids were utilized to test the therapeutic effect of a specific $BRAF^{V600E}$ inhibitor and to evaluate the potential role of $LGR5^{+}$ AM-EpiSCs in AM pathogenesis following subcutaneous transplantation into nude mice.

2.2 Tissue collection

The study was conducted in accordance with human subject research guidelines and a protocol approved by the institutional review board (IRB) at University of Pennsylvania (UPenn) (IRB#817407) and focused on solid AM, the most common histopathological variant of this benign tumor with a high recurrent rate. Three fresh primary solid AM samples, including one follicular type, one follicular/plexiform mixed type, and one desmoplastic type, were obtained immediately post-surgical procedures from the Department of Oral and Maxillofacial Surgery of Penn Medicine Hospital of UPenn. Meanwhile, six dentigerous cysts were also collected as the control. In addition, a total of 12 formalin-fixed paraffin-embedded blocks of solid AM samples were retrieved from the archives at Departments of Pathology of University of Pennsylvania School of Dental Medicine (IRB#817407), Dongguan Hospital Affiliated to Medical College of Jinan University, and the Fifth People's Hospital of Dongguan, which were also approved by the research and ethical committee of the two hospitals in China (Guangdong, China). Informed consent was obtained from all subjects. Diagnoses were made by two independent pathologists, including a board-certified oral and maxillofacial pathologist, based on the WHO classification (2017) of odontogenic tumors.

2.3 Cell culture

An immortalized AM cell line (AM-1) was generously provided by Dr. Hidemitsu Harada at Iwate Medical University and cultured with defined serum-

free keratinocyte growth medium (KGM-2 BulletKit, Lonza). Primary AM epithelial cells and AM-MSCs were isolated as previously described[24]. Briefly, at least 3-6 mm^3 of fresh human AM tissues were minced into 0.5-1 mm^3 pieces followed by enzymatic digestion with 0.2% collagenase I (Gibco) for 1 hour in a 37°C shaking incubator. For AM epithelial cells, the dissociated cells were seeded in gelatin-coated tissue culture dishes ($2x10^4/cm^3$) in defined KGM-2 culture medium (Lonza) at 37°C in a humidified incubator with 5% CO_2. For AM-MSCs, the dissociated cells were seeded in tissue culture dishes ($2x10^4/cm^3$) in complete α-MEM medium (α-MEM with 10% FBS and 1% penicillin/streptomycin) at 37°C in a humidified incubator with 5% CO_2 After 48 hours, the non-adherent cells were removed, and fresh media were replenished every three days. When cells were at 75%-95% confluence, AM epithelial cells were sub-cultured following cell dissociation with 1× Accutase solution (Sigma) and AM-MSCs were passaged using 0.05% Trypsin-EDTA solution (Fisher Scientific). The *ex vivo* expanded primary epithelial and mesenchymal stromal cells were characterized by immunocytochemical and flow cytometric analyses on the expression of epithelial markers, such as E-cadherin and Pan-cytokeratin and MSC markers, such as CD90 and CD105, respectively. In this study, the AM primary cells following≥ six passages appeared to become differentiated and lost their propagating ability. Primary cells at early passages were cryopreserved, and cells less than six passages were used for further experiments. Previous studies have shown the difference between primary cells and cell lines, and cell lines may undergo

chromosomal rearrangements/duplications or mutations, and epigenetic changes that make cell lines could not recapitulate the primary tumor behaviors[51,52]. Therefore, most experiments were performed by using primary AM cells.

2.4 Immunohistochemical (IHC) and immunofluorescence (IF) studies

The human tumor samples were fixed in 4% paraformaldehyde (Santa Cruz) for overnight at 4°C and embedded in either paraffin or Optimal Cutting Temperature (OCT) Compound. For IHC staining, paraffin-embedded sections were deparaffinized, unmasked with Antigen Unmasking Solution, Citric Acid Based (Vector) for twenty minutes at 95°C and followed by the protocol of avidin-biotin complex (ABC) kit (VECTASTAIN ABC Kit, Vector). Briefly, sections were incubated at 4°C overnight with primary antibodies for human LGR5 (Invitrogen, PA5-35304) or BRAF V600E (Invitrogen, MA5-24661). Next day, VECTASTAIN ABC Kit were applied to the sections, followed by color development using VECTOR NovaRED Peroxidase (HRP) Substrate Kit (Vector) and counterstained with hematoxylin. Isotype-matched control antibodies (BioLegend) were used as negative controls. Images were observed and photographed under a microscope (Olympus, IX73). Immunohistochemistry results were evaluated by a semiquantitative approach, H-score (“histo” score). Traditional H-score is based on the staining intensity (0=negative; 1=weak; 2=moderate; 3=intense) for each cell in a fixed field and calculated by the formula: [1 × (% cells of intensity 1) + 2 × (% cells of intensity 2) + 3 × (% cells of intensity 3)] to get the final score,

ranging from 0 to 300[53]. In this study, a digital quantification of H-Score was analyzed by Color Deconvolution of ImageJ software[54]. Briefly, each staining was observed and captured at least 3 fields by a microscope. Then each image was processed by “color deconvolution” using the “vector HDAB”, where the staining of hematoxylin and diaminobenzidine (DAB) was separated into 3 different panels: hematoxylin, DAB and background. Next, the area of epithelium or stroma in the DAB image was randomly selected, and the selected area were analyzed by “histogram”, which calculated the mean intensity of DAB in area (mm^2), ranging from 0 (black) to 255 (total white). Finally, the H-score was counted by subtracting the mean intensity of DAB from 255.

For dual-color immunofluorescence (IF) study, frozen sections were permeabilized in 0.5% triton X-100 in PBS for 15min and then blocked in 2.5% goat serum in PBS at room temperature for 1h, followed by incubation at 4°C overnight with a primary antibody for LGR5 (ORIGENE, TA503316, mouse IgG; or Invitrogen, PA5-35304, rabbit IgG) in combination with another primary antibody derived from a different host species, including Pan-Cytokeratin (BioLegend, 914204), ALDH1 (BD Biosciences, 611194), OCT4 (Abcam, ab18976), ZEB-1 (Santa Cruz, sc-25388), non-phospho (Active) β-catenin (Cell Signaling, 8814S), fibronectin (Sigma, F3648), human mitochondria (Novus, 113-1) and PCNA (Santa Cruz, sc-7907). Afterwards, the sections were incubated at room temperature for 1 h with appropriate fluorochrome-conjugated secondary antibodies: DyLight™ 488 Donkey anti-rabbit IgG, Alexa Fluor 594 Donkey anti-

rabbit IgG, DyLight™ 488 Goat anti-mouse IgG, and Alexa Fluor 594 Goat anti-mouse IgG (BioLegend). Isotype-matched control antibodies (BioLegend) were used as negative controls. Nuclei were counterstained with 4, 6-diamidino-2-phenylindole (DAPI) Staining Solution (Abcam) and images were captured with Olympus inverted fluorescence microscope (IX73). Correlation coefficient of dual-color IF study was calculated by CellProfiler software (Appendix III)[55]. Briefly, a pixel-based method was used and all pixels in an image were determine between the channels. Then the linear Pearson correlation coefficient between the two channels was computed by the slope a of the line y=ax +b, where y and x are the two channel intensities, indicating the overall relative intensity of the two channels.

2.5 Immunocytochemical studies

Cultured cells in eight-well chamber slides (Millicell EZ SLIDES) were fixed with cold methanol for 15 minutes at -20°C. Then cells were incubated with the following primary antibodies at 4°C overnight: β-catenin (Cell Signaling, 8480S), active β-catenin (Cell Signaling, 8814S), cyclin A (Sigma, C4710), cyclin B (Sigma, C8831), cyclin D1 (Cell Signaling, 2926), and cyclin E (Cell Signaling, 4129). The cells were then incubated with appropriate fluorochrome-conjugated secondary antibodies as described above. Isotype-matched control antibodies were used as negative controls. Nuclei were counterstained with DAPI Staining Solution and then images were captured using Olympus inverted fluorescence microscope (IX73). For quantitative analysis of mean fluorescence intensity (MFI),

cells with positive signals in at least six random fields were measured by Olympus cellSens software.

2.6 Flow cytometry

AM epithelial cells were harvested and suspended in cell staining buffer (0.5% BSA in PBS with 2mM EDTA) followed by incubation with primary antibody for LGR5 at 4°C for 30 min. After washing with PBS, the cells were incubated with appropriate fluorochrome-conjugated secondary antibody in the dark at 4°C for 30 min. Following immunostaining of the cell surface LGR5, the cells were fixed and permeabilized using True-Nuclear™ Transcription Factor Buffer Set (BioLegend) and then immunostained with a specific antibody for OCT4 (Abcam, ab18976), followed by staining with a fluorescein-conjugated secondary antibody. Isotype-matched IgG control antibodies were used as negative controls. ALDH activity was identified by a non-immunological method (ALDEFLUOR Kit, STEMCELL) and the inhibitor of ALDH enzyme (ALDEFLUOR DEAB Reagent, STEMCELL) was used as negative controls. Samples were analyzed by BD LSRII flow cytometer. Data were processed and analyzed by FlowJo software.

2.7 Cell proliferation assay

AM epithelial cells were seeded into 96-well culture plates in a density of $1x10^4$ cells/well in 100 µl of defined KGM-2 medium with five independent replicates per treatment condition. 24 h later, the cells were washed once with PBS and starved in Keratinocyte basal Medium 2 (KBM2, Lonza) overnight. Then R-spondin 1 (Rspo1, PeproTech) and Rspo2 (PeproTech) were administrated to

the starved AM epithelial cells at concentrations of 0, 5, 10, and 20 ng/ml, respectively. After 72 h, 10 µl of CCK-8 reagent (Cell Counting Kit-8 assay, BioLegend) was added into each well and incubated at 37 °C for 2 h. The absorbance at 450 nm wavelength was detected using an OPSYS Mr microplate reader (Thermo Fisher).

2.8 Cell cycle analysis

AM epithelial cells were seeded into 35-mm culture dishes at a density of $3x10^5$ cells per dish containing 2ml of defined KGM-2 medium. 24h later, the cells were washed once with PBS and starved in basal KBM2 medium overnight. Then 20 ng/ml Rspo2 were administrated to the starved AM epithelial cells while nontreated cells were used as the control. Both control and Rspo2-stimulated cells were labelled with Bromodeoxyuridine (BrdU) Labeling Reagent (Invitrogen) overnight and then harvested after stimulation with Rspo2 for 48h. Cells were then fixed with 70% cold ethanol for 2h and permeabilized in 2 N HCl/0.5% Triton X-100 at room temperature for 30min. Then, the cell pallet was treated with 0.1 M sodium tetraborate (pH8.5) for 2 min followed by washing twice with PBS. Afterwards, cells were incubated with a specific mouse monoclonal IgG for BrdU (Sigma, B8434) at room temperature for 1h followed by incubation with DyLight™ 488 Goat anti-mouse IgG at room temperature for 30 min. After washed cells with PBS, the pellet was resuspended in 0.5 ml PBS containing 10 µg/ml RNase A and 20 µg/ml propidium iodide (PI) solution and incubated at room temperature for 30 min in the dark. The samples were analyzed by BD LSRII flow cytometer

immediately. Data were processed and analyzed by FlowJo software.

2.9 Western blot

Cell lysates were prepared by incubation with radioimmunoprecipitation (RIPA) assay buffer (Santa Cruz) supplemented with a cocktail of protease inhibitors (Santa Cruz) and the total protein concentrations were determined using bicinchoninic acid (BCA) method (BioVision). Then 30μg of total proteins were subjected to SDS-polyacrylamide gel electrophoresis before being electroblotted onto a 0.2 μm nitrocellulose membrane (GE Healthcare). After blocking with 5% nonfat dry milk in TBST [25 mmol/L Tris (pH, 7.4), 137 mmol/L NaCl, 0.5% Tween20], membranes were incubated at 4°C overnight with following primary antibodies: LGR5 (Invitrogen, PA5-35304), ALDH1 (BD Biosciences, 611194), OCT4 (Abcam, ab18976), β-catenin (Cell Signaling, 8480S), Active β-catenin (Cell Signaling, 8814S), cyclin A (Sigma, C4710), cyclin B (Sigma, C8831), cyclin D1 (Cell Signaling, 2926) and cyclin E (Cell Signaling, 4129), ZEB-1 (Santa Cruz, sc-25388), fibronectin (Sigma, F3648) and E-Cadherin (BD Biosciences, 562869). β-actin (Santa Cruz, sc-47778) was used as loading control. After extensively washing, membranes were incubated with horseradish peroxidase (HRP)–conjugated secondary antibodies (Santa Cruz) and blot signals were developed with ECL^{TM} Western Blotting Detect Reagents (GE Health Care).

2.10 Cell sorting

LGR5^{+} AM epithelial cells were sorted by using magnetic Anti-LGR5

MicroBeads (Miltenyi Biotec) according to the manufacturer's protocol. Briefly, cultured AM epithelial cells were labeled with Anti-LGR5 MicroBeads at 4°C for 15 min. After washing, the cell suspension was applied to a LS Colum and separated with a magnetic MACS Manual Separator (Miltenyi Biotec). The purity of sorted $LGR5^-$ and $LGR5^+$ AM epithelial cells was examined by flow cytometry and confirmed by Western blot with a LGR5 antibody (Invitrogen, PA5-35304).

2.11 Spheroid formation assay

3D-spheroid formation assay was performed as described previously[56-58]. Briefly, unsorted (parental), sorted $LGR5^-$ and $LGR5^+$ AM epithelial cells were seeded at a density of 5×10^4 cells/well into Ultralow attached 6-well plates (Corning) with defined serum-free KGM-2 medium (n=3). For 3D-spheroid culture in Matrigel, parental, 5×10^5 of sorted $LGR5^-$ and $LGR5^+$ AM epithelial cells were suspended in 10μl KGM-2 medium, mixed with 40μl Matrigel (Corning), and seeded in 24-well plates with defined serum-free KGM-2 medium (n=3). After culturing for 2 weeks, each sample was observed and captured randomly (n=8) by Olympus microscope (IX73). Then spheroids with a size larger than 20μm were counted, and the size and number of spheroids were measured with Olympus cellSens software. To prepare the spheroids in Matrigel for IF study, the whole Matrigel containing spheroids was fixed in 4% PFA for 15 min followed by washing twice with PBS for 15 min each time. The spheroids with Matrigel were detached from the dish by a fine flat spatula and transferred to the mold. The whole Matrigel contained spheroids were embedded in OCT and frozen sections

at 10μm were cut for IF study.

2.12 Cell migration assay

Migration assay was performed by using 8μm permeable cell culture inserts in 24-well plate (CELLTREAT 230633) according to the manufacturer's protocol. The parental AM-1 cells were starved in KBM2 overnight and then sorted by magnetic Anti-LGR5 MicroBeads. The sorted LGR5 negative and positive AM-1 cells were seeded into the upper chambers of trans-wells ($7x10^4$ cells/well) with 200μl basal KBM2 medium and the lower chambers were filled with 600μl defined KGM-2 culture medium (n=3 for each group). After 16 hours, the trans-wells were gently washed with PBS twice and non-migrated cells were removed with cotton rods. Then the migrated cells on trans-wells were fixed with 70% ethanol for 10 min and dried for 10-15 min. The migrated cells were stained by 0.5% crystal violet in room temperature for 10 min and then gently washed with PBS. After air dry overnight, the migrated cells were photographed and counted under the microscope.

2.13 Preparation of AM-MSC derived conditioned medium/ secretomes

The AM-MSCs were culture in complete α-MEM. When cells reached 80% confluence, the cells were washed with PBS twice and then cultured in serum free α-MEM for 48 hours. After 48 hours, the culture medium of AM-MSC were collected and centrifuged at 4,400 rpm for 20 min to remove the cell debris. Then the supernatant was collected and concentrated by 30 kDa ultra centrifugal filter

unit (Millipore) at 4,400 rpm about 30 min twice with one wash with PBS between the two centrifuges to 100X concentrated medium. Then the protein concentration of AM-MSC derived conditioned medium was determined by bicinchoninic acid (BCA) assay (BioVision).

2.14 3D-organoids derived from AM epithelial cells

Single-cell suspensions of AM epithelial cells were directly dispersed into Growth Factor Reduced (GFR) Matrigel (Corning Life Sciences) at a density of 2×10^4 cells/μl (~$1x10^6$ each group) and seeded in a drop shape. The dish was inverted during solidification of Matrigel to prevent the cells attaching to the culture dish. After solidified for 20 minutes, the mixture of the cells and Matrigel were cultured in AM-organoid culture medium: 50% KGM2 and 50% Dulbecco's Modified Eagle Medium/Nutrient Mixture F-12 (DMEM/F12, Thermo Fisher). The organoid formation was observed under a microscope every 2-3 days and the whole Matrigel containing organoids was harvested on day 10. To prepare the Matrigel for frozen section, the gel was washed with PBS twice, and the whole Matrigel including organoids was fixed in 4% PFA for 15 minutes following by washing with PBS twice for 15 minutes each time. The organoids with Matrigel were detached from the dish by fine flat spatula and transferred to the mold. The whole Matrigel contained organoids was embedded in OCT for frozen section. Both H & E staining and immunofluorescence studies on the expression of Pan-Cytokeratin, LGR5 and active β-catenin were performed.

2.15 3D-organoids derived from AM epithelial cells and AM-MSCs

Single-cell suspensions of AM epithelial cells and AM-MSCs (with or without green fluorescent protein, GFP, lentivirus transduction) (cell ratio: 2:1) were directly dispersed into Matrigel at a density of 4×10^4 cells/μl (~1.5 x 10^6 each group) and seeded in a drop shape. The dish was inverted during solidification of Matrigel to prevent the cells attaching to the culture dish. After solidified for 20 minutes, the mixture of the cells and Matrigel were cultured in AM-organoid culture medium 2: 50% KGM2 and 50% Dulbecco's Modified Eagle Medium/Nutrient Mixture F-12 (DMEM/F12, Thermo Fisher), and supplemented with 10 ng/ml EGF, 20 ng/ml FGF and 0.5X Insulin-Transferrin-Selenium (Thermo Fisher). The organoid formation was observed under a microscope every day and the whole Matrigel containing organoids was passaged or cryopreserved on day 4. Briefly, after washing with PBS twice, the whole Matrigel containing organoids was broken down by 1000ul pipet tip and collected with 500ml iced 1% BSA in PBS to a 1.5 ml centrifuge tube. Then, spin down at 1,500 rpm for 5 min and carefully remove the supernatant. The pellet was dissociated with 400ml 1× Accutase solution in 37°C for 20-30 min, and washed with 1% BSA twice. The dissociated cells were directly dispersed into Matrigel at a density of 4×10^4 cells/μl or into the cryopreservation media followed by the normal cryopreservative procedure. The frozen organoid cells were thawed, washed and directly dispersed into Matrigel followed the same culture procedure. The preparation of the organoids in Matrigel for frozen section is same as AM-

organoids derived from AM epithelial cells. Both H & E staining and immunofluorescence studies on the expression of E-cadherin (24E10, Cell Signaling Technology), CD90 (5E10, BioLegend), vimentin (sc-32322, Santa Cruz Biotechnology) and LGR5 (ORIGENE, TA503316, mouse IgG; or Invitrogen, PA5-35304, rabbit IgG) were performed.

2.16 Subcutaneous transplantation of AM 3D-Organoids into nude mice

Eight-week-old female and male athymic NU/J mice were purchased from Charles River Laboratory. All animal procedures were handled according to the guidelines of the Institutional Animal Care and Use Committee of (IACUC) at University of Pennsylvania. Mice were group-housed in polycarbonate cages (five animals per cage) in the animal facility with controlled temperature, 40%-65% of humidity and a 12-hour light/dark cycle. Mice were acclimatized for at least 1 week before the study, fed with a standard laboratory diet and allowed ad libitum access to drinking water. For subcutaneous transplantation, nude mice were randomly assigned into six groups transplanted with 8×10^5 AM-EpiCs (parental, sorted $LGR5^-$ and $LGR5^+$) and 8×10^5 AM-EpiCs + AM-MSCs with 1:1 cell ratio (parental + MSCs, sorted $LGR5^-$ + MSCs and $LGR5^+$ +MSCs), respectively. Cells were pre-cultured in Matrigel for three weeks and then subcutaneously implanted into the dorsal skin of nude mice (n=3-4 in each group). Two to four weeks after transplantation, xenografted tumors were harvested for histologic analysis and IF studies on the expression of LGR5,

human mitochondria, PCNA, EMT- and stem cell-related genes. No blinding was carried out for animal experiments.

For cell-dilution assay, we sorted LGR5^{+} cells from parental primary AM epithelial cells and AM-1 cells and then cultured in Matrigel (50μl) for two weeks with different cell numbers: 10^3, 10^4, 10^5 and 10^6 (n=2 in each group). After two weeks, the organoids in Matrigel were transplanted subcutaneously into the dorsal skin of nude mice. 4-weeks post-transplantation, the volume of transplanted organoid xenografts was calculated; the histology was examined by H & E staining, and the expression of human LGR5 and PCNA was determined by IF studies.

2.17 Statistical analysis

All data are presented as mean ± SD and analyzed using unpaired Student's *t*-test for comparing two groups when appropriate. In cases of multiple groups, statistical analysis was performed through one-way ANOVA analysis with Tukey post-test. Fisher's exact test and Chi-square teat were used to compare proportions in one or more categories. All analyses were done using GraphPad Prism. A value of $P<0.05$ was considered to be statistically significant.

CHAPTER 3: RESULTS

3.1 LGR5 is highly expressed in epithelial cells in AM tissues

LGR5 has been reported as a stem cell marker in multiple normal and malignant tissues and recent studies revealed that LGR5^{+} CSCs promote EMT process and are essential for tumor metastasis[34,35]. Our recent studies have identified a subpopulation of AM epithelial cells with increased expression of both stemness- and EMT-related markers upon co-culture with AM-MSCs[24]. Herein, I further explored whether LGR5 represented a putative marker for epithelial stem-like cells in AM. To this purpose, the expression of LGR5 in a total of fifteen human AM tissues (ten follicular type; two plexiform type; three desmoplastic type) versus corresponding normal adjacent tissues (NATs), and six benign odontogenic cysts (OC) was initially evaluated. The results from IHC studies showed that LGR5 expression was consistently higher in different histological variants of solid AM (follicular, plexiform, and desmoplastic AM), as compared to OCs, and the corresponding NATs (Figure 3.1 A-C). Of note, the overall H-score of LGR5 expression in AM tumor tissues was much higher, 4-fold, than that in normal control and OCs (Figure 3.1 C). The immunoreactive signals of LGR5 expression are mainly localized in the AM epithelial islands, with an average 70.45% of LGR5+ cells in epithelial islands versus an average 18.62% of LGR5^{+} cells in stroma of the total fifteen AM tissues (Figure 3.1 D and E). The expression of LGR5 in AM epithelial islands was slightly higher in the plexiform (85.98%) than that in the follicular type (66.50%) ($p < 0.05$).

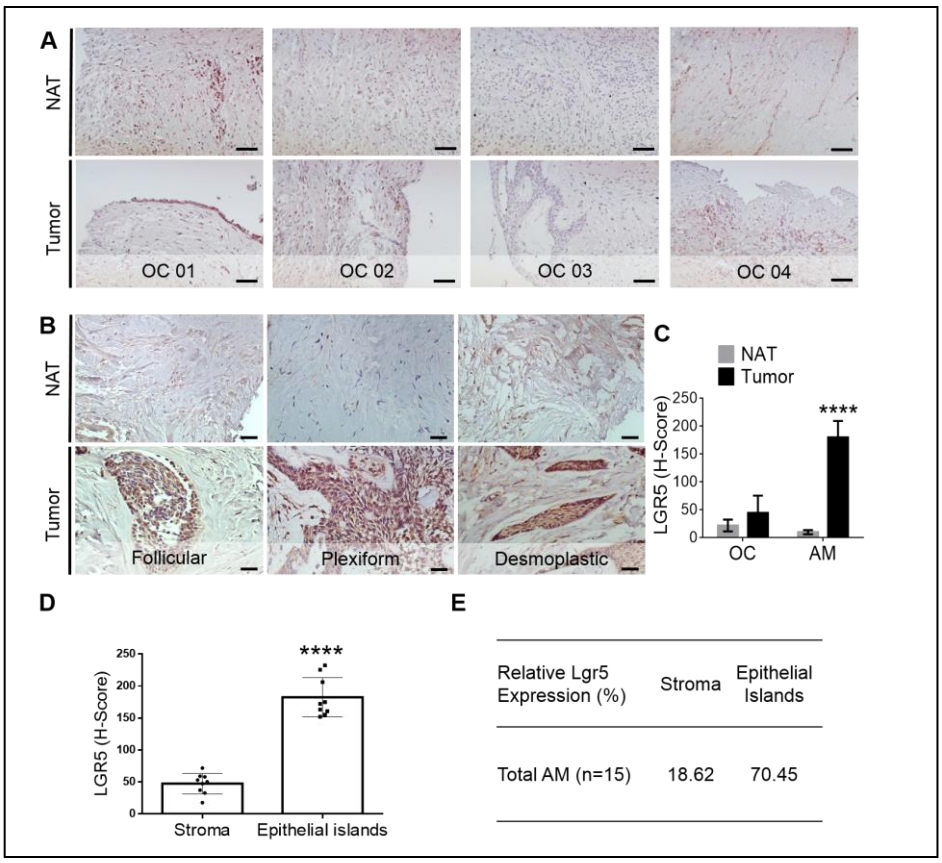

Figure 3.1 LGR5 is highly expressed in epithelial cells in AM tissues. A The paraffin-embedded sections of odontogenic cyst (OC) were processed for IHC staining with a specific antibody for human LGR5 (n=6). Scale bars, 50μm. NAT: normal adjacent tissue (same patient). **B** Expression of LGR5 in different histopathological types of AM (n=15). Scale bars, 20μm. NAT: normal adjacent tissue (same patient). **C** The quantification of H-score of LGR5 expression in AM (n=15) and odontogenic cyst (OC) (n=6). H-Score of each sample was analyzed at least 9 different areas by Color Deconvolution of ImageJ software and data are mean ± SD. Two-tailed unpaired Student's t-test. ****p<0.0001. **D** The quantification of H-score of LGR5 expression in stroma and epithelial islands of AM, respectively. Data are mean ± SD. Two-tailed paired Student's *t*-test. ****p<0.0001. **E** Relative percentage was converted from the H-Score values in (**D**). The immunoreactive signals of LGR5 expression are mainly localized in the AM epithelial islands, with an average 70.45% of $LGR5^+$ cells in epithelial islands versus an average 18.62% of $LGR5^+$ cells in stroma of the total fifteen AM tissues. H-Score of each sample was analyzed at least 5 different areas by Color Deconvolution of ImageJ software and data are mean ± SD.

3.2 Characterization of a subpopulation of LGR5$^+$ stem-like epithelial cells in AM

This study then determined whether LGR5 expression was associated with other stem cell-related genes in solid type of AM tissues. Dual-color immunofluorescence study showed that about 66.3% of LGR5 signal was co-localized with the pan-cytokeratin (Pan-CK) in AM tissues, indicating that LGR5 was mainly expressed by epithelial cells in AM (Figure 3.2). Since the solid type of AM accounts for about 80% of all AM cases and has a high recurrence rate[1,59], this study focused on this major type of AM. Dual-color immunofluorescence studies showed that within the epithelial islands of all three subtypes of solid type of AMs, LGR5 was simultaneously expressed with aldehyde dehydrogenase 1 (ALDH1) and octamer-binding transcription factor 4 (OCT4) (Figure 3.2 A, C and D), two well-recognized stem cell-regulatory genes identified in CSCs of multiple cancers[60-63]. Further analysis indicated that about 68.6% of LGR5$^+$ epithelial cells simultaneously expressed ALDH1 and 74.1% LGR5$^+$ epithelial cells simultaneously expressed OCT4 (Figure 3.2 B). These results suggest that solid type of AM tissues harbor a subpopulation of LGR5$^+$ epithelial cells expressing stem cell-related genes.

To characterize the stem cell properties of the subpopulation of LGR5$^+$ epithelial cells in AM, primary epithelial cells derived from solid follicular AM tissues (AM epithelial cells), as previously described[24] (Figure 3.3 A), were cultured under 3D-spheroid forming condition, an approach utilized for self-renewal and enrichment of stem cells[64-67]. The results showed that expression of

LGR5, ALDH1, and OCT4 was significantly increased in AM epithelial cells after 5 days in 3D-spheroid culture, as compared to those under 2D culture condition (Figure 3.3 B and C). Flow cytometric analysis showed that $LGR5^{+}$ cells grown in 3D-spheroid condition were consistently enriched by three-fold (from 9.95 ± 3.43 % to 27.1 ± 6.52 %) as compared to 2D culture (Figure 3.4 A). Meanwhile, $LGR5^{+}OCT4^{Low}$, $LGR5^{+}OCT4^{High}$, and total $OCT4^{High}$ cells in AM epithelial cells were further analyzed. The results showed that under 3D-culture *versus* 2D-culture, both $LGR5^{+}OCT4^{Low}$ and $LGR5^{+}OCT4^{High}$ cells were significantly enriched, from 3.98% to 21.8% and 2.09% to 14.7%, respectively; and total $OCT4^{High}$ cells were increased from 10.11% to 23.64% (Figure 3.4 B). In addition, ALDH1 activity increased about three-fold in AM epithelial cells in 3D-spheroid versus 2D cultures by evaluating ALDH activity using ALDEFLUOR assay (Figure 3.4 C). Similarly, $LGR5^{+}$ and $LGR5^{+}OCT4^{High}$ cells were enriched while ALDH1 activity increased in immortalized AM-1 cells when cultured under 3D-spheroid culture condition (Figure 3.5). Collectively, these results suggest that $LGR5^{+}ALDH1^{+}OCT4^{High}$ AM epithelial cells may have self-renewal capability and represent a subpopulation of tumor epithelial stem-like cells in solid AM (AM-EpiSCs).

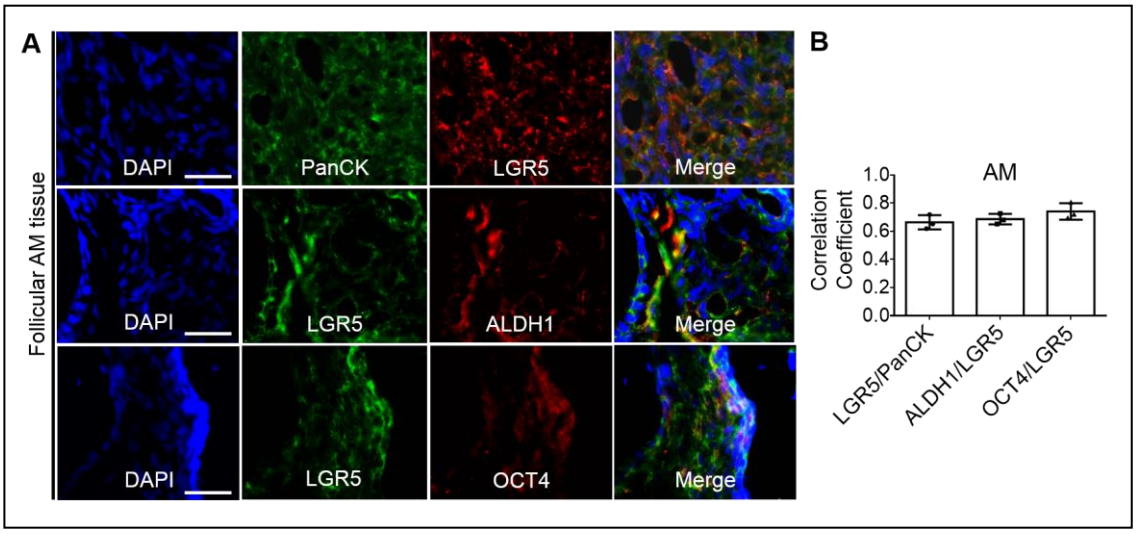

Figure 3.2 Simultaneous expression of LGR5 and certain stem cell-related markers in AM tissues. A Left: dual-color immunofluorescence study showed that simultaneous expression of LGR5 and Pan cytokeratin (PanCK), ALDH1 and OCT4 in the follicular tissue, respectively. Scale bars, 20μm. **B** The quantification of correlation coefficient of LGR5 and epithelial biomarker (PanCK) and stem cell-related markers (ALDH1 and OCT4) in the solid AMs (n=3). The results showed that about 66.3% of LGR5 signal was simultaneously expressed with the expression of PanCK in the solid AM tissues. About 68.6% and 74.1% of $LGR5^{+}$ cells simultaneously expressed ALDH1 and OCT4, respectively. Each group was calculated at least three different areas by CellProfiler software and data are mean ± SD.

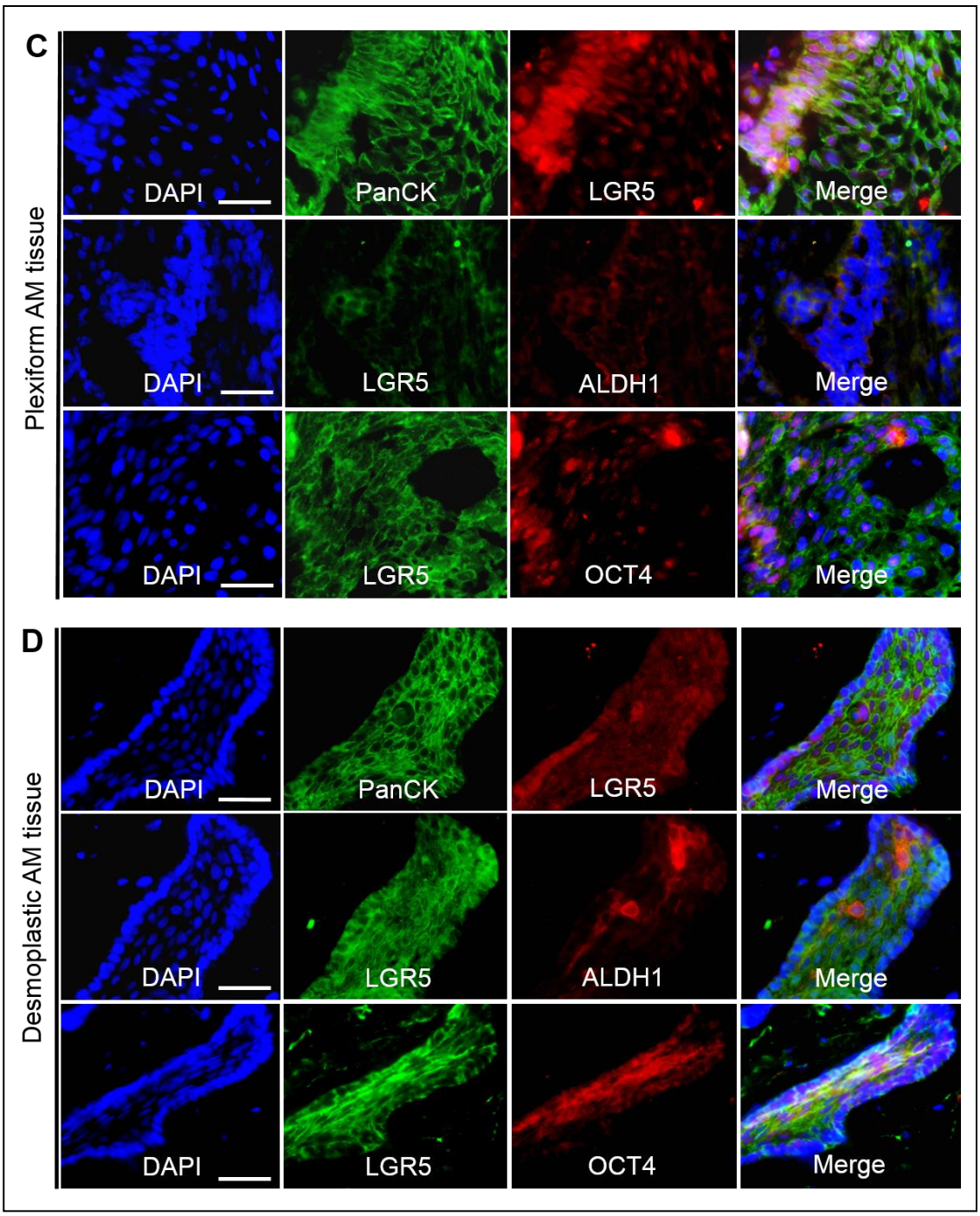

Figure 3.2 Cont'd. C Dual-color immunofluorescence study showed that simultaneous expression of LGR5 and PanCK, ALDH1 and OCT4 in the plexiform tissue, respectively. Scale bars, 20μm. **D** Dual-color immunofluorescence study showed that simultaneous expression of LGR5 and PanCK, ALDH1 and OCT4 in the desmoplastic tissue, respectively. Scale bars, 20μm.

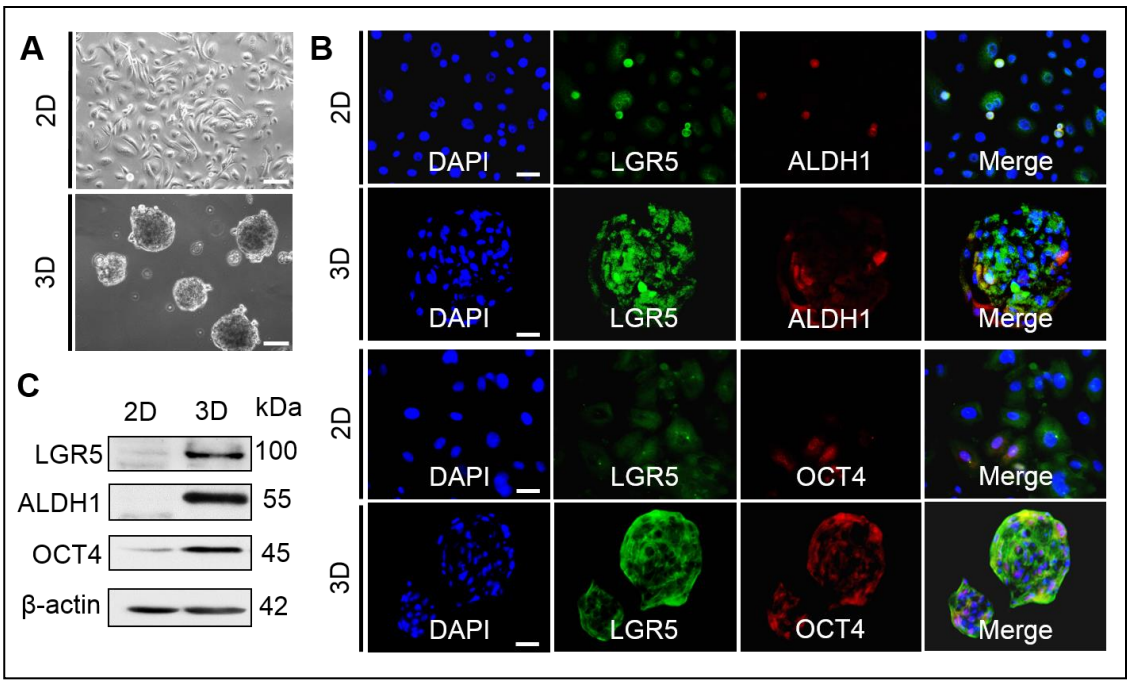

Figure 3.3 LGR5^{+}ALDH1^{+}OCT4^{High} AM epithelial cells are enriched in 3D-spheroid culture. A Morphology of AM epithelial cells derived from primary human AM tissues and cultured under 2D-monolayer or 3D spheroid-forming conditions. Scale bars, 100μm. **B** AM epithelial cells were cultured under 2D-monolayer or 3D-spheroid culture conditions for 5 days. The simultaneous expression of LGR5, ALDH1, and OCT4 was observed by immunofluorescence studies. Scale bars, 20μm. **C** Augmented expression of LGR5, ALDH1, and OCT4 in AM epithelial cells under 3D-spheroid culture versus 2D-monolayer culture as determined by Western blot analysis. All results are representative of at least three independent experiments.

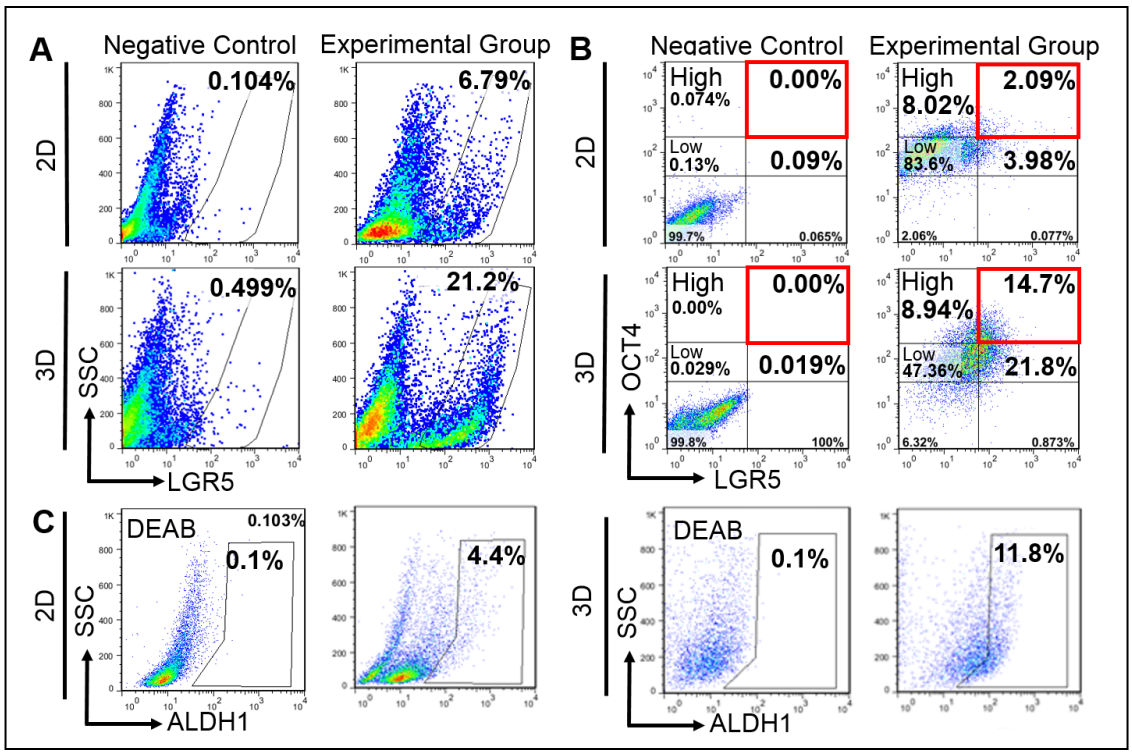

Figure 3.4 LGR5^{+}ALDH1^{+}OCT4^{High} AM epithelial cells are enriched in 3D-spheroid culture. A About three-fold enrichment of LGR5^{+} AM epithelial cells (from 6.79% to 21.2%) under 3D-spheroid culture versus 2D-monolayer culture as determined by flow cytometric analysis. **B** The proportion of LGR5^{+}OCT4^{Low}, LGR5^{+}OCT4^{High}, and total OCT4^{High} cells in AM epithelial cells cultured under 2D-monolayer culture and 3D-spheroid conditions was determined by flow cytometry. **C** The activity of ALDH1 was increased by about three-fold (4.4% to 11.8%) in AM epithelial cells under 3D-spheroid culture versus 2D-monolayer culture as determined by flow cytometric analysis. All results are representative of at least three independent experiments.

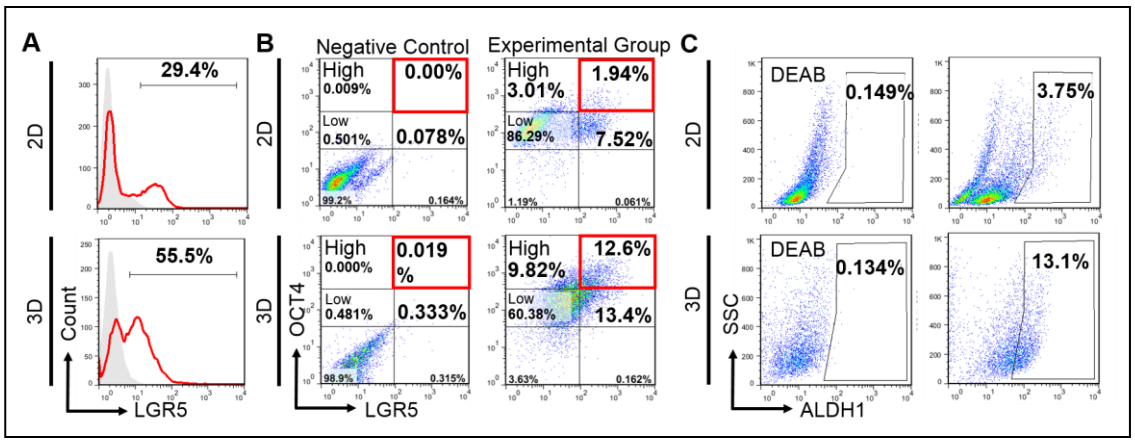

Figure 3.5 LGR5^{+}ALDH1^{+}OCT4^{High} are enriched in AM-1 cells under 3D spheroid-forming culture conditions. A Flow cytometric analysis showed that LGR5^{+} cells were enriched by about two-fold (from 29.4% to 55.5%) in AM-1 cells under 3D-spheroid culture for 5 days. Red: LGR5. Gray: negative control. **B** The proportion of LGR5^{+}OCT4^{Low}, LGR5^{+}OCT4^{High}, and total OCT4^{High} cells in AM-1 cells cultured under 2D-monolayer culture and 3D-spheroid conditions was determined by flow cytometry. **C** The ALDH1 activity was increased by about three-fold (3.75% to 13.1%) in AM-1 cells under 3D-spheroid culture for 5 days. All results are representative of at least three independent experiments.

3.3 LGR5^{+} AM epithelial cells are endowed with intermediate EMT phenotype and stem cell properties *in vitro*

The stem cell properties of LGR5^{+} AM epithelial cells were then further characterized. To this end, LGR5^{+} AM epithelial cells were sorted from parental primary AM epithelial cells using LGR5 antibody-conjugated with magnetic beads and confirmed by flow cytometry (Figure 3.8 A). 3D-spheroid forming assay under suspension culture conditions showed that LGR5^{+} AM epithelial cells formed more abundant and larger spheroids than LGR5^{-} counterparts (Figure 3.6 A and B). Meanwhile, sorted LGR5^{+} AM epithelial cells when cultured in 3D extracellular matrix (ECM) Matrigel for two weeks also readily formed larger 3D-spheroids as compared to LGR5^{-} counterparts (Figure 3.6 C and D). Similarly, LGR5^{+} cells sorted from AM-1 cells also exhibited increased 3D-spheroid forming capability as compared to the LGR5^{-} counterparts (Figure 3.8 B and C). These results suggest that LGR5^{+} AM epithelial cells are more capable of self-renewal than their LGR5^{-} counterparts.

Since EMT contributes to cell plasticity and cancer stem cell (CSC) formation[22], the expression profiles of stem cell-related and EMT-regulatory transcriptional factors (TFs) in sorted LGR5^{+} and LGR5^{-} AM epithelial cells were then compared. Western blot analysis demonstrated an increase in the expression of stem cell-related markers, ALDH1 and OCT4, as well as EMT-related markers, ZEB1, active β-catenin (ABC) and fibronectin, in LGR5^{+} cells sorted from both primary AM epithelial cells and AM-1 cell lines in comparison with their LGR5^{-} counterparts, respectively (Figure 3.6 E and Figure 3.8 D).

Additionally, the simultaneous expression of LGR5 and ZEB1, ABC, and fibronectin was further confirmed in different subtypes of solid AM tissues as determined by immunofluorescence studies (Figure 3.6 F and Figure 3.7). Functionally, $LGR5^+$ AM epithelial cells exhibited significantly increased migration ability as compared to their $LGR5^-$ counterparts ($p<0.001$) was found (Figure 3.8 E and F). Taken together, these findings suggest that $LGR5^+$ epithelial cells also possess features characteristic of an intermediate EMT phenotype.

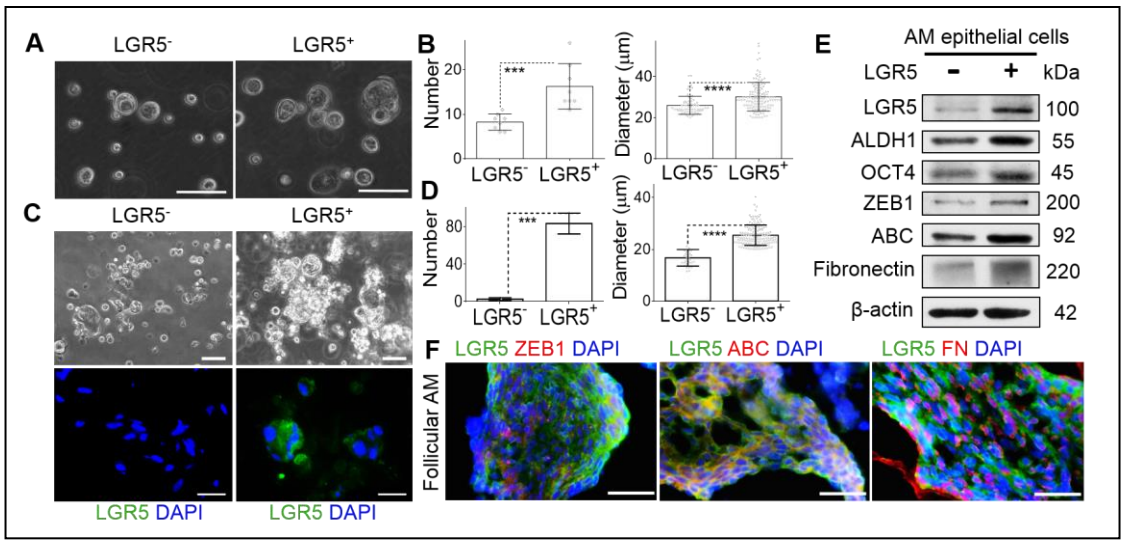

Figure 3.6 LGR5⁺ AM epithelial cells exhibit self-renewal ability and EMT phenotypes. A and **B** LGR5⁺ AM epithelial cells were sorted out from parental primary AM epithelial cells using LGR5 antibody-conjugated magnetic beads, which showed increased 3D spheroid-forming ability than their LGR5⁻ counterparts (n=3). Scale bars, 50μm. Data are Mean ± SD (each group was measured 8 different random areas under the microscope), two-tailed unpaired Student's *t*-test. *** $p<0.001$, **** $p<0.0001$. **C** Sorted LGR5⁺ AM epithelial cells formed more and larger 3D-spheroids as compared with LGR5⁻ counterparts after culturing in 3D extracellular matrix (ECM) Matrigel for two weeks (n=3). Scale bars, 20μm. **D** The quantification of spheroid formation as shown in (**C**). Data are Mean ± SD (each group was measured 3 different random areas under the microscope), two-tailed unpaired Student's *t*-test. *** $p<0.001$, **** $p<0.0001$. **E** Increased expression of stem cell-related markers, ALDH1 and OCT4, and EMT related markers, ZEB1, active β-catenin (ABC) and fibronectin (FN), in sorted LGR5⁺ AM epithelial cells as compared to that in LGR5⁻ counterparts. **F** Simultaneous expression of LGR5 and specific EMT related markers, ZEB1, ABC and FN in the follicular AM tissue. Scale bars, 20μm. All results are representative of three independent experiments.

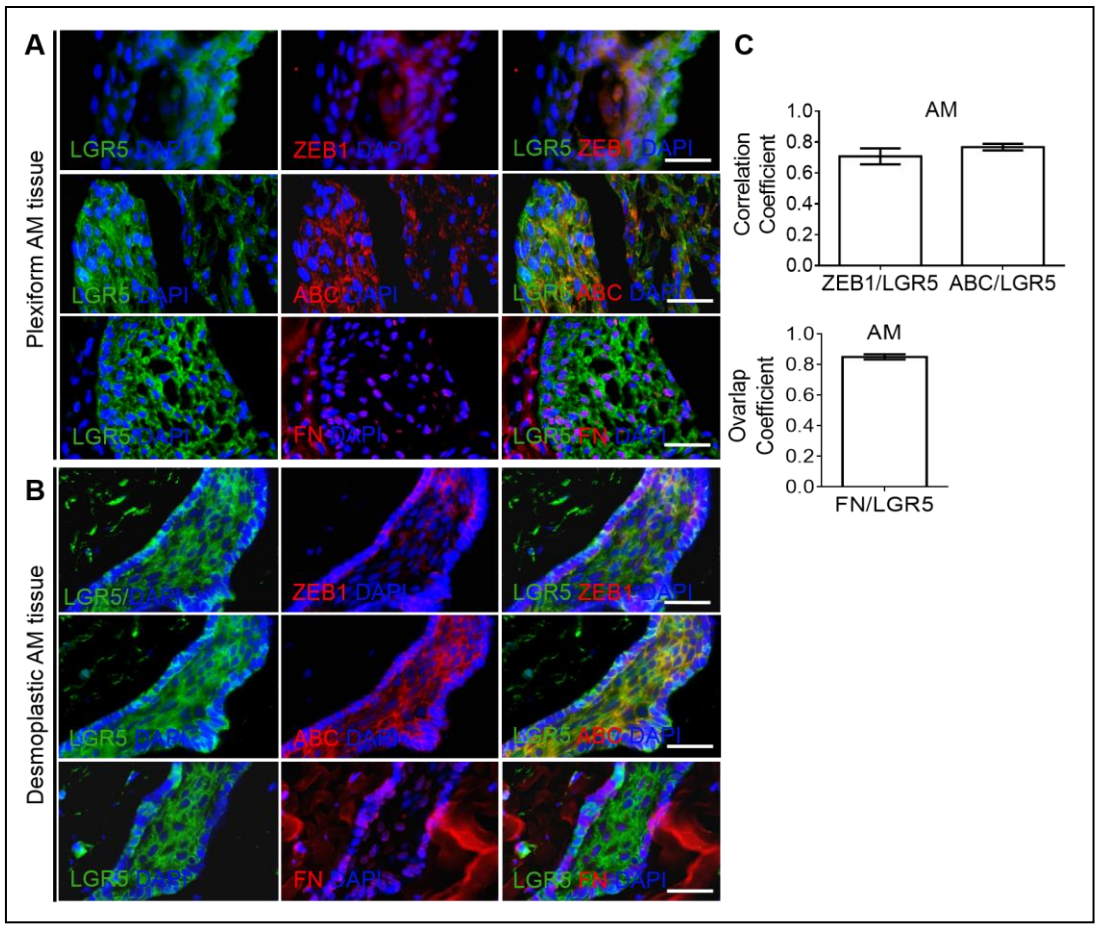

Figure 3.7 Simultaneous expression of LGR5 and certain EMT-related genes expressions in AM tissues. A and **B** Simultaneous expression of LGR5 and specific EMT related markers, ZEB1, ABC and fibronectin (FN) in the plexiform (**A**) and desmoplastic (**B**) AM tissues as determined by immunofluorescence studies. **C** The quantification of the results shown in (**A** and **B**), and **Figure 3.6 F** (follicular type). n=3, each group was calculated at least three different areas by CellProfiler software and data are mean ± SD. Scale bars, 20μm.

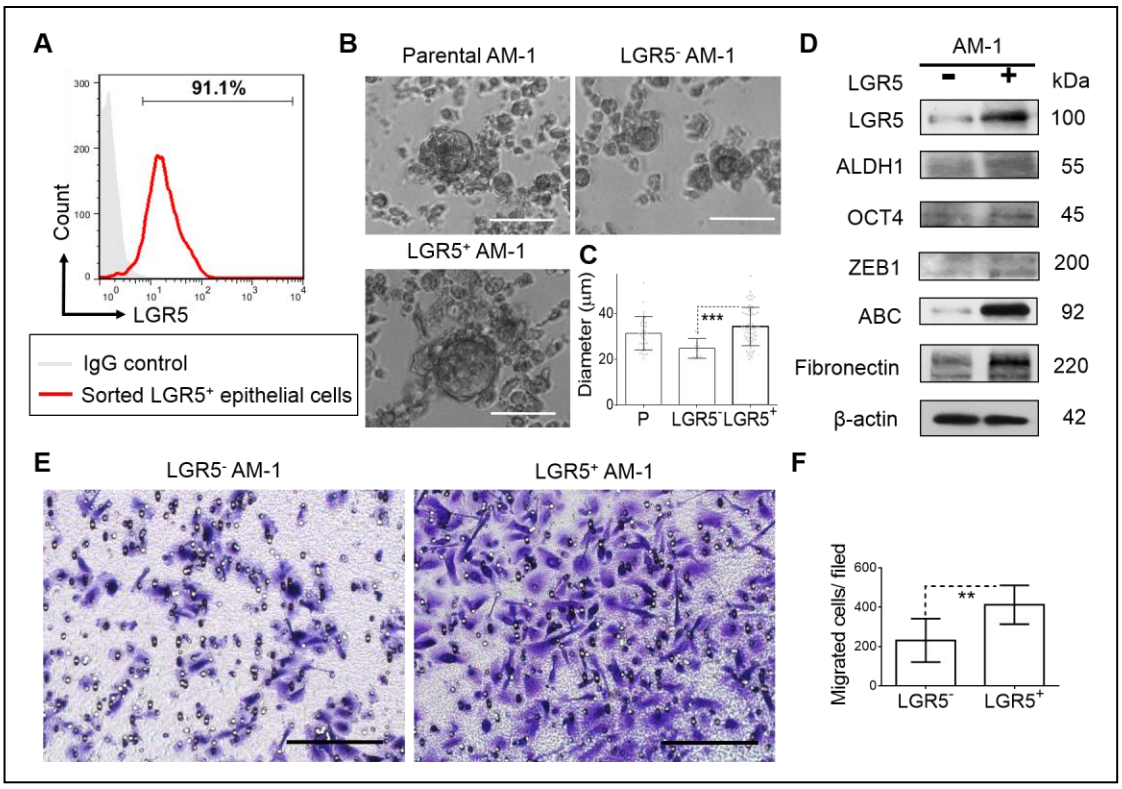

Figure 3.8 LGR5⁺ AM-1 cells exhibit self-renewal ability. A About 90% of sorted LGR5⁺ AM epithelial cells was positive for LGR5 as confirmed by flow cytometric analysis. **B** Sorted LGR5⁺ AM-1 formed larger 3D-spheroids than those by LGR5⁻ counterparts following cultured in 3D Matrigel for two weeks. Scale bars, 100μm. **C** The quantification of the results shown in (**B**). Data are Mean ± SD (each group was measured 3 different random areas under the microscope), Two-tailed unpaired Student's *t*-tests. ***p<0.001. **D** Increased expression of stem cell-related markers, ALDH1 and OCT4, and EMT related markers, ZEB1, active β-catenin (ABC) and fibronectin in sorted LGR5⁺ AM-1 cells in comparison to that in LGR5⁻ counterparts as determined by Western blot analysis. **E** The sorted LGR5⁻ and LGR5⁺ AM-1 ($7x10^4$ cells/well in 200μl basal KBM2 medium) were seeded onto the upper chamber of 24-transwells and the lower chambers were filled with 600μl defined KGM-2 culture medium (n=3 for each group). After culture overnight (16h), the migrated cells were stained with crystal violet and images were taken under a microscope. Scale bars, 100μm. **F** The quantification of the results shown in (**E**). Data are Mean ± SD (each trans-well was measured 6 different random areas under the microscope with 100x magnification), Two-tailed unpaired Student's *t*-tests. **p<0.01. All results are representative of at least two to three independent experiments.

3.4 LGR5/R-spondin stimulates proliferation and EMT/ stemness markers of AM epithelial cells

R-spondin 1 to 4 (Rspo1-4), four secreted Wnt agonists, can activate the canonical Wnt pathway through binding with their endogenous LGR receptor family members, LGR4, LGR5 and LGR6[25,68]. The biological function of LGR5 was then determined by stimulating AM epithelial cells with its ligands, R-spondin-1 or -2 (Rspo1 and Rspo2). To this purpose, primary AM epithelial cells were stimulated with Rspo1 and Rspo2 for 48h, respectively, and the proliferative activity was evaluated. The results showed that stimulation with either Rspo 1 or Rspo2 led to a dose-dependent increase in the proliferation in AM epithelial cells (Figure 3.9 A). Western blot analysis showed that treatment with Rspo1 and Rspo2 significantly increased the expression of active β-catenin (ABC), cyclin A, D1 and E in AM epithelial cells, while the stimulatory effect conferred by Rspo2 was more robust than that by Rspo1 (Figure 3.9 B). The increased expression of ABC, cyclin A, D1 and E in nuclei of AM epithelial cells following treatment with Rspo2 for 48h was further confirmed by immunofluorescence (IF) studies (Figure 3.9 C and D). Similarly, stimulation with Rspo2 increased the expression of ABC, cyclin A, D1 and E as well as the percentage of cells at S-phase (from 8.27% to 12.4%) in AM-1 cells (Figure 3.10 A and B). Of note, Rspo2 upregulated the expression of OCT4 and fibronectin but decreased the expression of E-cadherin in AM-1 cells (Figure 3.10 C). Meanwhile, ameloblastoma epithelial cells showed significantly enhanced 3D-spheroid forming capacity upon exposure to Rspo 2 as compared to the control (vehicle) group (Figure 3.10 D). These findings suggest

that functional LGR5/R-spondin may contribute to AM tumor growth through promoting proliferation, EMT, and acquisition of stem cell properties in AM epithelial cells.

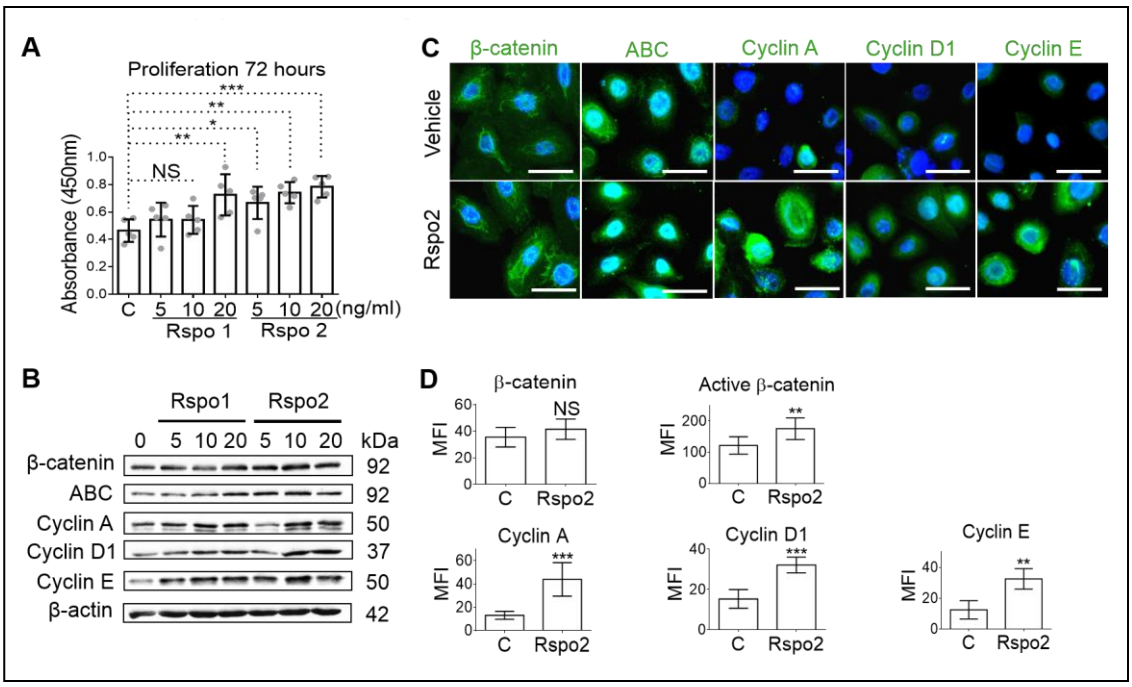

Figure 3.9 AM epithelial cells are responsive to R-spondin stimulation. A Stimulation with R-spondins (Rspo1 and Rspo2) for 72h increased proliferation in AM epithelial cells in a dose-dependent manner. Mean ± SD, n=5, one-way ANOVA and Dunnett's post-test for comparing treatments to untreated control. Control=PBS. NS=not significant. *p<0.05, **p<0.01, ***p<0.001. **B** Stimulation with R-spondins (Rspo1 and Rspo2) for 48h increased the expression of active β-catenin (ABC), cyclin A, D1, and E in AM epithelial cells in a dose-dependent manner as determined by Western blot analysis. **C** Stimulation with 20ng/mL of Rspo2 for 48h increased the expression of active β-catenin (ABC), cyclin A, D1, and E in nuclei of AM epithelial cells as determined by immunofluorescence studies. Scale bars, 20μm. **D** The quantification of the results from immunofluorescence studies shown in (**C**). MFI: mean fluorescence intensity. Each group was measured 6 different random areas and data are mean ± SD. Two-tailed unpaired Student's *t*-tests, NS=not significant, **p<0.01, ***p<0.001. All results are representative of three independent experiments.

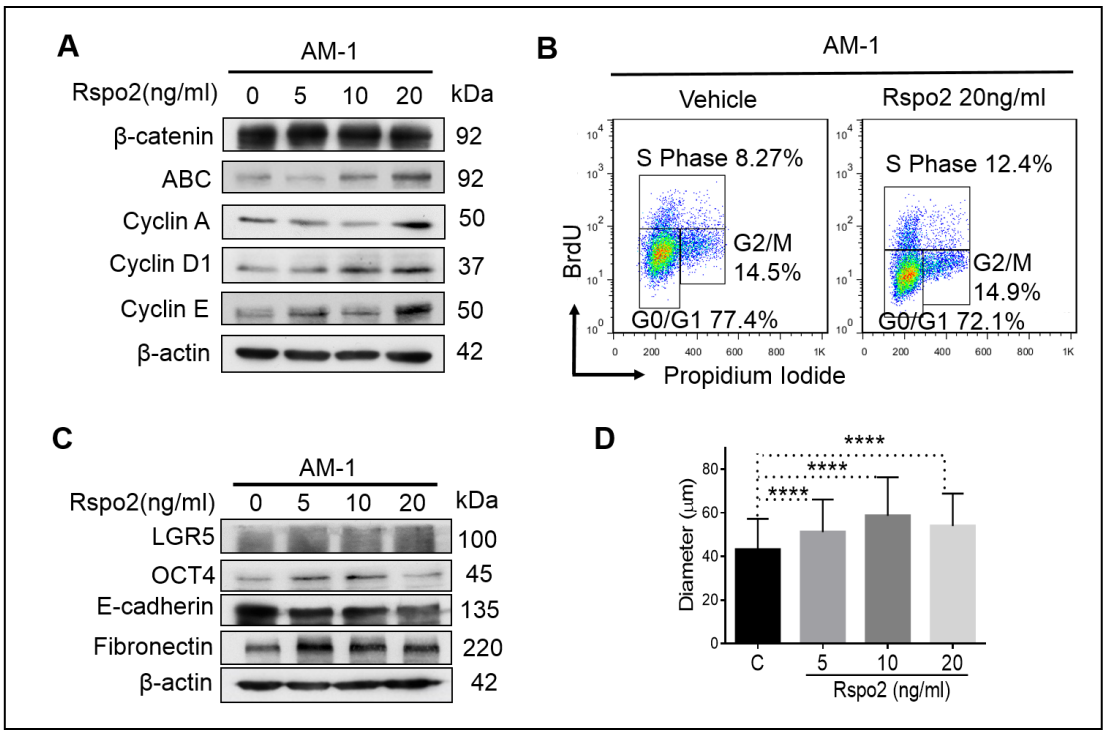

Figure 3.10 R-spondin stimulation promotes proliferation, EMT-related markers and self-renewal ability of AM-1. A The stimulation with Rspo2 for 48 h increased the expression of active β-catenin (ABC), cyclin A, D1 and E in AM-1 cells in a dose-dependent manner. **B** Flow cytometry showed increased proportion of AM-1 cells at S-phase after stimulation with Rspo2 (20ng/ml) for 48 h. **C** Stimulation with of Rspo2 for 48h led to a dose-dependent increase in the expression of OCT4 and fibronectin but decreased the expression of E-cadherin in AM-1 cells as determined by Western blot analysis. **D** Stimulation with of 20ng/mL of Rspo2 for 10 days significantly increased 3D-spheroid formation in AM-1 cells as compared with the control group. Mean ± SD, two-tailed unpaired Student's *t*-test (n=3 in each group). ****p<0.0001.

3.5 Generation of *ex vivo* AM three-dimensional organoid model with AM epithelial cells

In recent years, several progresses have been made in the development of novel 3D organoid models for a variety of cancers, to study tumorigenesis, cancer stem cell biology, tumor microenvironment, and drug screening, etc.[49,69-71]. Up to date, there are no experimental models to study benign tumor of jaw bone, especially ameloblastoma. Here, I explored feasibility to generate the human AM 3D organoids as a preclinical model for this benign/aggressive tumor. To this purpose, primary AM epithelial cells derived from follicular AM tissues or AM-1 cells (plexiform AM epithelial cell lines) were cultured in Matrigel and defined organoid culture medium. The formation of 3D organoid-like structure by both primary AM epithelial cells and AM-1 cells at day 2 following organoid culture were observed (Figure 3.11 A). At day 10, the organoids were harvested for further analysis. Histologically, the generated AM organoids recapitulated the distinct histopathologic features of follicular and plexiform subtypes of solid AM (Figure 3.11 B and C). Specifically, organoids generated from primary follicular AM epithelial cells displayed hyperchromic nuclei cuboidal (ameloblast-like) peripheral cells arranged in a palisading-like pattern and demonstrated reverse polarity (Figure 3.11 B); while organoids generated from AM-1 cells (plexiform type) exhibited irregular epithelial islands connected as anastomosing strands (Figure 3.11 C). Interestingly, highly co-expression of LGR5 and active β-catenin (ABC) was also observed in organoids generated from both primary follicular AM epithelial cells and plexiform AM-1 cell lines (Figure 3.11 B and C), similar to that

observed in both subtypes of solid AM tissues (Figure 3.6 F and 3.7). These findings have demonstrated for the first time the feasibility to generate *ex vivo* human AM 3D organoids, which recapitulated the histopathological features of AM subtypes, and to further confirm the potential role of $LGR5^{+}$ epithelial cells in the pathogenesis of AM.

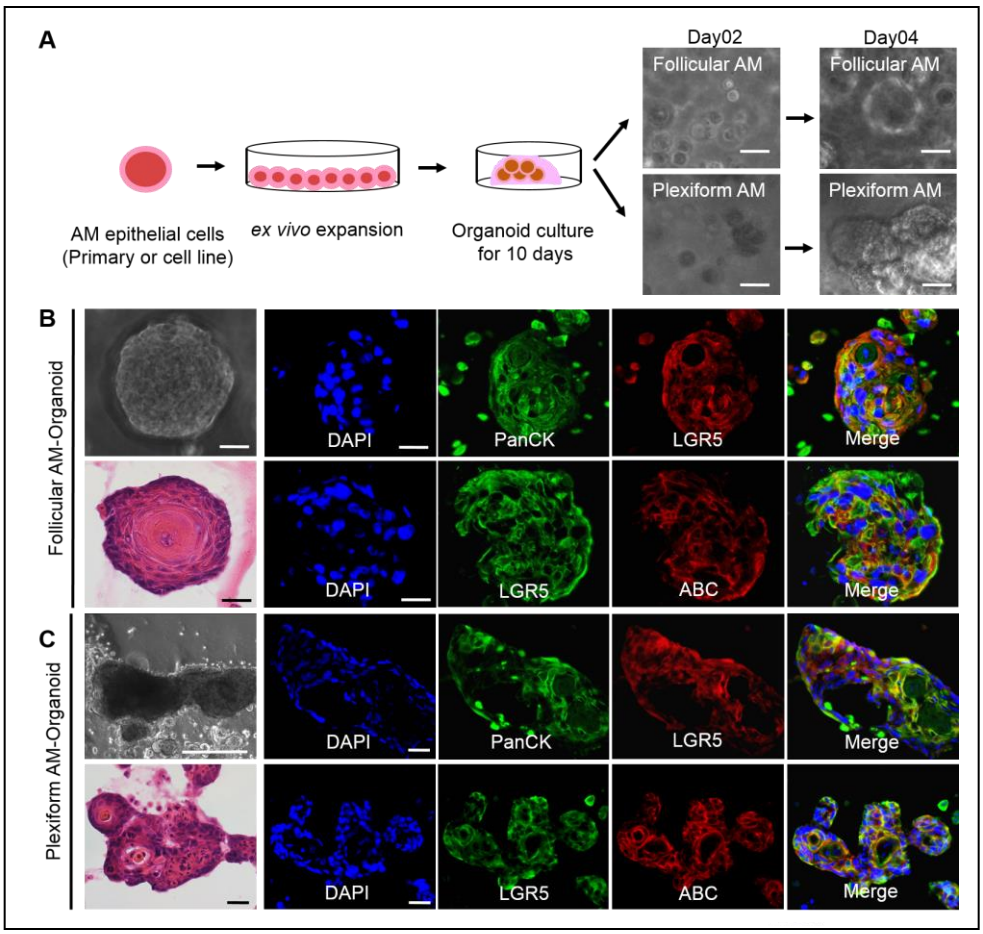

Figure 3.11 3D-organoids derived from AM epithelial cells recapitulate histopathological features of AM. A The diagram showing the generation of 3D-organoids by AM epithelial cells. *Ex vivo* expanded primary AM epithelial cells or AM-1 cells were transferred to 3D Matrigel and cultured for different days. Scale bars, 20μm. **B** 3D-organoid culture of follicular AM epithelial cells for 10 days. Left, H&E staining showed AM epithelial cells arranged into follicular-type organoids. AM-organoids recapitulated certain histopathological features of AM, including hyperchromic nuclei cuboidal (ameloblast-like) peripheral cells arranged in a palisading-like pattern and showed reverse polarity. Right: LGR5 was simultaneously expressed with pan-cytokeratin and activated β-catenin (ABC) in 3D organoids formed by AM epithelial cells as determined by immunofluorescence studies. Scale bars, 20μm. **C** 3D-organoid culture of AM-1 (plexiform type) for 10 days. Left, H&E staining showed generated organoids with irregular epithelial islands connected as anastomosing strands that were similar to the histopathological features of plexiform AM. Right, LGR5 was simultaneously expressed with pan-cytokeratin and activated β-catenin (ABC) in 3D organoids formed by AM epithelial cells as determined by immunofluorescence studies. Scale bars, left upper: 200μm; left lower and right: 20μm. All results are representative of three independent experiments.

3.6 Lg5^{+} AM epithelial cells possess self-renewal and propagating ability *in vivo*

Next, the self-renewal capability of LGR5^{+} AM epithelial cells *in vivo* was evaluated. To this purpose, parental and sorted LGR5^{+} and LGR5^{-} AM epithelial cells were cultured in Matrigel *in vitro* for three weeks and then subcutaneously transplanted into the flank of nude mice (Figure 3.12 A). At day 14 post-transplantation, histological analysis showed that parental and LGR5^{+} AM epithelial cells could proliferate and generate tumor-like structures, but transplanted LGR5^{-} cells could not survive and were almost completely resorbed (Figure 3.12 B), wherein the presence of human AM epithelial cells *in vivo* was confirmed by immunostaining with a specific antibody for human mitochondria (Figure 3.12 C). Meanwhile, in the tumor-like structures formed by transplanted parental and LGR5^{+} AM epithelial cells, about 60% of cells simultaneously expressed LGR5 and proliferating cell nuclear antigen (PCNA) (Figure 3.12 D). Further analysis showed that the percentage of cells co-expressing LGR5 and ALDH1, LGR5 and OCT4, LGR5 and ZEB1 in tumor-like structures formed by LGR5^{+} AM epithelial cells was significantly higher than that in those formed by parental AM epithelial cells (Fig. 3.13). To further evaluate the self-renewal capability of LGR5^{+} AM epithelial cells *in vivo*, sorted LGR5^{+} AM epithelial cells were cultured in Matrigel for two weeks and then performed cell-dilution assay by subcutaneously transplanting different number of cells (10^{6}, 10^{5}, 10^{4} and 10^{3}) into nude mice. The results showed that one-month post-transplantation, the implanted LGR5^{+} AM epithelial cells in all groups survived and exhibited

proliferative capability (Figure 3.14). Taken together, these results suggest that LGR5^{+} AM epithelial cells possess self-renewal and propagating capability *in vivo*.

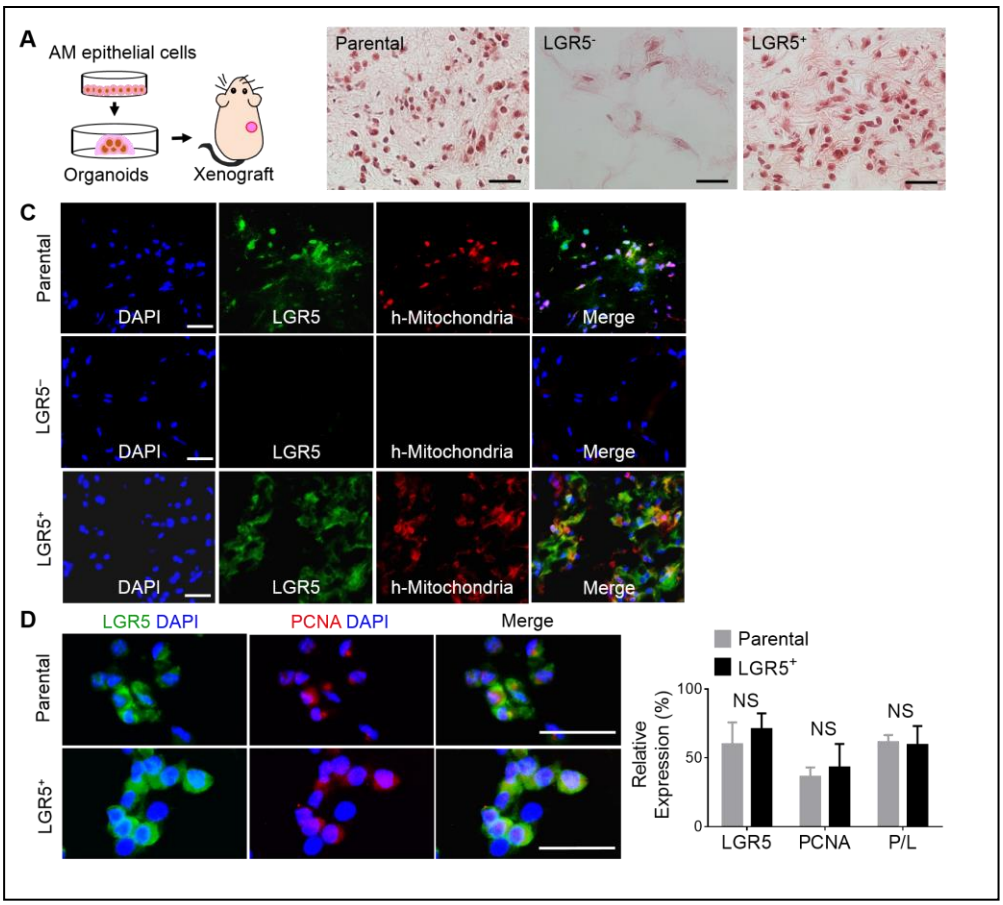

Figure 3.12 LGR5⁺ AM epithelial cells exhibit propagating ability *in vivo.* **A** The diagram showing the subcutaneous nude mice model using *ex vivo* organoids. Following culturing in 3D Matrigel for three weeks, the *ex vivo* organoids formed by parental, sorted LGR5⁺ or LGR5⁻ AM epithelial cells were harvested and subcutaneously transplanted into the flank of nude mice. **B** Two weeks post-transplantation, the tumor-like structures formed in nude mice were harvested for histological analysis by H & E staining. The LGR5⁻ AM epithelial cells were mostly resorbed while the LGR5⁺ and parental groups could generate some tumor-like structure. Scale bars, 20μm. **C** Immunofluorescence study showed co-expression of human mitochondria and LGR5 in xenografted tumor-like structures formed by transplanted LGR5⁺ and parental AM epithelial cells, but not by LGR⁻ counterparts. Scale bars, 50μm. **D** Co-expression of LGR5 and proliferating cell nuclear antigen (PCNA) in xenografted tumor-like structures formed by transplanted parental or LGR5⁺ AM epithelial cells as determined by immunofluorescence studies (Left panels). Scale bars, 100μm. Right panel: the quantification of relative expression of PCNA, LGR5 and PCNA/LGR5 (P/L) from the results shown in the left panels. Mean ± SD (n=4 in each group, xenografts of AM epithelial cells, each group was measured 5 different random areas under the microscope, two-tailed unpaired Student's *t*-test. NS=not significant).

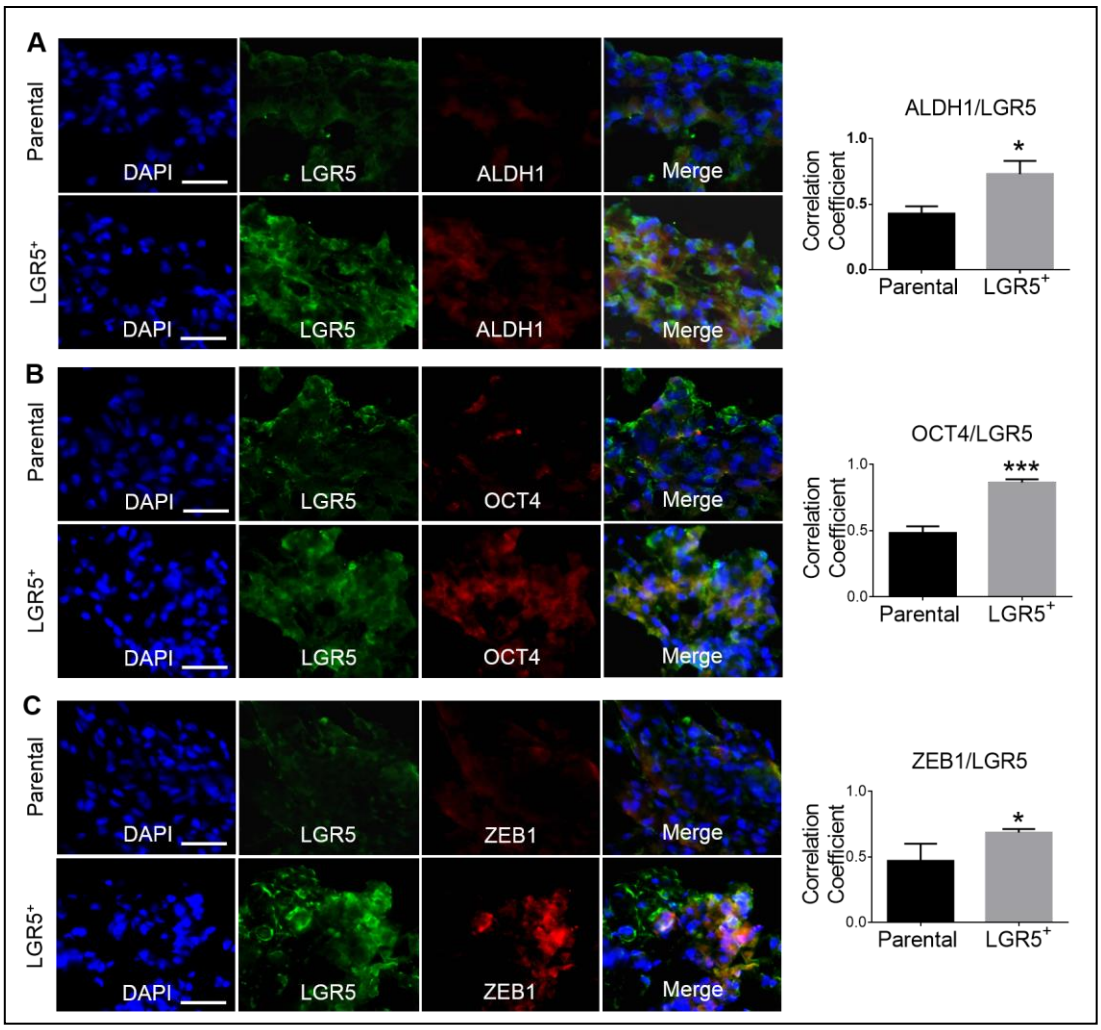

Figure 3.13 LGR5⁺ AM epithelial cells exhibit stemness and EMT markers *in vivo*. Following culturing in 3D Matrigel for three weeks, the *ex vivo* organoids formed by parental, sorted LGR5⁺ or LGR5⁻ AM epithelial cells were harvested and subcutaneously transplanted into the flank of nude mice. Two weeks post-transplantation, the tumor-like structures formed in nude mice were harvested for immunofluorescence studies. **A** Xenografted tumor-like structures formed by transplanted LGR5⁺ cells showed elevated simultaneous expression of ALDH1 and LGR5 in comparison to those formed by transplanted parental cells. Scale bars, 20μm. Mean ± SD, n=4, two-tailed unpaired Student's *t*-tests. **p*<0.05. **B** Xenografted tumor-like structures formed by transplanted LGR5⁺ cells showed elevated co-expression of OCT4 and LGR5 in comparison to those formed by transplanted parental cells. Scale bars, 20μm. Mean ± SD, n=4, two-tailed unpaired Student's *t*-tests. ****p*<0.001. **C** Xenografted tumor-like structures formed by transplanted LGR5⁺ cells showed elevated simultaneous expression of ZEB1 and LGR5 in comparison to those formed by transplanted parental cells. Scale bars, 20μm. Mean ± SD, n=4, two-tailed unpaired Student's *t*-tests. **p*<0.05.

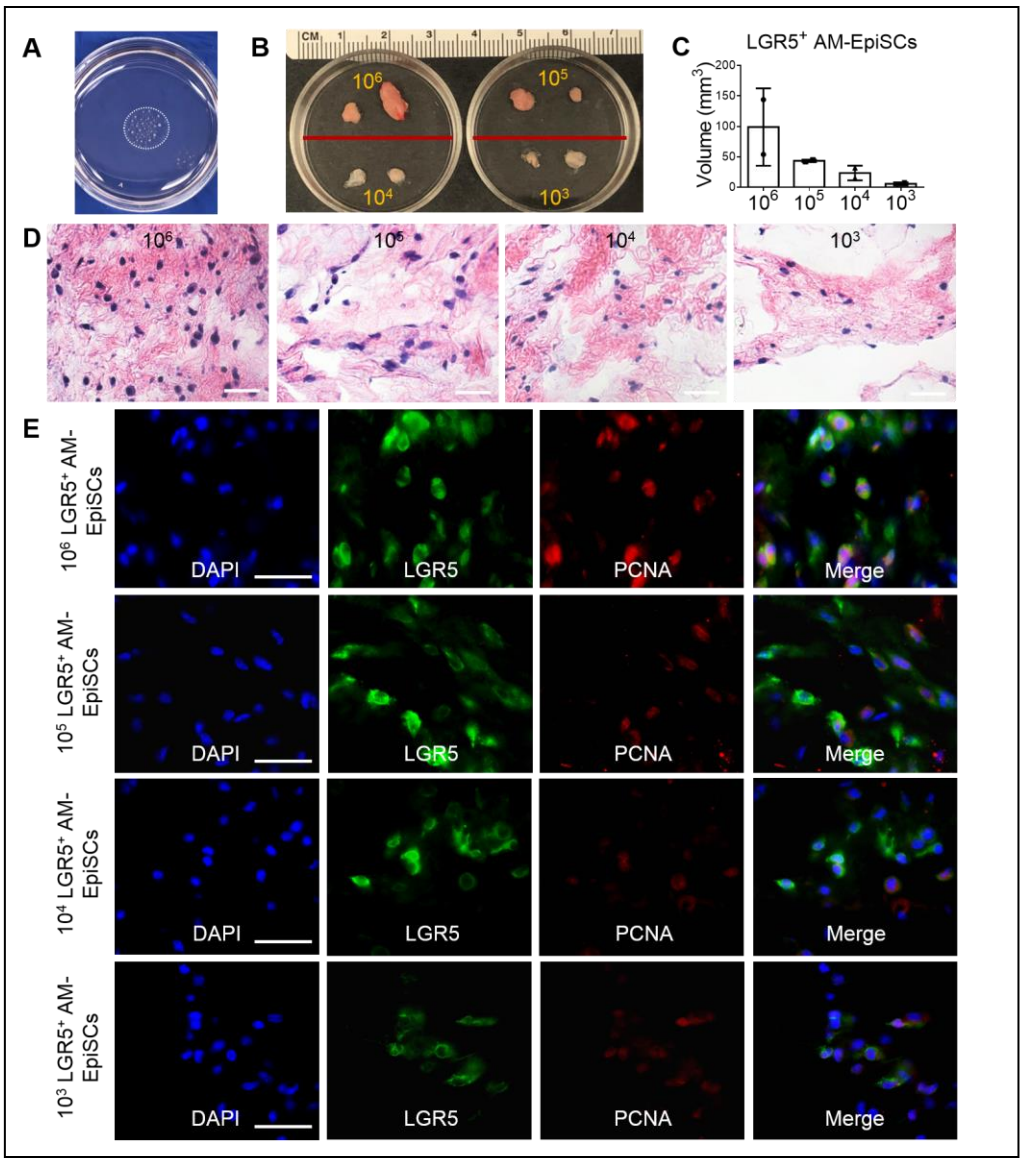

Figure 3.14 LGR5⁺ AM-EpiSCs exhibit self-renewal capability *in vivo*. For cell dilution assay, LGR5⁺ cells were sorted from primary AM epithelial cells and then cultured in Matrigel (50μl) for two weeks at different cell numbers: 10^3, 10^4, 10^5 and 10^6 (n=2 each group). After two weeks, the organoids in Matrigel were transplanted subcutaneously into the dorsal skin of nude mice for one month. **A** The organoids in Matrigel. **B** Organoid xenografts were harvested one-month post-transplantation. **C** Calculation of the mean volume of organoid xenografts from different groups of animals. **D** Histological analysis of organoid xenografts by H & E staining. Sale bars, 20μm. **E** The co-expression of human LGR5 and proliferating cell nuclear antigen (PCNA) in organoid xenografts were determined by immunofluorescence study. Scale bars, 20μm. All results are representative of two independent experiments.

3.7 LGR5^{+} AM-EpiSCs resistant to BRAF^{V600E} inhibitor are capable of tumor formation *ex vivo*

Previous studies have shown that about 46-82% of AM cases exhibit BRAF^{V600E} mutation [7-12]. BRAF^{V600E} mutation in some solid type of AM tissues was also confirmed by IHC studies (Figure 3.16 A). I next determined whether treatment of AM-1 cells with a specific BRAF^{V600E} inhibitor, Vemurafenib (PLX4032), could target the subpopulation of LGR5^{+} cells in AM epithelial cells. The results showed that treatment with PLX4032 reduced cell viability in a dose-dependent manner (Figure 3.15 A). Interestingly, flow cytometric analysis revealed that exposure to PLX4032 resulted in a dose-dependent enrichment of the subpopulation of LGR5^{+} cells (Figure 3.15 B). Furthermore, PLX4032 apparently interfered with organoid formation, with most of the residual cells positive for LGR5 (Figure 3.15 C and Figure 3.16 B). Western blot analysis further confirmed that treatment with PLX4032 not only enriched LGR5 expression, but also enhanced the expression of ALDH1, OCT4, active β-catenin, and fibronectin, and decreased the expression of E-cadherin in both primary AM epithelial cells and AM-1 cell lines (Figure 3.17 A).

LGR5^{+} and LGR5^{-} cells were sorted out from AM-1 cells following treatment with PLX4032 and compared the expression of these stem cell- and EMT-related genes. The results showed markedly elevated expression of ALDH1, OCT4, active β-catenin, and fibronectin in sorted PLX4032-resistant LGR5^{+} cells as compared to their LGR5^{-} counterparts (Figure 3.17 B). Additionally, the organoid-forming capacity of PLX4032-resistant LGR5^{+} AM-1 cells was determined. To

this end, AM-1 cells were treated with 20 μM of PLX4032 under 2D culture condition for 48h. Afterwards, unsorted parental (PLX-parental), sorted $LGR5^+$ (PLX- $LGR5^+$) and $LGR5^-$ (PLX-$LGR5^-$) cells were cultured in organoid culture condition, respectively, while AM-1 cells treated with vehicle (DMSO) were used as control (Figure 3.17 C). The results showed that PLX4032-treated AM-1 cells (PLX-parental cells) formed significantly more and larger organoids than AM-1 cells treated with vehicle (Figure 3.17 D and E). More compellingly, $LGR5^+$ cells sorted from PLX4032-treated AM-1 cells (PLX- $LGR5^+$) displayed more abundant and larger organoids than both their $LGR5^-$ counterparts (PLX-$LGR5^-$) and AM-1 cells treated with vehicle (Figure 3.17 D and E). Taken together, these findings have demonstrated that $LGR5^+$ AM epithelial cells can surmount resistance to the $BRAF^{V600E}$ inhibitor (PLX4032) and these PLX4032-resistant $LGR5^+$ AM epithelial cells are endowed with stem cell properties and an intermediate EMT phenotype with enhanced capacity for tumor organoid formation.

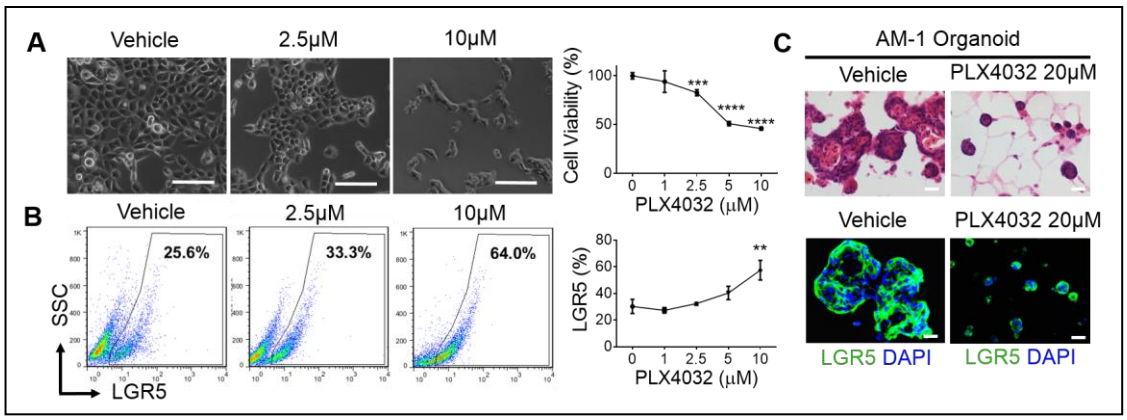

Figure 3.15 LGR5^{+} AM-EpiSCs resist BRAFV600E inhibitor in AM-organoids. A Left: AM-1 cells were seeded on a 24 well plate in a cell density of 10^5/well and treated with different concentrations of a specific BRAF^{V600E} inhibitor (Vemurafenib, PLX4032) for 48 h (n=3). Residual cells arranged into irregular epithelial islands connected as anastomosing strands. Right: AM-1 cells were seeded into 96-well plates ($5x10^4$ cells/well) followed by exposure to different concentrations of PLX4032 for 48 h and the cell viability was determined by cell count kit-8. Data are Mean ± SD, n=4, two-tailed unpaired Student's *t*-test. ****p*<0.001, *****p*<0.0001. **B** Left: enriched expression of LGR5 on AM-1 cells following treatment with different concentrations of PLX4032 for 48h as determined by flow cytometry. Right: graphs showing the results from flow cytometric analysis as shown in the left panels. Data are Mean ± SD, n=3, two-tailed unpaired Student's *t*-test. ***p*<0.01. **C** 3D-organoids formed by AM-1 cells for 4 days were treated with PLX4032 (20μM) for 6 days. Upper: PLX4032 interfered with 3D-organoid formation as determined by H & E staining. Lower: the residual PLX4032-resistant AM-1 cells in 3D-organoids were positive for LGR5 as determined by immunofluorescence study. Scale bars, 20μm. All results are representative of at least three independent experiments.

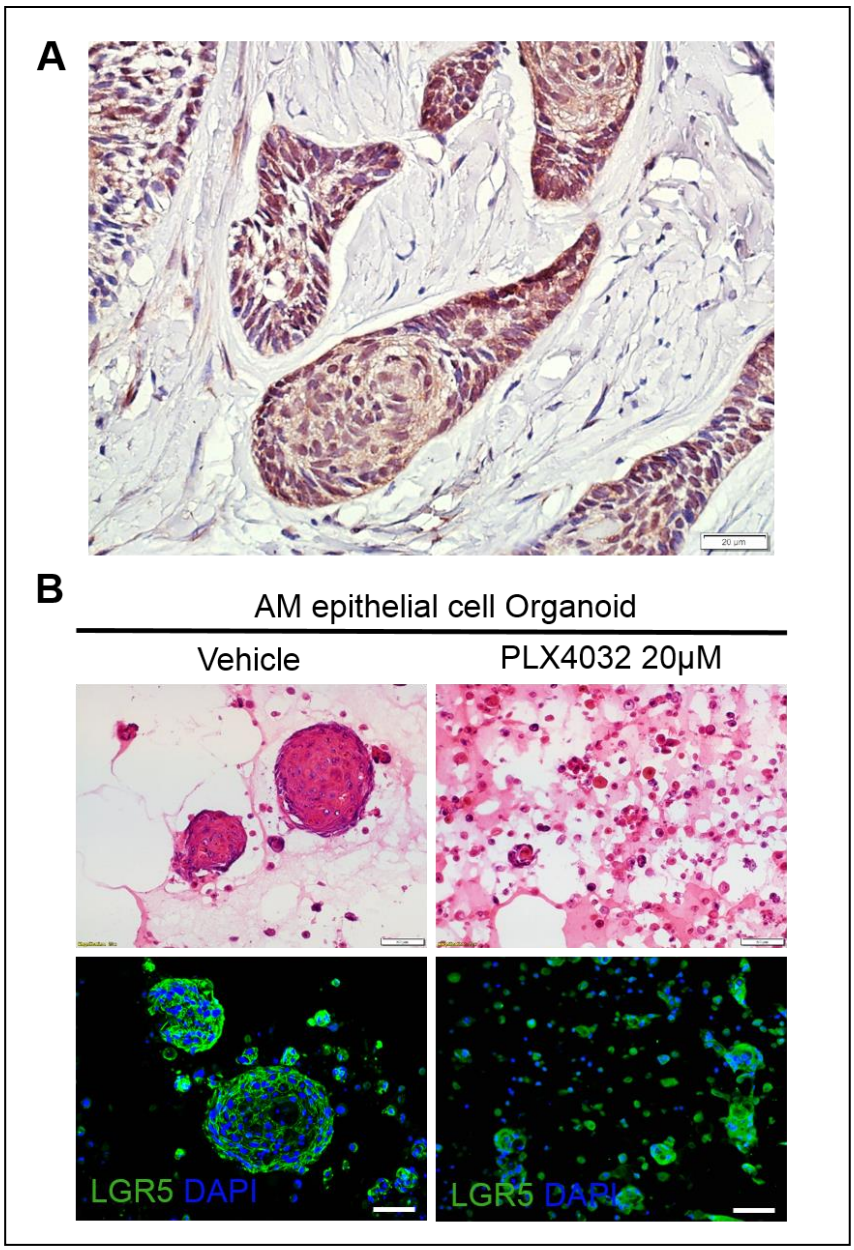

Figure 3.16 LGR5^{+} AM-EpiSCs resist to the BRAF inhibitor. A Immunohistochemistry study showed BRAF^{V600E} mutation in primary AM tissues. **B** 3D-organoids formed by AM epithelial cells for 4 days were treated with PLX4032 (20μM) for 6 days. Upper: PLX4032 interfered with 3D-organoid formation as determined by H & E staining. Lower: the residual PLX4032-resistant AM epithelial cells cells in 3D-organoids were positive for LGR5 as determined by immunofluorescence study. N=3. Scale bars, 20μm.

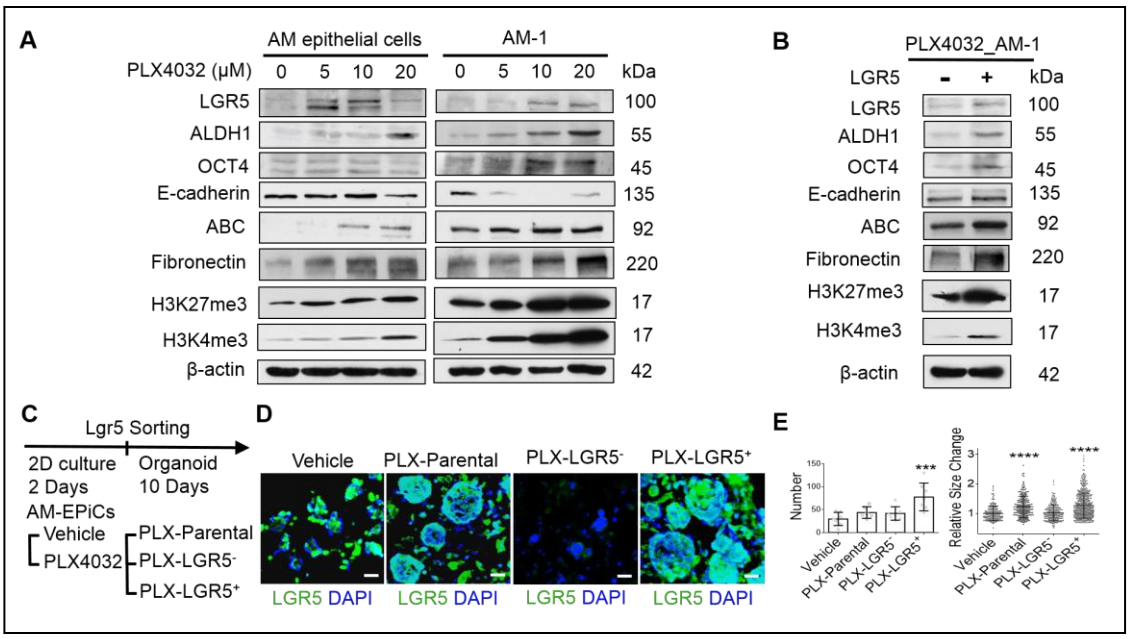

Figure 3.17 LGR5$^+$ AM-EpiSCs resist BRAFV600E inhibitor and drug-resistant LGR5$^+$ AM-EpiSCs possess propagating ability to generate AM organoids. A LGR5$^+$ epithelial cells were enriched with a concomitant dose-dependent increase in the expression of ALDH1, active β-catenin (ABC) and fibronectin but decreased E-cadherin expression in either primary AM epithelial cells or AM-1 cells following treatment with different concentrations of PLX4032 under 2D-monolayer culture condition for 48h. **B** AM-1 cells were treated with PLX4032 (20μM) under 2D monolayer culture conditions for 48h and then LGR5$^-$ and LGR5$^+$ AM epithelial cells were sorted by anti-LGR5 microbeads. The expression of stem cell- and EMT-related genes/markers was significantly increased in LGR5$^+$ AM epithelial cells in comparison to that in LGR5$^-$ counterparts as determined by Western blot analysis. **C** and **D** AM-1 were treated with PLX4032 (20μM) or vehicle under 2D-monolayer culture condition for 48h and LGR5$^-$ and LGR5$^+$ AM epithelial cells were sorted by anti-LGR5 microbeads. Unsorted PLX4032-treated parental cells (PLX-parental) and sorted PLX4032-treated LGR5$^+$ (PLX-LGR5$^+$) cells generated significantly larger and more organoids than the PLX-LGR5$^-$ counterparts and even the vehicle-treated parental group. Vehicle: Dimethyl sulfoxide (DMSO). **E** Measurements of organoid number and size as shown in (**D**). Data are Mean ± SD, n=3, one-way ANOVA and Dunnett's post-test. ****p<0.0001. All results are representative of at least two to three independent experiments.

3.8 AM-MSC-derived secretomes promote the formation of LGR5$^+$ AM-EpiSC *in vitro*

Our recent studies have shown that AM-MSCs promoted EMT and acquisition of stem cell properties in AM epithelial cells[24]. This study then aimed to explore whether AM-MSCs can promote the formation of LGR5$^+$ AM-EpiSCs. To this purpose, AM-1 cells were co-cultured with AM-MSCs in a trans-well system or with the AM-MSC derived conditioned medium (CM) for 3 days. The results showed that co-culture with AM-MSCs or stimulation with AM-MSC derived CM significantly changed the morphology of AM-1 from epithelial islands to anastomosing strands (Figure 3.18 A). The Western blot study showed an increase in the expression of LGR5, ALDH1, active β-catenin and fibronectin, but decreased expression of E-cadherin in AM-1 cells following co-culture with AM-MSCs or stimulation with AM-MSC derived CM (Figure 3.18 B), suggesting that AM-MSC derived secretomes can promote EMT process and the formation of LGR5$^+$ AM-EpiSCs in AM epithelial cells. Then, AM-1 cells were further stimulated with concentrated AM-MSC derived CM for 72h. The results showed that stimulation with concentrated AM-MSC derived CM increased the expression of LGR5, active β-catenin (ABC), and fibronectin in AM-1 cells as determined by flow cytometry (Figure 3.18 C and D) and Western blot analysis (Figure 3.18 E), respectively. To further define whether AM-MSC derived EVs play a role in this process, AM-MSCs were pretreated with GW4869, a specific exosome secretory blocker, for 24 or 72h, and then the conditioned medium was harvested for functional studies. The results showed that pretreatment with GW4869 partially

abrogated the upregulation of active β-catenin (ABC) and fibronectin expression in AM-1 induced by AM-MSCs derived CM (Figure 3.18 F and G). These results implicate that AM-MSC derived secretomes containing EVs contribute an important role in promoting EMT process and formation of $LGR5^{+}$ AM-EpiSCs in AM epithelial cells.

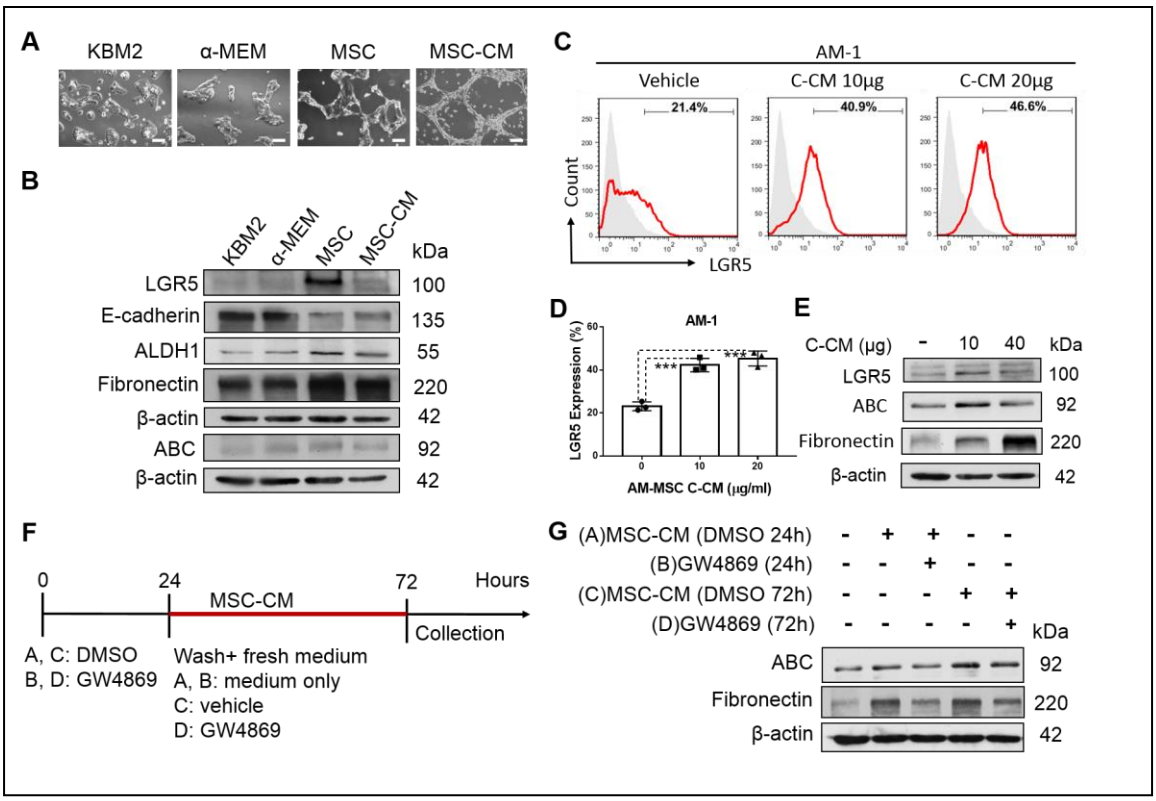

Figure 3.18 AM-MSC derived secretomes promote the subpopulation of LGR5⁺ AM-EpiSC *in vitro*. A and B, AM-1 cells were seeded on a 6-well plate ($3x10^5$/well) overnight and then co-cultured with AM-MSCs ($2x10^5$ cells) in serum free α-MEM or treated with AM-MSC condition medium (CM) (collected from the AM-MSC cultured in serum free α-MEM for 48h) for 3 days. Control: normal epithelial culture medium (KGM2) and serum free α-MEM. **A** The morphology of AM-1 was changed by AM-MSC co-culture or CM form multiple epithelial islands (KGM2 and α-MEM groups) to anastomosing strands (MSC and MSC-CM groups). **B** Western blots study showed increased expression of LGR5, stemness-related marker (ALDH1) and EMT- related markers (ABC and fibronectin) and decreased expression E-cadherin. **C** AM-1 cells treated with concentrated condition medium (C-CM) of AM-MSC for 3 days and the flow cytometric results showed significantly increased expression of LGR5. Red: LGR5. Gray: negative control. **D** The quantification of data shown in (**C**). Mean ± SD, two-tailed unpaired Student's *t*-tests. ****p*<0.001. **E** Western blot study showed increased expression of LGR5 and EMT-related makers (ABC and fibronectin) in AM-1 after stimulated with concentrated condition medium (C-CM) of AM-MSC for 3 days. **F** The diagram of AM-MSC treated with DMSO or GW4869 for 24h or 72h. The treated AM-MSC CM were collected after 48h culturing. **G** AM-1 cells were stimulated with AM-MSC CM (the AM-MSCs were treated with DMSO or GW4869 as the diagram shown in **F**) showed either 24h or 72h treated AM-MSC derived CM reduced the expression of ABC and fibronectin.

3.9 Generation of 3D organoid model from AM epithelial cells and AM-MSCs

To recapitulate the microenvironment of AM, AM epithelial cells and AM-MSCs were combined to generate 3D organoid model. AM epithelial cells were mixed with AM-MSCs in different cell ratios (1:1, 1:2, 1:4 and 2:1) and different culture medium (data unshown), and defined an optimal cell ratio (2:1), cell density ($4x10^4$ cells/μl Matrigel) and the culture condition that could facilitate AM 3D-organoid formation to recapitulate the histopathological properties and maintained a similar expression of biomarkers in AM tissues. The AM epithelial cells maintained the repropagating ability through several passages and cryopreservation/thaw procedures (Figure 3.19). The cryopreserved organoids were thawed into Matrigel to maintain in the organoid culture condition. The AM organoids derived from AM epithelial cells and AM-MSCs self-organized to cystic structures within 2 days under the microscopic examination (Figure 3.20 A). The H & E study of the organoids derived from AM-1 mixed with AM-MSCs showed plexiform-like anastomosing strands (Figure 3.20 B). To maintain a sufficient nutrition supply in the central part of organoids, the AM organoids were dissociated on day 4 and passaged to new Matrigel or cryopreserved. The immunofluorescence study of day 2 organoids showed the expression of E-cadherin, CD90, vimentin and LGR5 in the AM organoids derived from AM-1 and AM-MSCs (Figure 3.20 C and 3.21), and the day 4 organoids showed higher expression of LGR5 than day 2 and day 8. Besides, the MSC marker (vimentin) was losing in the Matrigel-culture condition (Figure 3.22). These present results

have provided a short-term AM 3D-organoid platform to evaluate the potential role of stromal cells in pathogenesis of AM.

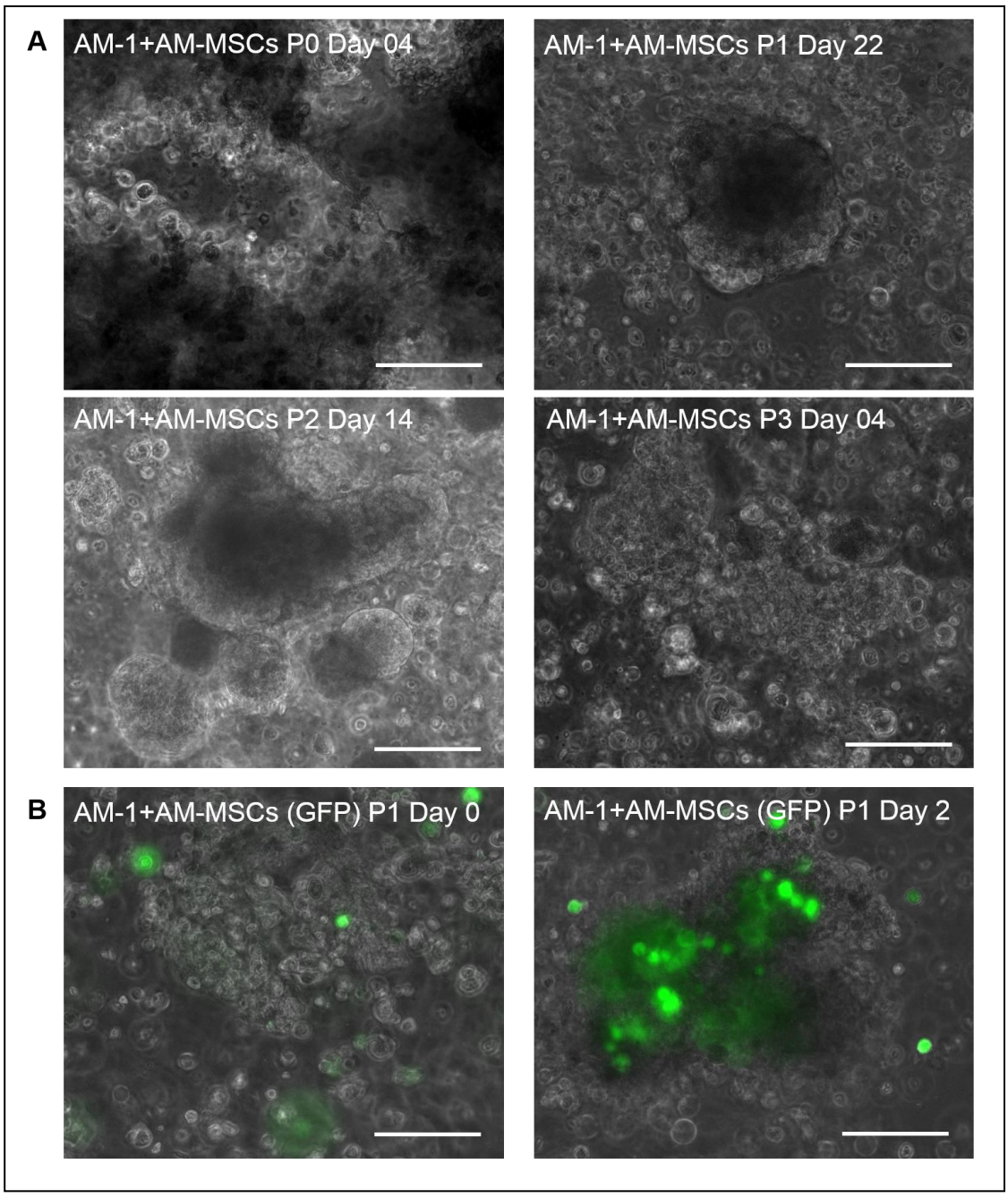

Figure 3.19 Long-term AM-organoid culture. A AM-organoids derived from AM-1 mixed with AM-MSCs (without GFP). The AM-organoids were passaged and cryopreserved between P2 and P3. Each passage of AM-organoids maintained propagating ability and continuingly generated new AM-organoids. Scale bars, 100μm. **B** AM-organoids derived from AM-1 mixed with AM-MSCs-GFP were successfully passaged and both AM-1 and AM-MSCs had cell viability and capacity to aggregate together. Scale bars, 100μm.

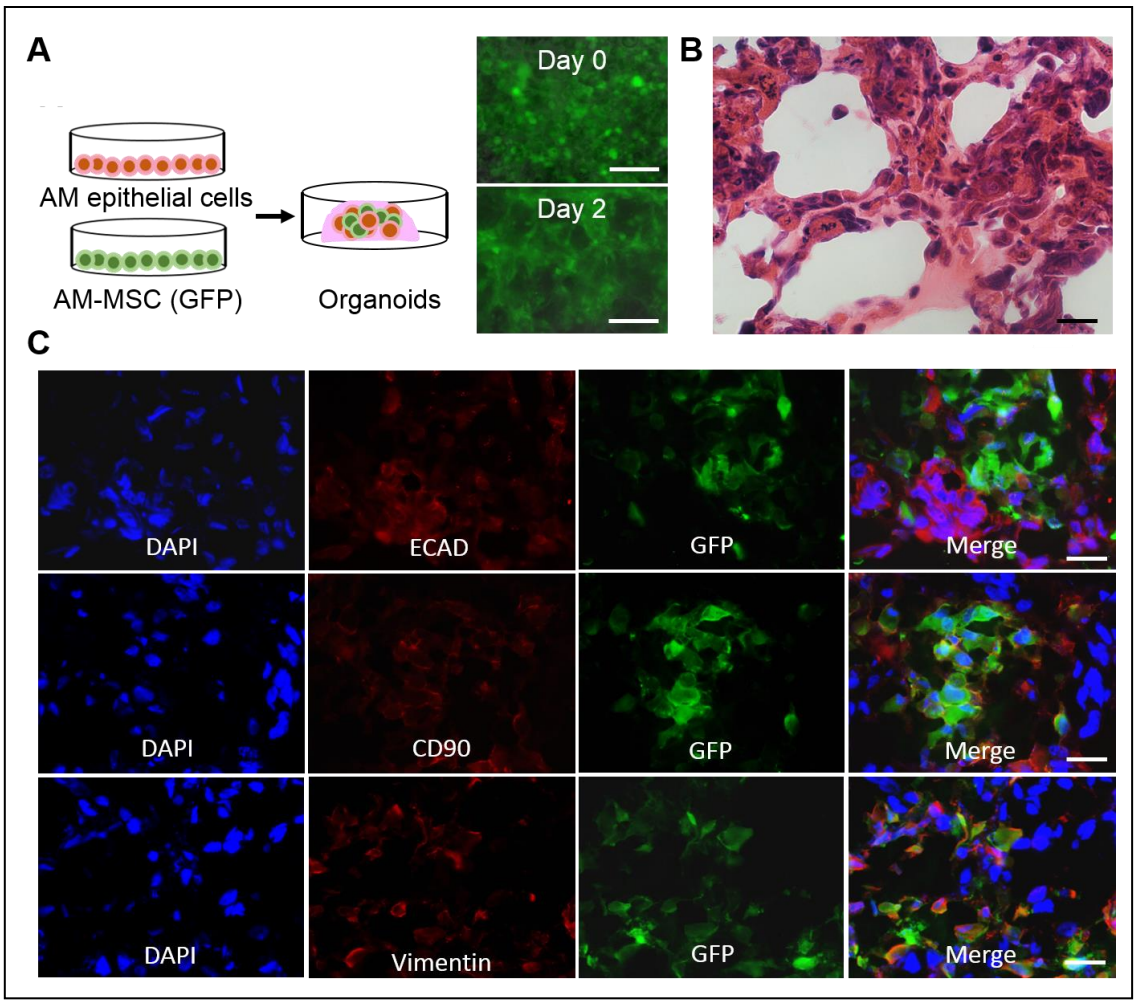

Figure 3.20 AM 3D-organoids derived from AM epithelial cells and AM-MSCs. A Left: the diagram showing the generation of 3D-organoids by AM epithelial cells and AM-MSCs. *Ex vivo* expanded primary AM epithelial cells/ AM-1 cells and primary AM-MSCs (with GFP). Then primary AM epithelial cells or AM-1 were mixed with AM-MSCs (cell ratio 2:1) and transferred to 3D Matrigel ($4x10^4$ cells/μl Matrigel). Right: Organoids derived from AM-1 mixed with AM-MSCs (with GFP) under microscopic study. On day 0, every single cell was suspended in Matrigel and then re-arranged into multicystic structures within 2 days. Scale bars, 100μm. **B** 3D-organoid culture of plexiform AM-1 with AM-MSCs for 2 days. H&E staining showed generated organoids with irregular epithelial islands connected as anastomosing strands that recapitulated the histopathological features of plexiform AM. Scale bars, 20μm **C** 3D-organoid culture of AM-1 (plexiform type) mixed with AM-MSCs (with GFP) for 2 days. Both epithelial (E-cadherin) and MSC (CD90 and vimentin) markers were showed in the organoids. Scale bars, 20μm. All results are representative of three independent experiments.

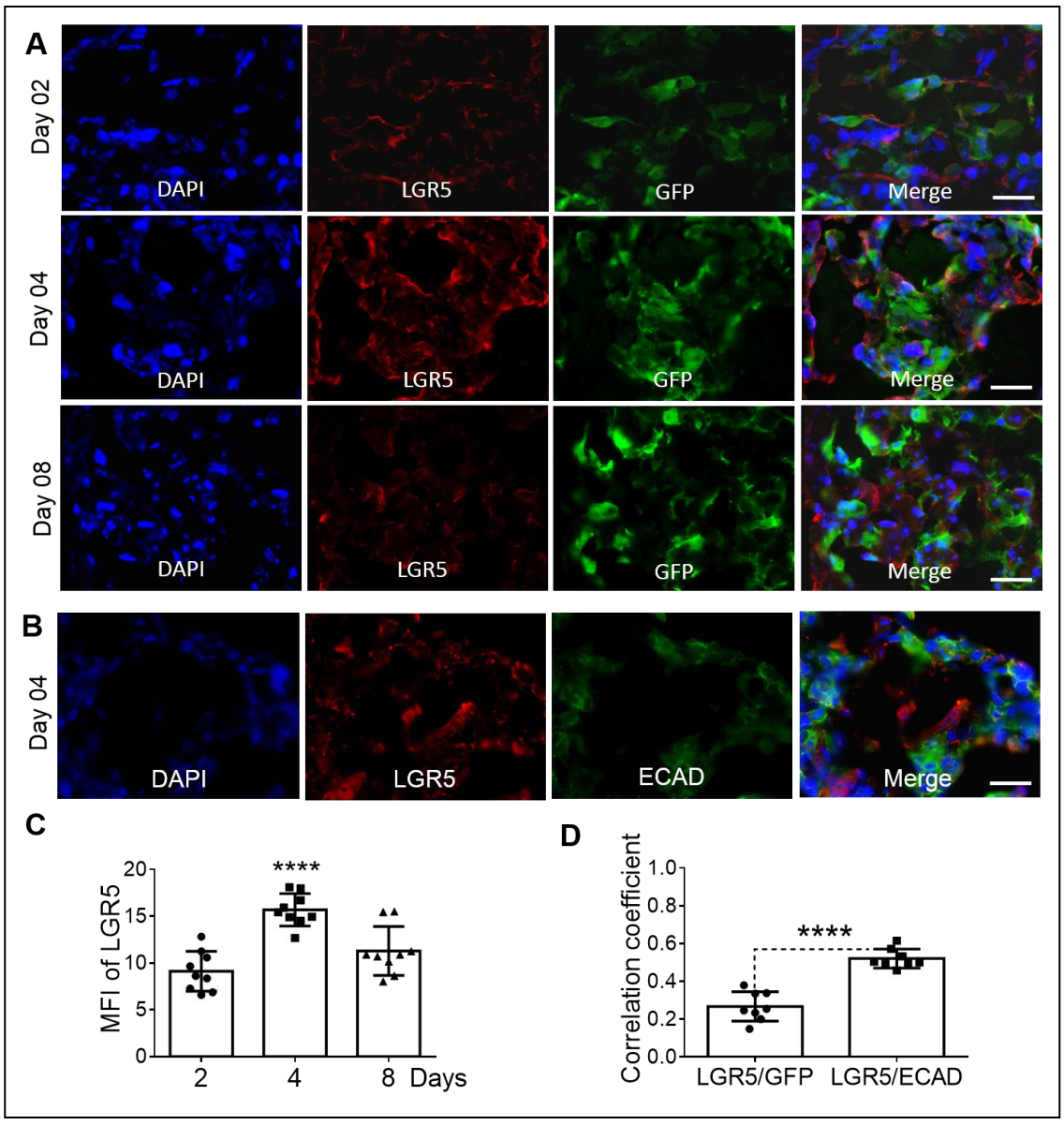

Figure 3.21 Expression of LGR5 in AM 3D-organoids derived from AM epithelial cells and AM-MSCs. A AM-1 cells were mixed with AM-MSCs (with GFP) in cell ratio 2:1, and transferred to 3D Matrigel ($4x10^4$ cells/μl Matrigel) and the organoids were harvested on day 2, 4 and 8. The expression of LGR5 was higher on day 4 while compared with day 2 and day 8. Scale bars, 20μm. **B** Day 4 organoids derived from AM-1 cells and AM-MSCs (without GFP). The immunofluorescence study showed the majority of LGR5 signal was colocalized with E-cadherin (ECAD). Scale bars, 20μm. **C** The quantification of the mean fluorescence intensity of the expression of LGR5 in the AM organoids on day2, day4 and day8. Mean ± SD, one-way ANOVA. ****p<0.0001. **D** The quantification of correlation coefficient of the expression of LGR5 and GFP; LGR5 and ECAD in the day 4 AM organoids. Mean ± SD, two-tailed unpaired Student's t-tests. ****p<0.0001. All results are representative of two independent experiments.

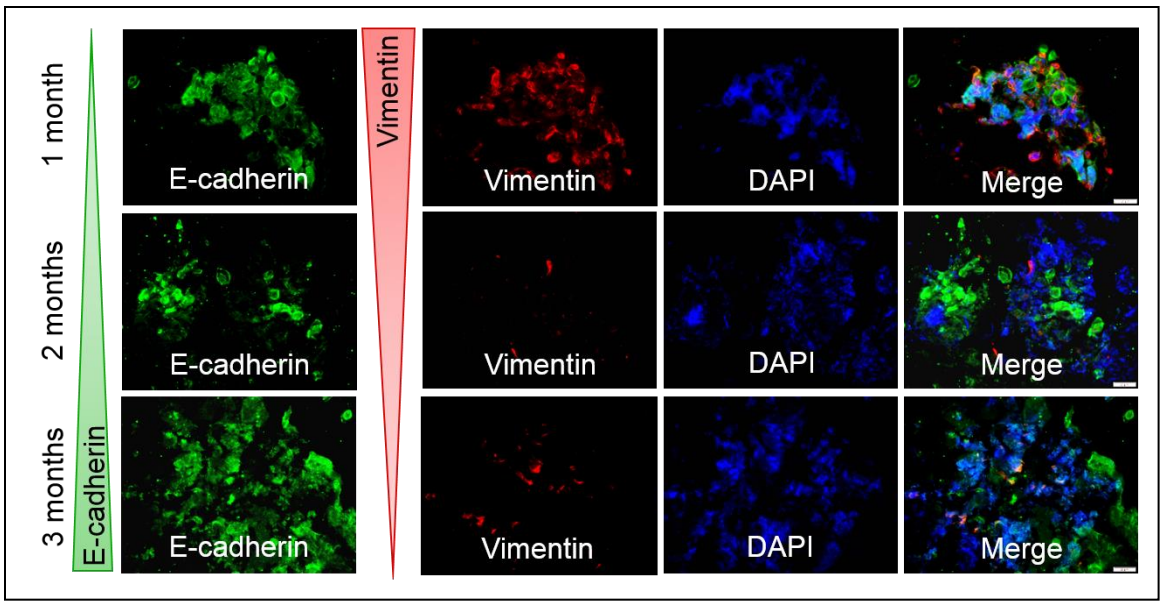

Figure 3.22 Loss of MSC-related gene (vimentin) expression in long-term AM-organoid culture. AM epithelial cells (follicular type) mixed with AM-MSCs in 3D organoid culture for 3 months. During the 3D-organoid culturing, the epithelial marker (E-cadherin) was increased, but the EMT marker (vimentin) was decreased. Scale bars, 20μm. This long-term observation was performed once.

3.10 AM-MSC derived secretomes promote the formation of LGR5^{+} AM-EpiSC *in vivo*

To identify whether the AM-MSCs promote the generation of LGR5^{+} AM-EpiSCs in vivo, AM epithelial cells (parental, sorted LGR5^{-} and sorted LGR5^{+}) were mixed with AM-MSCs in 1:1 ratio, respectively, and cultured in Matrigel for three weeks. Then the organoids with Matrigel were implanted into the flank of nude mice (n=3 for each group) (Figure 3.23 A). After two weeks, the xenografts were harvested and embedded in OCT for frozen section. Interestingly, the organoid xenografts with LGR5^{-} AM epithelial cells alone could not survive *in vivo* (Figure 3.12 B), but LGR5^{-} AM epithelial cells mixed with AM-MSCs could form tumor-like structures (Figure 3.23 B) similar to those formed by parental AM epithelial cells or LGR5^{+} AM-EpiSCs mixed with AM-MSCs as shown by H & E staining. In addition, dual-color immunofluorescence studies showed colocalized expression of human LGR5 and proliferating cell nuclear antigen (PCNA) in tumor-like structures formed by all groups of AM epithelial cells mixed with AM-MSCs (Figure 3.23 C and D). Collectively, these findings suggest that AM-MSCs can promote the formation of LGR5^{+} AM-EpiSCs both *in vitro* and *in vivo* through their secretomes.

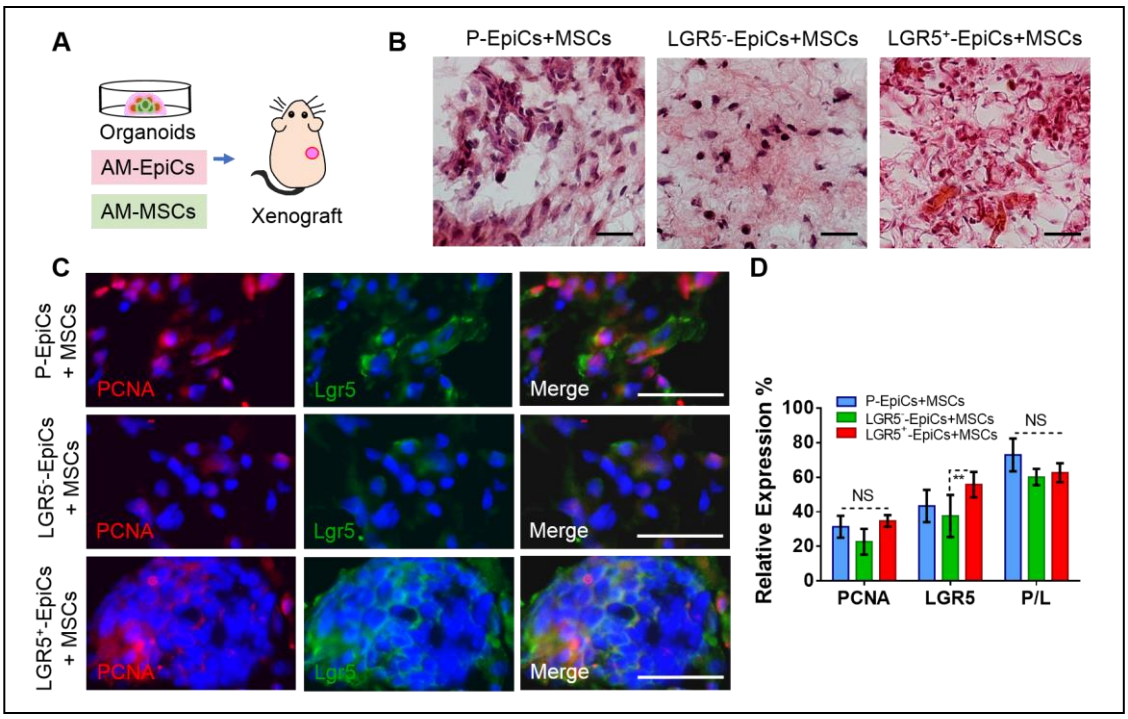

Figure 3.23 AM-MSC promote the subpopulation of LGR5$^+$ AM-EpiSC *in vivo*. A The diagram showing the subcutaneous nude mice model using *ex vivo* organoids derived from the mixture of AM epithelial cells and AM-MSCs. Following culturing in 3D Matrigel for three weeks, the ex vivo organoids formed by AM epithelial cells (parental, sorted LGR5$^+$ or LGR5$^-$) mixed with AM-MSCs were harvested and subcutaneously transplanted into the flank of nude mice. **B** Two weeks post-transplantation, the tumor-like structures formed in nude mice were harvested for histological analysis by H & E staining. The group of LGR5$^-$ AM epithelial cells with AM-MSCs could generate some similar tumor-like structures as the groups of LGR5$^+$/ parental with AM-MSCs. Scale bars, 20μm. **C** Co-expression of LGR5 and proliferating cell nuclear antigen (PCNA) in xenografted tumor-like structures formed by transplanted LGR5$^-$ AM epithelial cells with AM-MSCs and parental epithelial cells/ LGR5$^+$ AM-EpiSCs with MSCs as determined by immunofluorescence studies. Scale bars, 100μm. **D** The quantification of relative expression of PCNA, LGR5 and PCNA/LGR5 (P/L) from the results shown in (**C**). Mean ± SD (n=4 in each group, each group was measured 5 different random areas under the microscope, two-tailed unpaired Student's *t*-test. NS=not significant).

CHAPTER 4: DISCUSSIONS AND CONCLUSIONS

4.1 The intermediate EMT stem-like LGR5^{+} epithelial cells in ameloblastoma

Most solid tumors are composed of heterogeneous populations of tumor cells with subpopulations endowed with increased self-renewal and tumor repropagating capabilities termed cancer stem cells (CSCs) or tumor initiating cells (TICs)[19]. To date, a panel of cell surface molecules such as CD133, CD44, epithelial cell-adhesion molecule (EpCAM), CD166, CD151, etc., has been utilized for identification of CSCs in distinct types of cancer[19,72]. LGR5, upon binding with R-spondins, triggers the activation of downstream Wnt/β-catenin signaling pathway[25], and has also been used as a putative marker for CSCs in several types of cancers[29-34]. However, like other adult stem cells, no single molecule can serve as an exclusive marker for a specialized CSC compartment. Multiple markers alone or in combination with ALDH enzyme activity and/or the expression of stemness-regulatory genes, like OCT4, Nanog, and SOX2, have been utilized to identify a special CSC subpopulation in different tumors[72]. In the last decade, the critical role of CSCs or TICs in tumorigenesis, progression and therapeutic relapse has been extensively explored and CSC-targeting therapies are emerging as novel strategies in therapeutics of various cancers[19,20]. However, up to date, limited work has been done to explore the potential role of tumor stem cells in the pathogenesis and therapy of various benign tumors of jaw bones, including the most common type of odontogenic benign, yet most aggressive and

devastating tumor, ameloblastoma. Developmentally, ameloblastoma may have possibly derived from remnants of odontogenic epithelium, the migrating epithelium at the cervical loop, and lining of odontogenic cyst[36,37], while LGR5 has been well recognized as putative marker for odontogenic epithelial stem cells[38-41]. Herein, this study demonstrated that different subtypes of solid ameloblastoma (AM) tissues harbored a subpopulation of $LGR5^+$ epithelial cells co-expressing stemness-related genes such as active β-catenin (ABC), OCT4 and ALDH1 as well as EMT-related genes such as ZEB1 and fibronectin, all of which were significantly increased in isolated epithelial cells (AM-EpiSCs) when cultured under 3D spheroid-forming conditions (Figure 3.1-3.8). Meanwhile, purified $LGR5^+$ AM epithelial cells displayed enhanced capacities to form 3D-spheroid *in vitro* and to generate tumor-like structures *in vivo* (Figure 3.6, 3.8 and 3.12-3-14). These findings support the hypothesis that $LGR5^+$ epithelial cells in ameloblastoma (AM) represent a subpopulation of epithelial tumor stem-like cells ($LGR5^+$ AM-EpiSCs) harboring an intermediate EMT phenotype, which may contribute to the pathogenesis and recurrence of this benign/yet aggressive odontogenic tumor.

$BRAF^{V600E}$ mutation has been implicated in the progression of several types of carcinoma by RAS-independent activation of MEK/ERK signaling pathways[73]. This mutation has also been reported in about 46-82% of AM cases[7-12], but it has no relation to the high recurrence of AM. To date, several small molecular inhibitors that specifically target $BRAF^{V600E}$ mutation have been developed as therapeutic drugs for cancers with this mutant, but the development of intrinsic

and acquired resistance to these drugs has become an ongoing challenge for the treatment of these cancer patients[73]. Currently, an active clinical trial (NCT02367859) is undergoing with the combinatory use of Dabrafenib and Trametinib in the treatment of AM, but the clinical outcome is still unknown. In the present study, the 3D-organoid platform generated by AM epithelial cells were utilized to evaluate their response to treatment with Vemurafenib (PLX4032), a selective inhibitor of $BRAF^{V600E}$ mutation. Even though PLX4032 interfered with the cell viability and organoid formation by AM epithelial cells, it simultaneously enriched the proportion of $LGR5^{+}$ AM-EpiSCs with EMT phenotype and enhanced capacity for organoid formation (Figure 3.15-3.17). Previous study also showed increased LGR5 positive cells in colorectal xenograft after BRAF inhibitor treatment[74]. These findings suggest that $LGR5^{+}$ AM-EpiSCs are resistant to a selective $BRAF^{V600E}$ inhibitor and the 3D-organoids derived from AM epithelial cells could be a helpful platform to further screen small molecules that can specifically target $LGR5^{+}$ AM-EpiSCs and treat one of the most aggressive benign tumors of the jaw bones.

4.2 Establishment of 3D-organoid culture for tumor study

Traditional two-dimensional (2D) monolayer cell culture has long been a mainstay in the field of biomedical research. However, it is a great challenge to maintain the intrinsic cell properties and retain the molecular and epigenetic repertoire due to the lack of supporting niche factors. In recent years, 3D-organoid culture is emerging as a novel approach in cell biology, particularly in

stem cell research and cancer cell biology, which enables modeling the tumor microenvironment and maintaining the major genetic and phenotypic features of individual tumors in an efficient and cost-effective manner[49,69,71]. Organoid and spheroid cultures allow for better modeling cell behaviors in a recapitulating *in vivo*-like natural tumor microenvironment such as cell-cell interactions, hypoxia, pH gradients, extracellular matrix, and different profile of bioactive molecules[50]. For instance, the cell-cell and cell-ECM interactions and cell geometry in 3D culture can increase self-renewal ability and the expression of stem cell-related genes, such as OCT4 and Nanog[75-77], thus allowing for maintenance and expansion of normal and cancer stem cells[50]. Under most conditions, 3D organoid cultures require mouse-derived extracellular matrix (ECM) substitutes with variant stiffness or rigidity e.g. Matrigel or basement membrane extract, which may affect the outcome of experiments[49]. Most recently, mechanically and chemically defined hydrogel matrices with controllable substrate stiffness and rigidity have been developed for organoid culture of patient-derived colorectal tumors[78]. In the present study, mouse-derived ECM were utilized for AM organoid culture, which led to maintenance and expansion of $LGR5^+$ AM-EpiSCs (Fig. 3.11). However, further studies are warranted to explore the mechanisms whereby mechanical properties of ECM and other factors enhance the self-renewal and expansion of this subpopulation of AM-EpiSCs.

In addition, organoids can be used, to certain degrees, as preclinical alternative models to animal models because they can reduce experimental

complexity, allow real-time imaging and high-throughput screening, and enable the study of diseases that are not easily and accurately modelled in animals[48]. To date, numerous organoids have been reported for various types of cancers for multiple purposes, e.g. disease modeling, mechanistic study, biobanking, drug screening, prediction of treatment response, and so on[49,69,71]. However, much less work has been done to develop an organoid platform to model a benign tumor even though it is usually challengeable to establish an appropriate animal model for most types of benign tumors. This study demonstrated for the first time the feasibility to generate 3D organoid structures of human ameloblastoma by using AM epithelial cells with or without AM-MSCs, which recapitulated the histopathological features and LGR5 expression profile of distinct subtypes of solid ameloblastoma and could be passaged and cryopreserved (Figure 3.11 and 3.19-3.21). Interestingly, in the 3D-orgnoid model derived from both AM epithelial cell and AM-MSCs, the MSC markers were losing during long-term culture (Figure 3.22), and the similar finding was reported that only epithelial markers were detected in patient derived organoids from other tissues including head and neck cancers[79]. In the transplanted organoid xenograft model, the $LGR5^+$ AM-EpiSCs had propagating ability and could generated some tumor-like structures. However, it is noteworthy that, even though a short-term subcutaneous transplantation of AM 3D-organoids into nude mice led to xenograft formation (Fig. 3.12-3.14), demonstrating the self-renewal and propagating capabilities of $LGR5^+$ EpiSCs *in vivo*, this study still cannot establish an appropriate animal model for long-term observation of the role of this unique subpopulation of

epithelial stem-like cells in the initiation and progression of AM, a common challenge for most types of benign tumors due to their intrinsically benign and slow progression properties.

4.3 The reciprocal crosstalk of tumor microenvironment and tumor stem cells

To date, several hypotheses have been proposed on different origins of CSCs in individual tumors, such as normal tissue stem and progenitor cells, the more differentiated somatic cells, and lineage infidelity switching triggered by microenvironmental stress signals[19,80]. Accumulating evidence support the notion that CSCs represent a dynamic or plastic status, whereby tumor cells can convert or reprogram between stem and non-stem cell state or phenotype due to the signals they encounter within the tumor microenvironment (TME), e.g. chronic inflammation and therapeutic insults[19,22]. The dynamic bidirectional phenotypic conversion between non-CSCs and CSCs may contribute to the development of heterogeneity of CSCs, e.g. distinct quiescence, therapeutic sensitivity, and capabilities for EMT, invasion, and metastasis[19,22]. EMT is a complex reprogramming process through which epithelial cells acquire a mesenchymal or epithelial/mesenchymal hybrid cell phenotype, which plays an important role in regulating plasticity of CSCs[21-23]. A large panel of growth factors, cytokines, chemokines and other stimuli within the tumor microenvironment can trigger epithelial tumor cells to undergo EMT and acquire stem cell properties[72]. In the present study, R-spondin 2 could stimulate the proliferation and induce

EMT in ameloblastoma epithelial cells (AM epithelial cells) was showed, suggesting that LGR5/R-spondin 2 may functionally contribute to the development and maintenance of the hybrid EMT phenotype of ameloblastoma epithelial stem-like cells (AM-EpiSCs). Most recently, this study have shown that ameloblastoma mesenchymal stromal cells (AM-MSCs) promote EMT and increase the expression of certain stemness-regulatory genes in AM epithelial cells through their secretion of interleukin (IL)-6[24]. In this study, to elucidate the role of AM-MSCs in regulating the plasticity and homeostasis of $LGR5^+$ AM-EpiSCs, the AM-MSC derived conditioned medium was utilized to stimulate the AM epithelial cells. The results showed the AM-MSC derived secretomes/EVs enhanced the expression of EMT markers (active β-catenin and fibronectin) and contributed to the subpopulation of $LGR5^+$ AM-EpiSCs (Figure 3.18). Of note, the AM-MSC derived EVs may play partial role to promote the EMT process of AM epithelial cells, and the EV dependent and independent effects on AM epithelial cells are warranted to define in future studies. Besides, the AM-MSCs promoted the $LGR5^-$ AM epithelial cells to form some tumor-like structures and increased the subpopulation of $LGR5^+$ cells in nude mice as the parental and $LGR5^+$ groups that implicated AM-MSCs could maintain the homeostasis of $LGR5^+$ AM-EpiSCs *in vivo* (Figure 3.23). These results support the hypothesis that AM-MSCs contribute to the homeostasis of $LGR5^+$ AM-EpiSCs, however, further studies are needed in an appropriate animal model for long-term observation to demonstrate the roles of stromal cells in the homeostasis of $LGR5^+$ stem-like cells in AM.

4.4 Limitations and future directions

The major limitation of this study is limited resource of fresh samples. Therefore, AM cell lines were utilized to validate the results of the primary cells and for mechanism studies. However, cell lines may undergo chromosomal rearrangements/duplications or mutations, and epigenetic changes that make cell lines could not recapitulate the primary tumor behaviors[51,52]. In the future, we would like to collaborate with multicenter in the USA and worldwide, such as China and Taiwan, to establish a cell/tissue bank of ameloblastoma. After establishing the AM cell/tissue bank, we want to create a patient derived organoid platform and animal models for small molecular screenings and further mechanistic studies.

This study demonstrated that AM-MSC derived secretomes maintain the homeostasis of $LGR5^+$ AM-EpiSCs. In future non-surgical adjuvant therapeutic studies, directly targeted inhibition of LGR5 and blockage of the microenvironment factors that promote the homeostasis of $LGR5^+$ AM-EpiSCs serve novel approaches for this aggressively benign jaw tumor. Hence, it is vital to dissect major factors of AM-MSC derived secretomes or EVs that govern the EMT process and stem cell properties in $LGR5^+$ AM epithelial cells, and we will define stroma derived EV dependent and independent effects on AM epithelial cells. First, AM-MSC derived EVs and characterize its size, markers and interactions with AM epithelial cells will be isolated. Secondly, we will determine and compare the major components, such as R-spondin, IL-6 and PGE2, of AM-MSC derived EVs and non-EVs by microarray analysis. We will identify whether

these defined major factors can promote the EMT process and stem cell properties in LGR5$^+$ AM-EpiSCs and promote the formation of LGR5$^+$ AM-EpiSCs. Finally, elusive molecular mechanisms of these defined major factors from stroma derived EVs and non-EVs that govern the EMT process and stem cell properties in LGR5$^+$ AM-EpiSCs will be determined.

In addition, the *ex vivo* 3D organoid models are possible for quick drug screening, but limited in a short-term culturing, that obstructs further mechanistic studies. To supply consistent nutrition and mimic the physiological microenvironment, we will optimize the *ex vivo* culture condition and the *in vivo* subcutaneous organoid model and hope to develop an intraosseous organoid model in the jaw of nude mice for mechanistic and therapeutic intervention studies.

4.5 Clinically relevant and conclusion

In conclusion, this is the first study to identify a subpopulation of LGR5$^+$ epithelial cells endowed with tumor stem-like cell properties and intermediate EMT phenotype in solid AM (LGR5$^+$ AM-EpiSCs), which may play an important role in its pathogenesis and recurrence. In addition, this study established conditions for generation of 3D AM-organoids which recapitulate certain degree of different histological subtypes of AM, thus allowing us to generate 3D AM organoids by directly using both biopsy and final excisional tissues from AM in the future. In the short term, the human AM 3D-organoids may be utilized as a platform for further mechanistic studies and screening small molecules that can

specifically target LGR5^{+} AM-EpiSCs due to the lack of an animal model for AM. In the long run, further studies are warranted to optimize the conditions for generation and transplantation of 3D AM-organoids in order to generate a consistent animal model of AM for deep mechanistic and interventional studies *in vivo*.

APPENDIX I: Supplemental data of Western blots

Figure 3.3 C

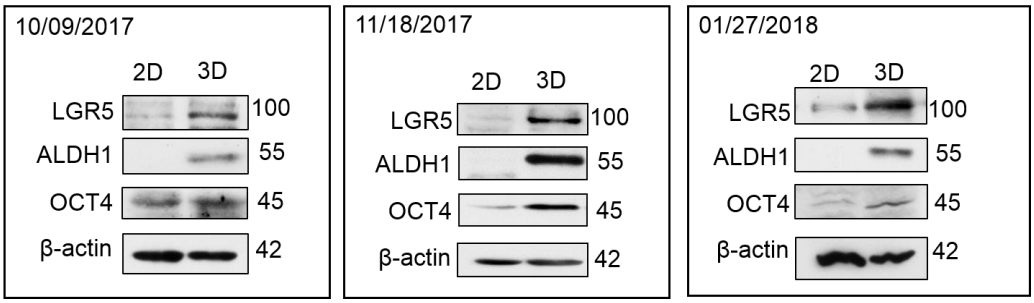

Figure 3.6 E

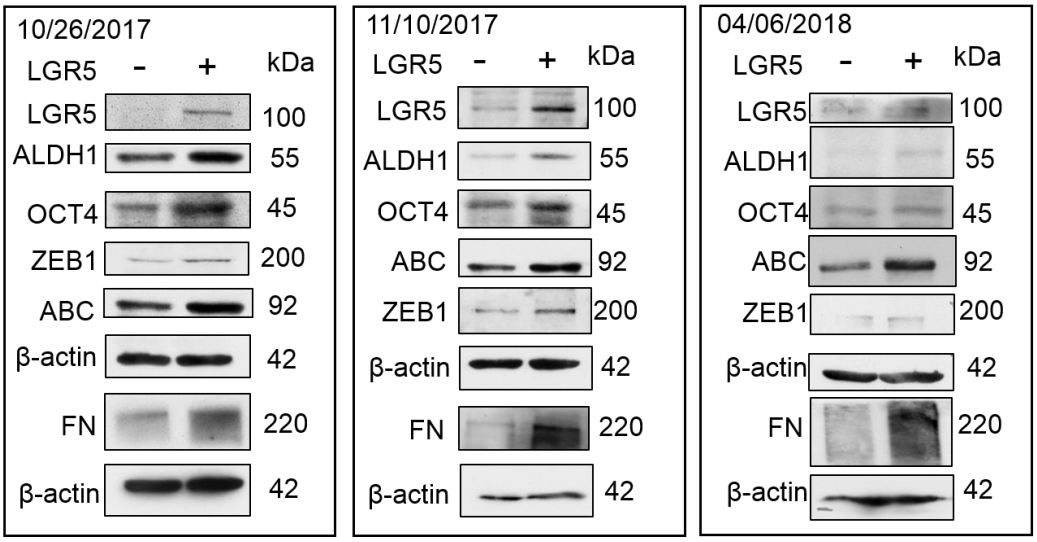

Figure 3.8 D

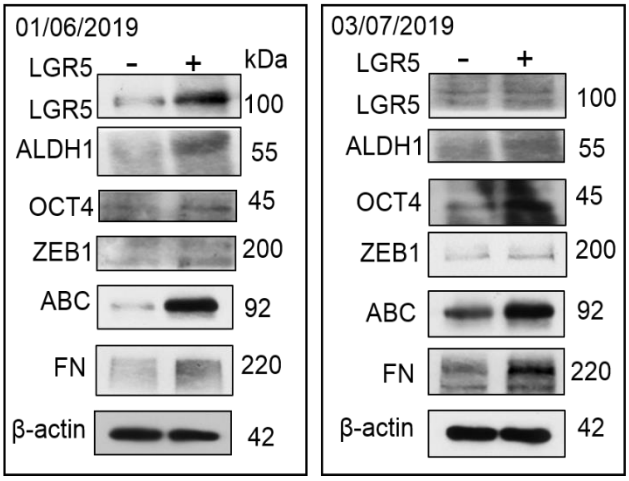

Figure 3.9 B

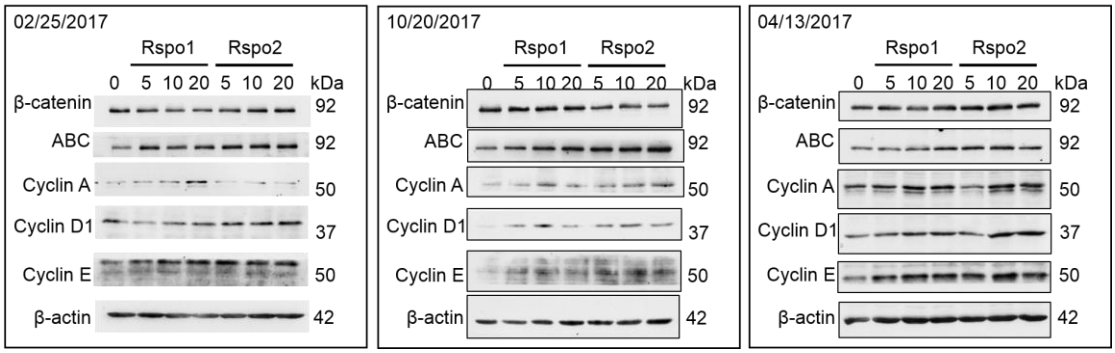

Figure 3.10 A

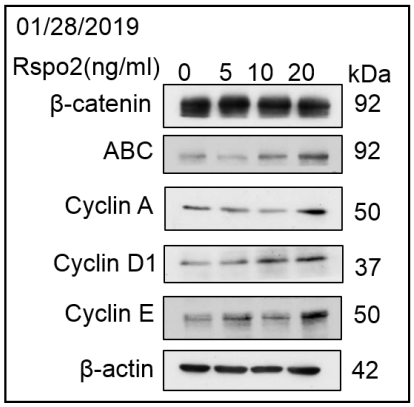

Figure 3.10 C

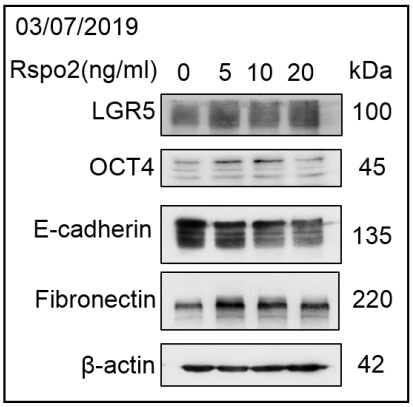

Figure 3.17 A

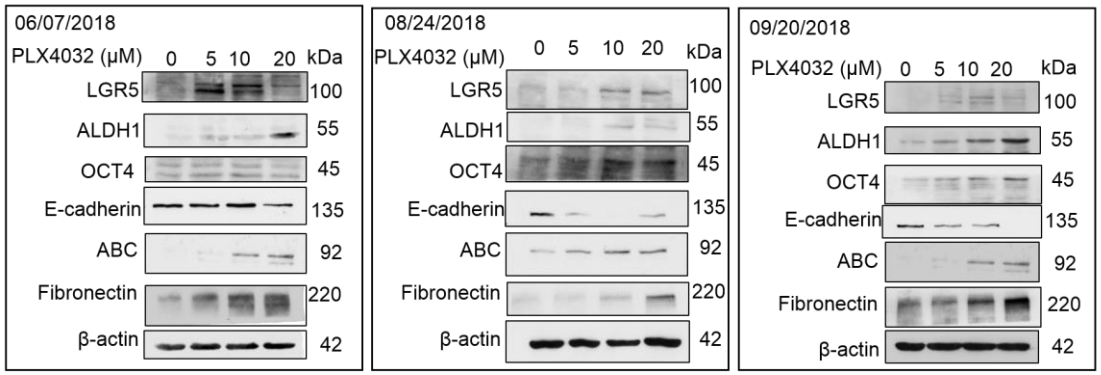

Figure 3.17 B

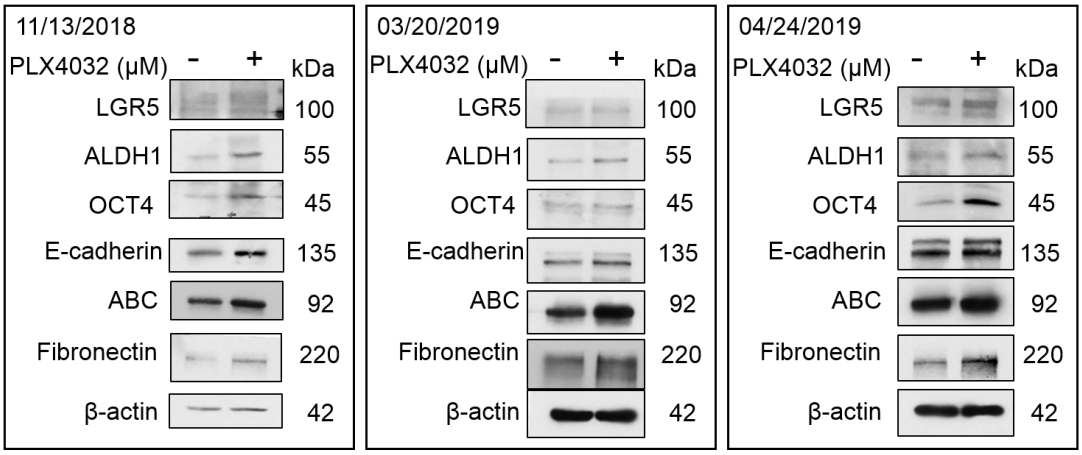

Figure 3.18 B

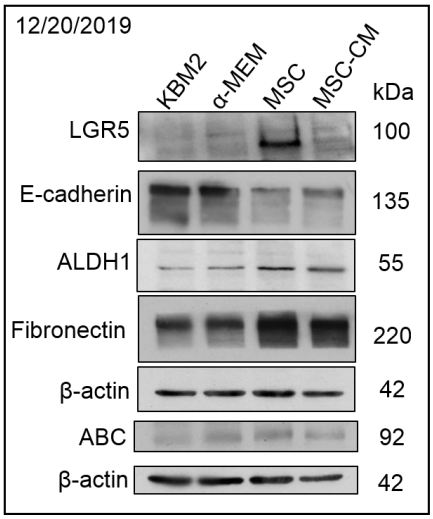

Figure 3.18 G

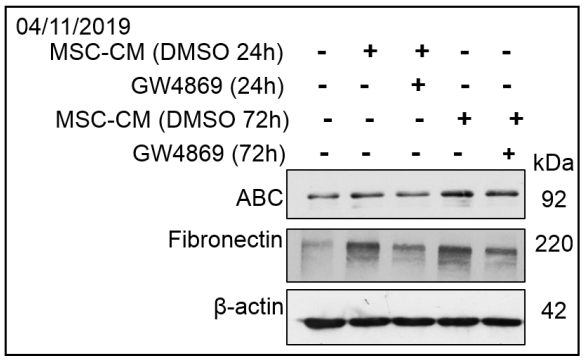

Figure 3.18 E

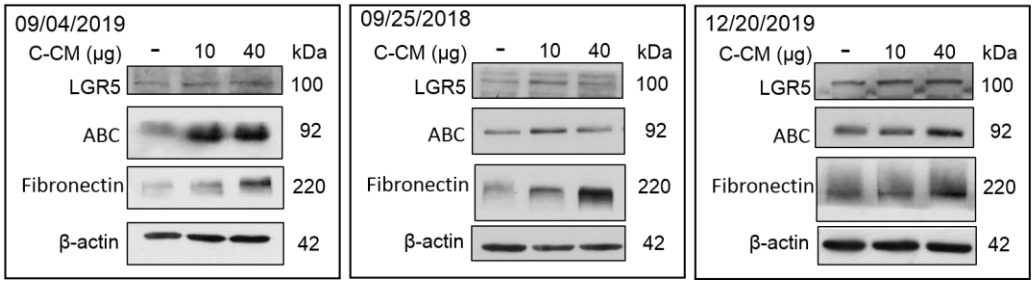

APPENDIX II: Negative controls of

Immunohistochemical and immunofluorescence studies

Figure 3.1 A and B

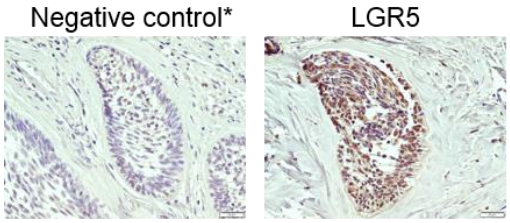

Figure 3.2

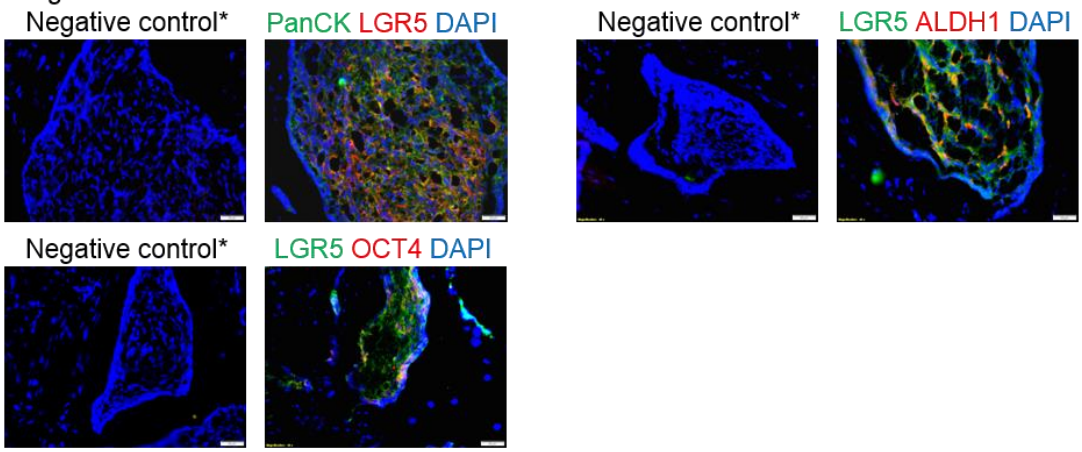

Figure 3.3 B

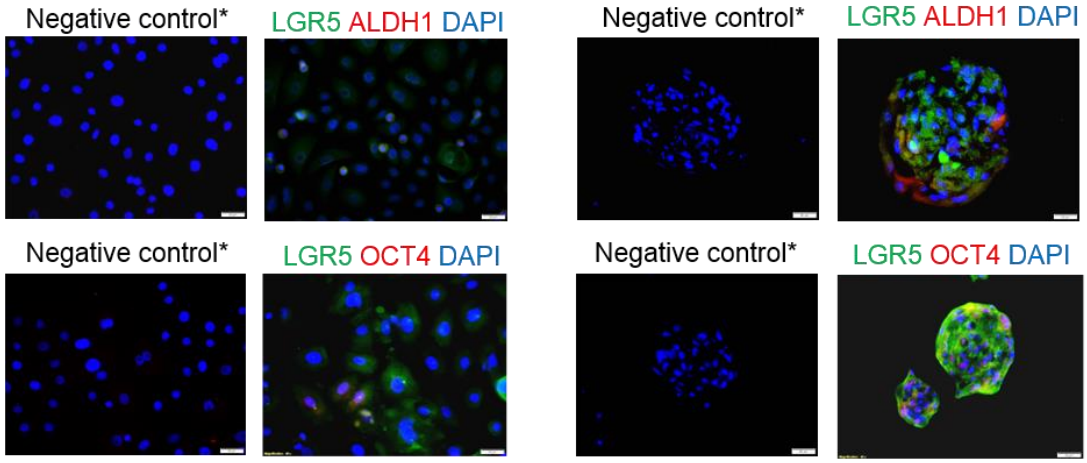

*The negative control was representative of images whereby sections or cells were incubated at 4 degree overnight with the appropriate isotype-matched negative control IgG with an equal concentration of the match primary antibody, followed by incubation with the corresponding secondary antibody as described in Materials & Methods.

Figure 3.6 C

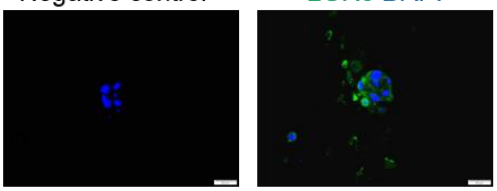

Figure 3.6 F and Figure 3.7

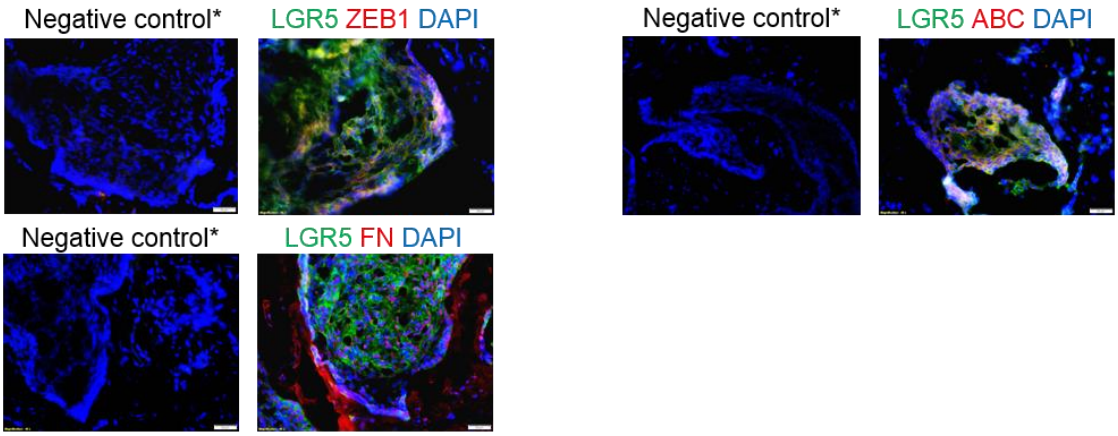

Figure 3.9 C

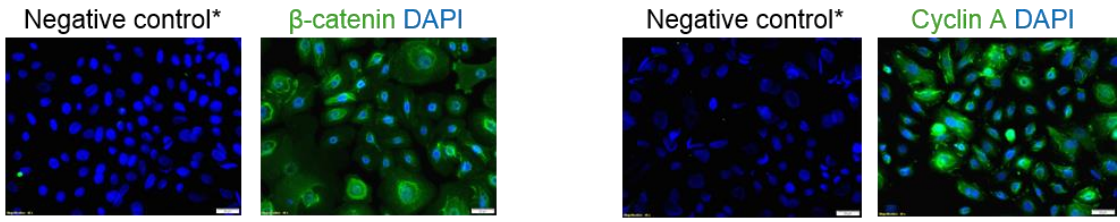

Figure 3.11 B and C

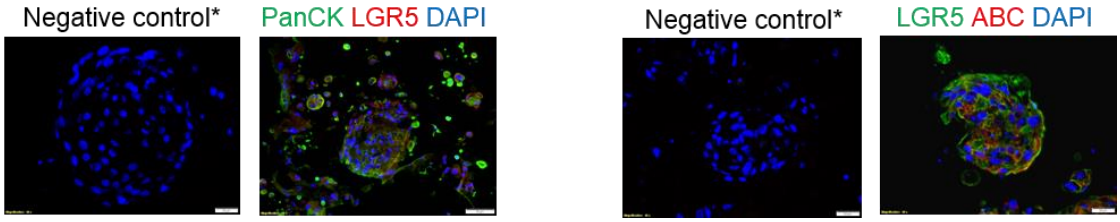

*The negative control was representative of images whereby sections or cells were incubated at 4 degree overnight with the appropriate isotype-matched negative control IgG with an equal concentration of the match primary antibody, followed by incubation with the corresponding secondary antibody as described in Materials & Methods.

Figure 3.12 C and D, 3.13

Negative control* LGR5 h-mitochondria

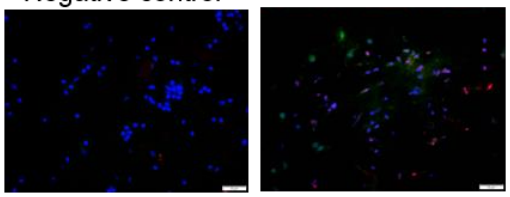

Negative control* LGR5 ZEB1

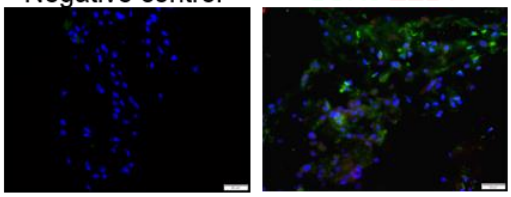

Figure 3.14 E

Negative control* LGR5 PCNA

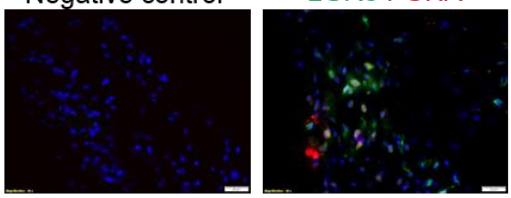

Figure 3.15 C and 3.16

Negative control* LGR5 DAPI

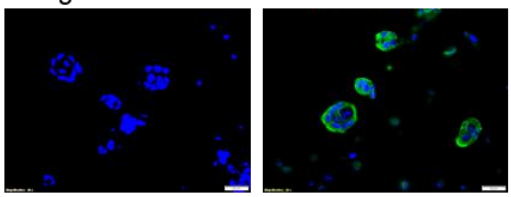

Figure 3.17 D

Negative control* LGR5 DAPI

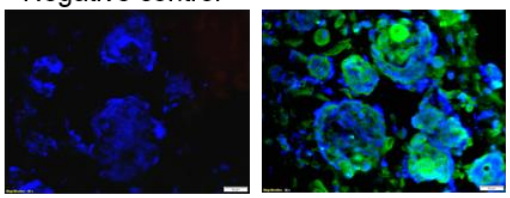

Figure 3.20 C. 3.21 A and B

Negative control* ECAD GFP DAPI

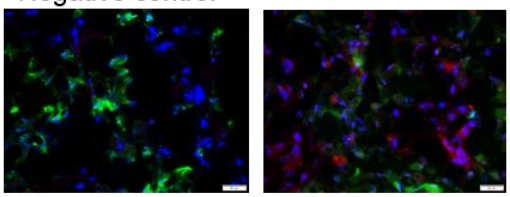

Negative control* Vimentin GFP DAPI

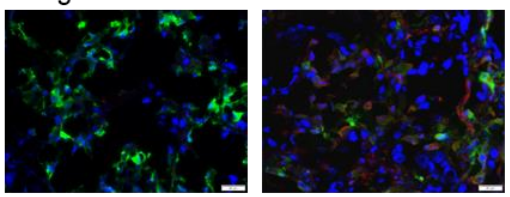

Figure 3.22

Negative control* ECAD Vimentin DAPI

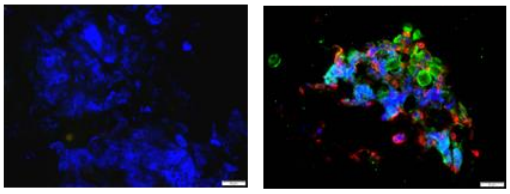

Figure 3.23 C

Negative control* LGR5 PCNA DAPI

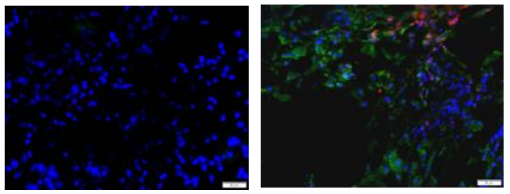

*The negative control was representative of images whereby sections or cells were incubated at 4 degree overnight with the appropriate isotype-matched negative control IgG with an equal concentration of the match primary antibody, followed by incubation with the corresponding secondary antibody as described in Materials & Methods.

APPENDIX III: Measurement of coefficient

In this study, the coefficient of two channels in the immunofluorescence study was processed by the CellProfiler software, and one demo is presented below.

1. Load images

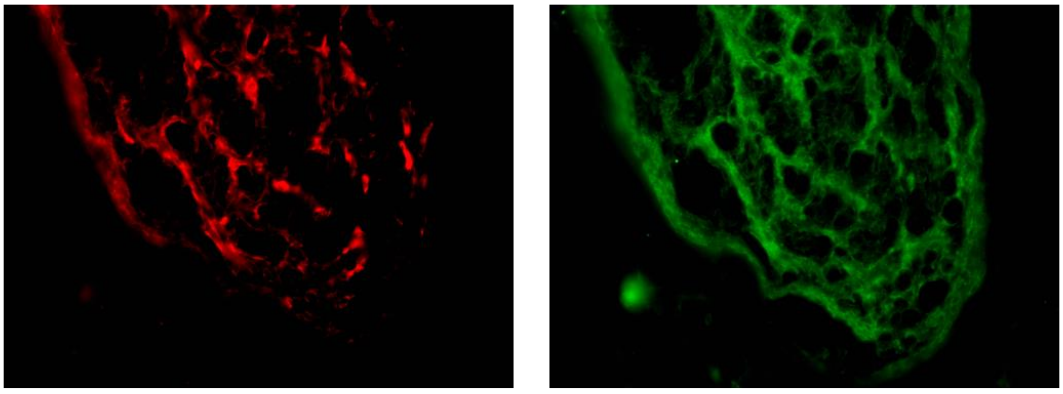

2. Correct illumination-calculate

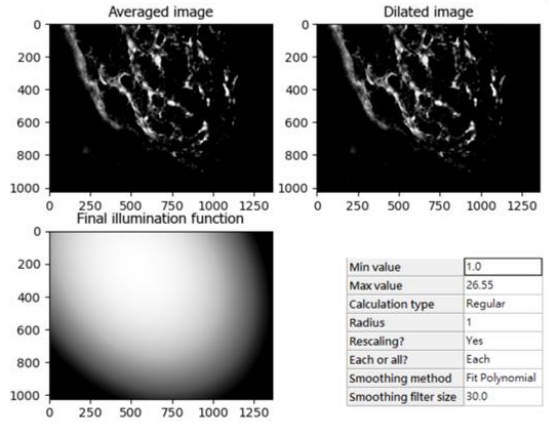

Min value	1.0
Max value	26.55
Calculation type	Regular
Radius	1
Rescaling?	Yes
Each or all?	Each
Smoothing method	Fit Polynomial
Smoothing filter size	30.0

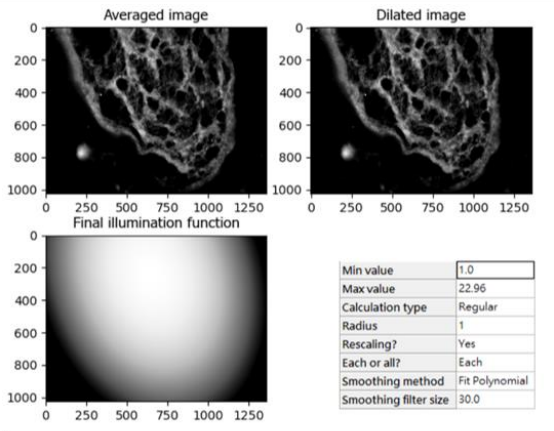

Min value	1.0
Max value	22.96
Calculation type	Regular
Radius	1
Rescaling?	Yes
Each or all?	Each
Smoothing method	Fit Polynomial
Smoothing filter size	30.0

3.Correct Illumination-Apply

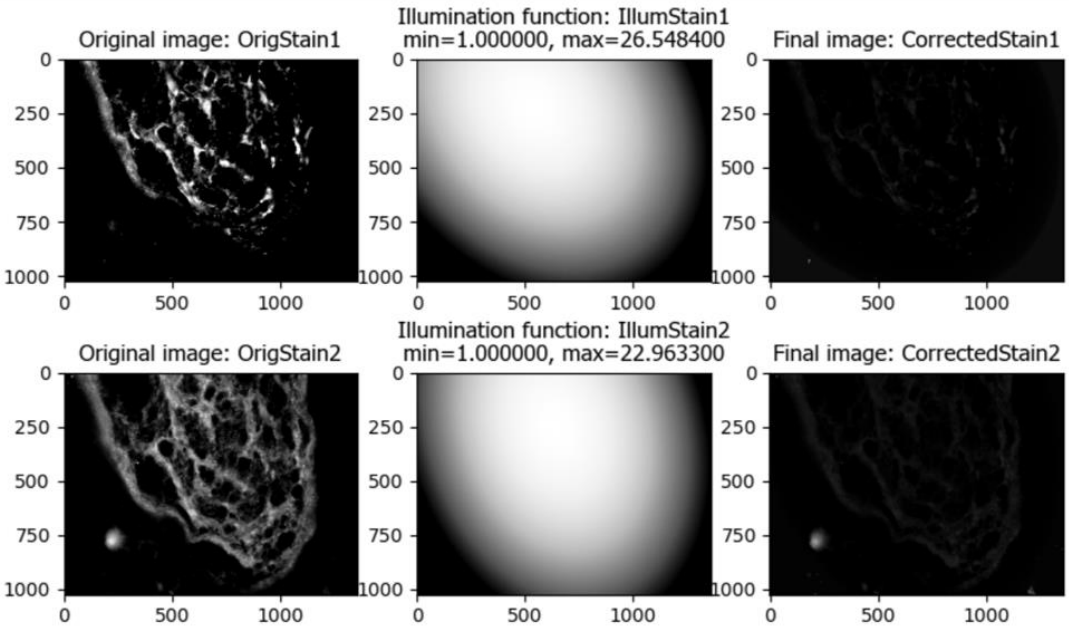

4. Align

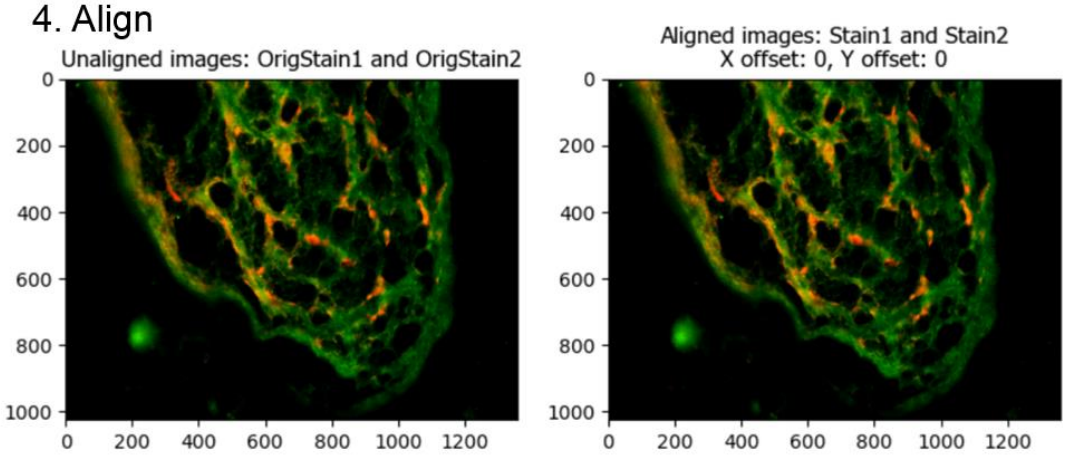

5. Measure correlation

First image	Second image	Objects	Measurement	Value
Stain1	Stain2	-	Correlation	0.677
Stain1	Stain2	-	Slope	2.306
Stain1	Stain2	-	Manders Coefficient	0.982
Stain2	Stain1	-	Manders Coefficient	0.500
Stain1	Stain2	-	RWC Coefficient	0.834
Stain2	Stain1	-	RWC Coefficient	0.406
Stain1	Stain2	-	Manders Coefficient (Costes)	1.000
Stain2	Stain1	-	Manders Coefficient (Costes)	0.610
Stain1	Stain2	-	Overlap Coefficient	0.900

BIBLIOGRAPHY

1 Effiom, O. A., Ogundana, O. M., Akinshipo, A. O. & Akintoye, S. O. Ameloblastoma: current etiopathological concepts and management. *Oral diseases*, doi:10.1111/odi.12646 (2017).

2 McClary, A. C. *et al.* Ameloblastoma: a clinical review and trends in management. *Eur Arch Otorhinolaryngol* **273**, 1649-1661, doi:10.1007/s00405-015-3631-8 (2016).

3 EI-Naggar A.K., C. J. K. C., Grandis J.R., Takata T., Slootweg P.J. *WHO Classification of Head and Neck Tumors* 4th edn, 215-218 (2017).

4 Hendra, F. N. *et al.* Global incidence and profile of ameloblastoma: A systematic review and meta-analysis. *Oral Dis*, doi:10.1111/odi.13031 (2019).

5 Peacock, Z. S., Ji, Y. D. & Faquin, W. C. What Is Important for Confirming Negative Margins When Resecting Mandibular Ameloblastomas? *J Oral Maxillofac Surg* **75**, 1185-1190, doi:10.1016/j.joms.2016.11.016 (2017).

6 Pogrel, M. A. & Montes, D. M. Is there a role for enucleation in the management of ameloblastoma? *Int J Oral Maxillofac Surg* **38**, 807-812, doi:10.1016/j.ijom.2009.02.018 (2009).

7 Brown, N. A. *et al.* Activating FGFR2-RAS-BRAF mutations in ameloblastoma. *Clin Cancer Res* **20**, 5517-5526, doi:10.1158/1078-0432.CCR-14-1069 (2014).

8 Sweeney, R. T. *et al.* Identification of recurrent SMO and BRAF mutations in ameloblastomas. *Nat Genet* **46**, 722-725, doi:10.1038/ng.2986 (2014).

9 Kurppa, K. J. *et al.* High frequency of BRAF V600E mutations in ameloblastoma. *J Pathol* **232**, 492-498, doi:10.1002/path.4317 (2014).

10 Diniz, M. G. *et al.* Assessment of BRAFV600E and SMOF412E mutations in epithelial odontogenic tumours. *Tumour Biol* **36**, 5649-5653, doi:10.1007/s13277-015-3238-0 (2015).

11 Gultekin, S. E. *et al.* The landscape of genetic alterations in ameloblastomas relates to clinical features. *Virchows Arch* **472**, 807-814, doi:10.1007/s00428-018-2305-5 (2018).

12 Soltani, M. *et al.* Genetic study of the BRAF gene reveals new variants and high frequency of the V600E mutation among Iranian ameloblastoma patients. *J Oral Pathol Med* **47**, 86-90, doi:10.1111/jop.12610 (2018).

13 Yao, Z. *et al.* Tumours with class 3 BRAF mutants are sensitive to the inhibition of activated RAS. *Nature* **548**, 234-238, doi:10.1038/nature23291 (2017).

14 Kaye, F. J., Ivey, A. M., Drane, W. E., Mendenhall, W. M. & Allan, R. W. Clinical and radiographic response with combined BRAF-targeted therapy in stage 4 ameloblastoma. *J Natl Cancer Inst* **107**, 378, doi:10.1093/jnci/dju378 (2015).

15 Faden, D. L. & Algazi, A. Durable treatment of ameloblastoma with single agent BRAFi Re: Clinical and radiographic response with combined BRAF-targeted therapy in stage 4 ameloblastoma. *J Natl Cancer Inst* **109**, doi:10.1093/jnci/djw190 (2017).

16 Tan, S., Pollack, J. R., Kaplan, M. J., Colevas, A. D. & West, R. B. BRAF inhibitor treatment of primary BRAF-mutant ameloblastoma with pathologic assessment of response. *Oral Surg Oral Med Oral Pathol Oral Radiol* **122**, e5-7, doi:10.1016/j.oooo.2015.12.016 (2016).

17 Fernandes, G. S., Girardi, D. M., Bernardes, J. P. G., Fonseca, F. P. & Fregnani, E. R. Clinical benefit and radiological response with BRAF inhibitor in a patient with recurrent

ameloblastoma harboring V600E mutation. *BMC Cancer* **18**, 887, doi:10.1186/s12885-018-4802-y (2018).

18 Brunet, M., Khalifa, E. & Italiano, A. Enabling Precision Medicine for Rare Head and Neck Tumors: The Example of BRAF/MEK Targeting in Patients With Metastatic Ameloblastoma. *Front Oncol* **9**, 1204, doi:10.3389/fonc.2019.01204 (2019).

19 Saygin, C., Matei, D., Majeti, R., Reizes, O. & Lathia, J. D. Targeting Cancer Stemness in the Clinic: From Hype to Hope. *Cell stem cell* **24**, 25-40, doi:10.1016/j.stem.2018.11.017 (2019).

20 Clarke, M. F. Clinical and Therapeutic Implications of Cancer Stem Cells. *The New England journal of medicine* **380**, 2237-2245, doi:10.1056/NEJMra1804280 (2019).

21 Nieto, M. A., Huang, R. Y., Jackson, R. A. & Thiery, J. P. Emt: 2016. *Cell* **166**, 21-45, doi:10.1016/j.cell.2016.06.028 (2016).

22 Varga, J. & Greten, F. R. Cell plasticity in epithelial homeostasis and tumorigenesis. *Nat Cell Biol* **19**, 1133-1141, doi:10.1038/ncb3611 (2017).

23 Thiery, J. P. Epithelial-mesenchymal transitions in tumour progression. *Nat Rev Cancer* **2**, 442-454, doi:10.1038/nrc822 (2002).

24 Jiang, C. *et al.* Mesenchymal Stromal Cell-Derived Interleukin-6 Promotes Epithelial-Mesenchymal Transition and Acquisition of Epithelial Stem-Like Cell Properties in Ameloblastoma Epithelial Cells. *Stem Cells* **35**, 2083-2094, doi:10.1002/stem.2666 (2017).

25 Barker, N., Tan, S. & Clevers, H. Lgr proteins in epithelial stem cell biology. *Development* **140**, 2484-2494, doi:10.1242/dev.083113 (2013).

26 Birchmeier, W. Stem cells: Orphan receptors find a home. *Nature* **476**, 287-288, doi:10.1038/476287a (2011).

27 Suomalainen, M. & Thesleff, I. Patterns of Wnt pathway activity in the mouse incisor indicate absence of Wnt/beta-catenin signaling in the epithelial stem cells. *Dev Dyn* **239**, 364-372, doi:10.1002/dvdy.22106 (2010).

28 Yee, K. K. *et al.* Lgr5-EGFP marks taste bud stem/progenitor cells in posterior tongue. *Stem Cells* **31**, 992-1000, doi:10.1002/stem.1338 (2013).

29 Tanese, K. *et al.* G-protein-coupled receptor GPR49 is up-regulated in basal cell carcinoma and promotes cell proliferation and tumor formation. *Am J Pathol* **173**, 835-843, doi:10.2353/ajpath.2008.071091 (2008).

30 Becker, L., Huang, Q. & Mashimo, H. Lgr5, an intestinal stem cell marker, is abnormally expressed in Barrett's esophagus and esophageal adenocarcinoma. *Dis Esophagus* **23**, 168-174, doi:10.1111/j.1442-2050.2009.00979.x (2010).

31 Yamamoto, Y. *et al.* Overexpression of orphan G-protein-coupled receptor, Gpr49, in human hepatocellular carcinomas with beta-catenin mutations. *Hepatology* **37**, 528-533, doi:10.1053/jhep.2003.50029 (2003).

32 Leushacke, M. & Barker, N. Lgr5 and Lgr6 as markers to study adult stem cell roles in self-renewal and cancer. *Oncogene* **31**, 3009-3022, doi:10.1038/onc.2011.479 (2012).

33 de Sousa e Melo, F. *et al.* A distinct role for Lgr5(+) stem cells in primary and metastatic colon cancer. *Nature* **543**, 676-680, doi:10.1038/nature21713 (2017).

34 Zhang, J. *et al.* LGR5, a novel functional glioma stem cell marker, promotes EMT by activating the Wnt/beta-catenin pathway and predicts poor survival of glioma patients. *J Exp Clin Cancer Res* **37**, 225, doi:10.1186/s13046-018-0864-6 (2018).

35 Liu, J. *et al.* LGR5 promotes hepatocellular carcinoma metastasis through inducting epithelial-mesenchymal transition. *Oncotarget* **8**, 50896-50903, doi:10.18632/oncotarget.15143 (2017).
36 Brown, N. A. & Betz, B. L. Ameloblastoma: A Review of Recent Molecular Pathogenetic Discoveries. *Biomarkers in cancer* **7**, 19-24, doi:10.4137/BIC.S29329 (2015).
37 Effiom, O. A., Ogundana, O. M., Akinshipo, A. O. & Akintoye, S. O. Ameloblastoma: current etiopathological concepts and management. *Oral diseases* **24**, 307-316, doi:10.1111/odi.12646 (2018).
38 Binder, M. *et al.* Functionally distinctive Ptch receptors establish multimodal Hedgehog signaling in the tooth epithelial stem cell niche. *Stem cells*, doi:10.1002/stem.3042 (2019).
39 Athanassiou-Papaefthymiou, M., Papagerakis, P. & Papagerakis, S. Isolation and Characterization of Human Adult Epithelial Stem Cells from the Periodontal Ligament. *Journal of dental research* **94**, 1591-1600, doi:10.1177/0022034515606401 (2015).
40 Jiang, N. *et al.* Postnatal epithelium and mesenchyme stem/progenitor cells in bioengineered amelogenesis and dentinogenesis. *Biomaterials* **35**, 2172-2180, doi:10.1016/j.biomaterials.2013.11.061 (2014).
41 Yoshida, T. *et al.* Promotion of mouse ameloblast proliferation by Lgr5 mediated integrin signaling. *Journal of cellular biochemistry* **114**, 2138-2147, doi:10.1002/jcb.24564 (2013).
42 Peng, W. C. *et al.* Structure of stem cell growth factor R-spondin 1 in complex with the ectodomain of its receptor LGR5. *Cell Rep* **3**, 1885-1892, doi:10.1016/j.celrep.2013.06.009 (2013).
43 Sahai, E. *et al.* A framework for advancing our understanding of cancer-associated fibroblasts. *Nat Rev Cancer*, doi:10.1038/s41568-019-0238-1 (2020).
44 Raposo, G. & Stoorvogel, W. Extracellular vesicles: exosomes, microvesicles, and friends. *J Cell Biol* **200**, 373-383, doi:10.1083/jcb.201211138 (2013).
45 Kalluri, R. The biology and function of exosomes in cancer. *J Clin Invest* **126**, 1208-1215, doi:10.1172/JCI81135 (2016).
46 Steinbichler, T. B., Dudas, J., Riechelmann, H. & Skvortsova, II. The role of exosomes in cancer metastasis. *Semin Cancer Biol* **44**, 170-181, doi:10.1016/j.semcancer.2017.02.006 (2017).
47 Mashouri, L. *et al.* Exosomes: composition, biogenesis, and mechanisms in cancer metastasis and drug resistance. *Mol Cancer* **18**, 75, doi:10.1186/s12943-019-0991-5 (2019).
48 Li, M. & Izpisua Belmonte, J. C. Organoids - Preclinical Models of Human Disease. *N Engl J Med* **380**, 569-579, doi:10.1056/NEJMra1806175 (2019).
49 Drost, J. & Clevers, H. Organoids in cancer research. *Nature reviews. Cancer* **18**, 407-418, doi:10.1038/s41568-018-0007-6 (2018).
50 Vasyutin, I., Zerihun, L., Ivan, C. & Atala, A. Bladder Organoids and Spheroids: Potential Tools for Normal and Diseased Tissue Modelling. *Anticancer Res* **39**, 1105-1118, doi:10.21873/anticanres.13219 (2019).
51 Lorsch, J. R., Collins, F. S. & Lippincott-Schwartz, J. Cell Biology. Fixing problems with cell lines. *Science* **346**, 1452-1453, doi:10.1126/science.1259110 (2014).
52 Kaur, G. & Dufour, J. M. Cell lines: Valuable tools or useless artifacts. *Spermatogenesis* **2**, 1-5, doi:10.4161/spmg.19885 (2012).

53 Fedchenko, N. & Reifenrath, J. Different approaches for interpretation and reporting of immunohistochemistry analysis results in the bone tissue - a review. *Diagn Pathol* **9**, 221, doi:10.1186/s13000-014-0221-9 (2014).
54 Fuhrich, D. G., Lessey, B. A. & Savaris, R. F. Comparison of HSCORE assessment of endometrial beta3 integrin subunit expression with digital HSCORE using computerized image analysis (ImageJ). *Anal Quant Cytopathol Histpathol* **35**, 210-216 (2013).
55 Carpenter, A. E. *et al.* CellProfiler: image analysis software for identifying and quantifying cell phenotypes. *Genome Biol* **7**, R100, doi:10.1186/gb-2006-7-10-r100 (2006).
56 Miyoshi, H. & Stappenbeck, T. S. In vitro expansion and genetic modification of gastrointestinal stem cells in spheroid culture. *Nat Protoc* **8**, 2471-2482, doi:10.1038/nprot.2013.153 (2013).
57 Cui, T. X. *et al.* Myeloid-derived suppressor cells enhance stemness of cancer cells by inducing microRNA101 and suppressing the corepressor CtBP2. *Immunity* **39**, 611-621, doi:10.1016/j.immuni.2013.08.025 (2013).
58 Fang, M. *et al.* IL33 Promotes Colon Cancer Cell Stemness via JNK Activation and Macrophage Recruitment. *Cancer Res* **77**, 2735-2745, doi:10.1158/0008-5472.CAN-16-1602 (2017).
59 Milman, T., Ying, G. S., Pan, W. & LiVolsi, V. Ameloblastoma: 25 Year Experience at a Single Institution. *Head Neck Pathol* **10**, 513-520, doi:10.1007/s12105-016-0734-5 (2016).
60 Zhu, S. *et al.* Reprogramming of human primary somatic cells by OCT4 and chemical compounds. *Cell Stem Cell* **7**, 651-655, doi:10.1016/j.stem.2010.11.015 (2010).
61 Ginestier, C. *et al.* ALDH1 is a marker of normal and malignant human mammary stem cells and a predictor of poor clinical outcome. *Cell Stem Cell* **1**, 555-567, doi:10.1016/j.stem.2007.08.014 (2007).
62 Kumar, S. M. *et al.* Acquired cancer stem cell phenotypes through Oct4-mediated dedifferentiation. *Oncogene* **31**, 4898-4911, doi:10.1038/onc.2011.656 (2012).
63 Piskounova, E. *et al.* Oxidative stress inhibits distant metastasis by human melanoma cells. *Nature* **527**, 186-191, doi:10.1038/nature15726 (2015).
64 Singh, S. K. *et al.* Identification of a cancer stem cell in human brain tumors. *Cancer Res* **63**, 5821-5828 (2003).
65 Ponti, D. *et al.* Isolation and in vitro propagation of tumorigenic breast cancer cells with stem/progenitor cell properties. *Cancer Res* **65**, 5506-5511, doi:10.1158/0008-5472.CAN-05-0626 (2005).
66 Chaichana, K., Zamora-Berridi, G., Camara-Quintana, J. & Quinones-Hinojosa, A. Neurosphere assays: growth factors and hormone differences in tumor and nontumor studies. *Stem Cells* **24**, 2851-2857, doi:10.1634/stemcells.2006-0399 (2006).
67 Pastrana, E., Silva-Vargas, V. & Doetsch, F. Eyes wide open: a critical review of sphere-formation as an assay for stem cells. *Cell Stem Cell* **8**, 486-498, doi:10.1016/j.stem.2011.04.007 (2011).
68 de Lau, W. *et al.* Lgr5 homologues associate with Wnt receptors and mediate R-spondin signalling. *Nature* **476**, 293-297, doi:10.1038/nature10337 (2011).
69 Driehuis, E. *et al.* Oral mucosal organoids as a potential platform for personalized cancer therapy. *Cancer discovery*, doi:10.1158/2159-8290.CD-18-1522 (2019).

70 Mullenders, J. *et al.* Mouse and human urothelial cancer organoids: A tool for bladder cancer research. *Proceedings of the National Academy of Sciences of the United States of America*, doi:10.1073/pnas.1803595116 (2019).
71 Tuveson, D. & Clevers, H. Cancer modeling meets human organoid technology. *Science* **364**, 952-955, doi:10.1126/science.aaw6985 (2019).
72 Yadav, A. K. & Desai, N. S. Cancer Stem Cells: Acquisition, Characteristics, Therapeutic Implications, Targeting Strategies and Future Prospects. *Stem cell reviews* **15**, 331-355, doi:10.1007/s12015-019-09887-2 (2019).
73 Obaid, N. M., Bedard, K. & Huang, W. Y. Strategies for Overcoming Resistance in Tumours Harboring BRAF Mutations. *International journal of molecular sciences* **18**, doi:10.3390/ijms18030585 (2017).
74 Chen, G. *et al.* Wnt/beta-Catenin Pathway Activation Mediates Adaptive Resistance to BRAF Inhibition in Colorectal Cancer. *Mol Cancer Ther* **17**, 806-813, doi:10.1158/1535-7163.MCT-17-0561 (2018).
75 Gilbert, P. M. *et al.* Substrate elasticity regulates skeletal muscle stem cell self-renewal in culture. *Science* **329**, 1078-1081, doi:10.1126/science.1191035 (2010).
76 Zhou, Y., Chen, H., Li, H. & Wu, Y. 3D culture increases pluripotent gene expression in mesenchymal stem cells through relaxation of cytoskeleton tension. *J Cell Mol Med* **21**, 1073-1084, doi:10.1111/jcmm.12946 (2017).
77 Du, J. *et al.* Compression Generated by a 3D Supracellular Actomyosin Cortex Promotes Embryonic Stem Cell Colony Growth and Expression of Nanog and Oct4. *Cell Syst* **9**, 214-220 e215, doi:10.1016/j.cels.2019.05.008 (2019).
78 Ng, S., Tan, W. J., Pek, M. M. X., Tan, M. H. & Kurisawa, M. Mechanically and chemically defined hydrogel matrices for patient-derived colorectal tumor organoid culture. *Biomaterials* **219**, 119400, doi:10.1016/j.biomaterials.2019.119400 (2019).
79 Driehuis, E. *et al.* Oral Mucosal Organoids as a Potential Platform for Personalized Cancer Therapy. *Cancer Discov* **9**, 852-871, doi:10.1158/2159-8290.CD-18-1522 (2019).
80 Ge, Y. *et al.* Stem Cell Lineage Infidelity Drives Wound Repair and Cancer. *Cell* **169**, 636-650 e614, doi:10.1016/j.cell.2017.03.042 (2017).